Constraining mechanical and permeability properties of the Krafla geothermal reservoir, North-East Iceland

Thesis submitted in accordance with the requirements of the University of Liverpool for the degree of Doctor of Philosophy

by

Guðjón Helgi Eggertsson

May 2019

Declaration of authorship

I, Guðjón Helgi Eggertsson, declare that this thesis, entitled "Constraining mechanical and permeability properties of the Krafla geothermal reservoir, North-East Iceland" and the work presented in it are my own. I confirm that:

- This thesis was completed as a part of a research degree at the University of Liverpool.
- The material contained in the thesis has not been presented, nor is currently being presented, either wholly or in parts, for any other degree or qualifications.
- Where I have consulted published studies, this has been clearly referenced.
- Where the work was part of a collaborative effort, I have made clear what others have done and what I have contributed myself.
- Parts of the thesis have been published or in preparation for publication as:
    - **G. H. Eggertsson**, Y. Lavallée, J. E. Kendrick, S. H. Markússon. (published in *Journal of Volcanology and Geothermal Research*). **Improving fluid flow in geothermal reservoirs by thermal and mechanical stimulation: The case of Krafla volcano, Iceland.**
    - **G. H. Eggertsson**, Y. Lavallée, P. A. Wallace, J. Weaver, J. E. Kendrick, S. H. Markússon. (in preparation for the *Journal of Volcanology and Geothermal Research*). **Mechanical behaviour of geothermal reservoir rocks at Krafla volcano, Iceland.**
    - **G. H. Eggertsson**, J. E. Kendrick, J. Weaver, P. A. Wallace, J. E. P. Utley, J. D. Bedford, M. J. Allen, S. H. Markússon, R. H. Worden, D. R. Faulkner and Y. Lavallée. (submitted to *Geofluids*). **Compaction of hyaloclastite from the active geothermal system at Krafla volcano, Iceland.**

Signed:

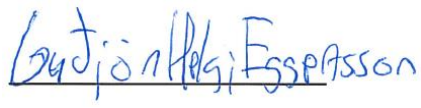

Guðjón Helgi Eggertsson

Abstract

Krafla volcano, located in North-East Iceland, holds an active hydrothermal system, that has been exploited for geothermal energy since 1978. Today it is exploited by Landsvirkjun National Power Company of Iceland and the system is generating ~60 MW_e from ~18 wells, tapping into fluids at 200-300°C. But as the geothermal industry is heading into a new era, with aims to drill further and reach the roots of geothermal reservoirs, sourcing higher enthalpy (possibly supercritical) fluids, understanding the physical properties rocks at these conditions is vital. In relation to this, the first well of the Icelandic Deep Drilling Project (IDDP) was drilled in Krafla in 2009. Drilling was terminated at a depth of 2.1 km, when the drill string penetrated a rhyolitic magma body, which could not be bypassed despite attempts to side-track the well. This pioneering effort demonstrated that the area close to magma had great energy potential, even though the well did not reach its initial target of 4-5 km depth.

In this thesis, I have employed laboratory experiments to describe the physical behaviour of reservoir rocks at Krafla under different conditions. During two field surveys in 2015 and 2016, and information gathered from drilling of geothermal wells, six main rock types were identified and sampled [and their porosities (i.e., storage capacities) where determined]: three groups of basalts (a lava with 10 to 27 % porosity, a basalt dyke with 31-36% porosity, and a porous lava with 34 to 60 % porosity), hyaloclastites (<35-45% porosity), obsidians (0-5% porosity), ignimbrites (13-18% porosity), and intrusive felsite's and micro-gabbro's (9-16% porosity). Samples are primarily from surface exposures, but selected samples of hyaloclastite core were sampled from cores drilled within the Krafla caldera. The permeability properties of both intact and fractured reservoir rocks were investigated using a hydrostatic cell, simulating stress conditions extant in the geothermal reservoir. The impact of thermal stimulation and pressure fluctuations was also investigated to further simulate reservoir conditions. The mechanical properties were investigated, especially how they might change in response to pressure changes, and how this might impact the effect of thermal- or mechanical stimulation. To further investigate the complex post-deposition evolution of rocks within the geothermal system, samples of hyaloclastite cores were compared to samples from the surface. As hyaloclastite gets buried within the caldera, it is subjected to increased pressure, temperature and fluid flow through the rock, causing alteration that decreases the permeability and increases the strength of the material within the reservoir with increasing depth.

As volcanically active areas are constantly changing and evolving, the properties of reservoir rocks can vary greatly. Thus, site exploration relies on understanding the physical- and mechanical properties of the rocks from geophysical surveys and real-time drilling data. For a successful drilling campaign and economically viable extraction from the hydrothermal reservoir, knowledge of the rock behaviour under various conditions is vital to seek ways to increase the permeability of the reservoir to enhance productivity of the exploited geothermal wells.

Contents

List of figures

List of tables

Acknowledgements

During my time in Liverpool, I have been fortunate to meet many great people that have supported me and helped in various ways. First, I would like to thank my supervisor, Prof. Yan Lavallée, for his guidance, support, patience and enthusiasm to make things happen. After only meeting over a short cup of coffee when he was in Reykjavík for a meeting, he was willing to scope a project based on a vague idea, and then fund the project to make it happen. I doubt that many supervisors would go the same distance as he has done to realise this project. I would also like to thank Jackie E. Kendrick, for her great supervision, support and assistance throughout my time in Liverpool.

The project would also never had been realised if it had not been for the support of Landsvirkjun, who partly funded the project, allowed us to stay in Krafla during our fieldwork, provided core samples and were always open for discussions and to listen to our ideas. Their feedback was very valuable and helped to improve the work even further.

I also want to thank my two examiners, Dr. Silvio De Angelis and Dr Hugh Tuffen, for their interest in this work. I very much looked forward to my Viva and they did not disappoint, with a lot of great questions, insight and knowledge, which made the Viva one of the most memorable moments of this journey.

I was assisted and supported by many friends and colleges at the Institute of Earth, Ocean and Ecological science. First and foremost, I would like to thank Paul Anthony Wallace (i.e. my work-wife and future six figure babysitter $$$), Josh Weaver and James Ashworth for all their help and great companionship during my time at the University. I'm also very grateful for all the great moments in the lab shared with the Volcanology group in Liverpool, with a lot of laughter and good stories. They helped to make the long hours in the lab bearable during bad days.

But mainly and especially, I want to thank my beautiful partner, Fjóla Daníelsdóttir, who in the years we have been together, has not only made me a man and a proud father of two beautiful kids, but also showed me how to be brave and firm during tough times. She has twice moved with me to cities she had never been to and with all her courage, showed how easy it can be. With her bright smile and easy-going attitude, it did not take long for her to meet and fit right in with the other Scouse stay-at-home moms. This made us feel very much at home in Liverpool and it became much harder to move back "home" to Iceland, because Liverpool had become our hometown, with lots of great friends and neighbours, that were always there if we needed.

Finally, I need to thank all my friends and family for their support during my PhD. The numerous visits we had in Liverpool helped us keep a bit if Iceland with us in Liverpool and make our stay even better.

Chapter 1:

Introduction

Exploration of geothermal energy is when heat is extracted from the ground for utilization, either for direct use, such as district heating, or extraction of steam and hot water. The hot water might be used to heat up groundwater through heat exchangers for district heating or industrial use. The steam is commonly utilised to power a turbine, producing electricity. For a hydrothermal reservoir to be economically viable, the reservoir needs to contain three things; 1) heat, 2) sufficient permeability and 3) water. For electricity production within high temperature fields (>230°C; e.g. Sanyal, 2005), the common practice is to drill production geothermal wells, usually about 1-3 km deep into a hydrothermal reservoir and extract hot water and steam (Fig. 1.1; e.g. Fridleifsson and Elders, 2005; Fridleifsson et al., 2014).

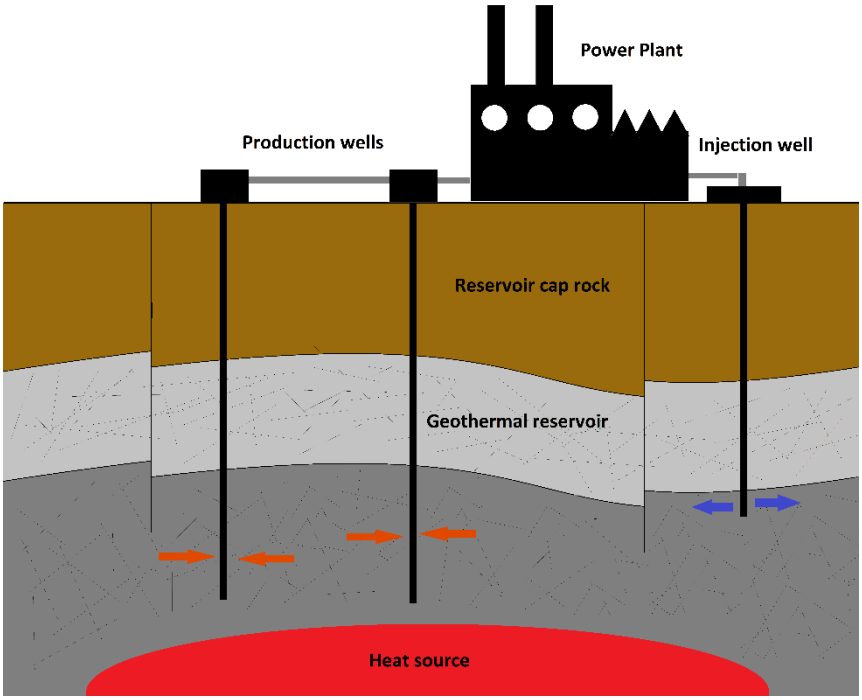

Figure 1.1: Schematic of the exploitation of a hydrothermal system. Fluids (steam and water) are extracted from production wells that have been drilled 1-3 km into the reservoir. The steam is used to spin turbines at the power plant and then the water is injected back into the reservoir.

A production well within the reservoir aims to source fluids at high temperature, where the recharge of the reservoir is high (i.e. high permeability), thus, the wells aim to intersect possible feed zones (fluid-filled high permeable zones or fractures and faults). To make sure each production well is optimised to its full potential, the well is usually stimulated directly after drilling and possibly later during its lifetime (e.g. Axelsson et al., 2006). The stimulation process might either aim to clean out any cuttings or drilling mud washed into the feed zones during drilling, restoring their permeability, or to open hydrological pathways and enhance the fluid flow in initially low permeability zones. To clean the well during or after drilling, water is injected through the drill string at the base at different rates

(Axelsson et al., 2006). To create or enhance any hydrological pathways the presence of hydrologically active fractures is often said to be the key for successful exploration of the reservoir (e.g. Barton et al., 1995), and a number of stimulation methods have been used. The three most common stimulation methods used are: 1) Hydraulic fracturing, where the pore pressure within a well or within a chosen zone in the well, is raised above the minor principal stress (σ_3; see section 1.1.2) and a fracture forms (Axelsson et al., 2006; Legarth et al., 2005; McClure and Horne, 2014; Miller, 2015; Murphy et al., 1981); 2) Thermal stimulation, where cycled injection of cold water is executed into the well, either from the top or through a deeper drill string. Pauses between cycles allow the well to thermally recover in-between injection periods. The method aims to cycle thermal contraction and expansion of the rock, causing cracking and is the most common stimulation method applied in high-temperature fields in Iceland (e.g. Axelsson et al., 2006; Grant et al., 2013; Siratovich et al., 2015a; Stefánsson et al., 1982). 3) Acidising, by injection of acidic fluids through the wellhead or drill string. The method aims to remove calcite scale, often present within fractures (e.g. Axelsson et al., 2006; Zimmermann et al., 2011).

Within exploited hydrothermal systems, pressure decline is commonly seen (e.g. Allis et al., 2009; Allis and Zhan, 2000; Bodvarsson, 1988; Bodvarsson et al., 1987; Bromley et al., 2013; Majer and Peterson, 2007; Scott et al., 2005). The pressure decline is a consequence of mass extraction from the reservoir, where the natural recharge of the reservoir is lower than mass extraction. The recharge rate within a reservoir is very dependent on permeability, pressure difference between the reservoir and the surrounding fluid pressure and the presence of fluids, as low permeability reservoirs will experience greater pressure decrease due to production, but high permeability reservoirs might see cold water inflow, as the fluids flows relatively fast through the reservoir, not allowing the fluids to heat up sufficiently in time. Well located injection sites can also help balance extraction from the reservoir and provide enough pressure support to the system, maintaining its pressure and power output (e.g. Arnorsson, 1995; Arnorsson et al., 2008).

As many of the more economical reservoirs have already been exploited, the focus has in many cases shifted towards more unusual reservoirs. These reservoirs include, for example, low permeability reservoirs, that are stimulated to create a viable source for geothermal water and steam (e.g. Ghassemi, 2012; Miller, 2015; Zimmermann et al., 2009), referred to as enhanced geothermal systems (EGS). Another example is in the search for deep reservoirs with supercritical fluids. Supercritical fluids have much higher enthalpies and lower viscosity than two-phase mixtures of water and steam; thus they hold the promise of greater heat and energy production, possibly increasing the energy output from wells by an order of magnitude (Fridleifsson et al., 2014). In this respect, the Iceland Deep Drilling Project (IDDP) and the DeepEGS project, both aim to investigate processes at higher pressures and temperatures than within conventional geothermal fields (Elders et al., 2014b; Fridleifsson and Elders, 2005; Friðleifsson et al., 2017). The concept of the IDDP project is to drill deeper than what is typically done in Iceland high temperature geothermal fields, aiming to source supercritical fluids (>374°C and 221 bars for pure water, increasing with increased salinity; Fridleifsson et al., 2017). The first well drilled in the IDDP project was IDDP-1, located at Krafla Volcano. The well was designed to reach 4-5 km depth, but the drilling was terminated at 2.1 km depth, as the drilling penetrated a shallow rhyolitic magma body. The well, however, showed great potential for production as it was able to produce

super-heated steam from the contact zone to the magma (Fig. 1.2), becoming the world's hottest geothermal well at the time. The theoretical output reached 35 MW_e during flow testing (Ingason et al., 2014) but the extreme conditions caused failure of the master valve and the well had to be closed shortly after (Hauksson et al., 2014; Hjartarson et al., 2014; Karlsdottir et al., 2014). This later sparked a new project, the Krafla Magma Testbed (KMT), seeking to observe and conduct scientific research on magma in-situ (Eichelberger et al., 2018).

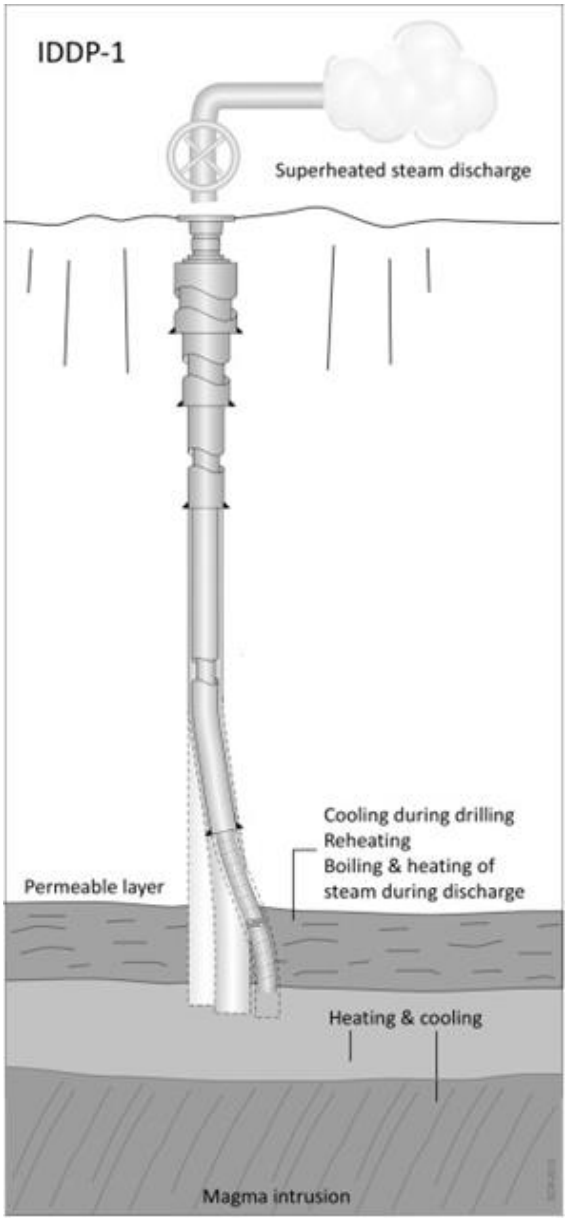

Figure 1.2: A simplified sketch of IDDP-1 well at Krafla, modified from Axelsson et al. (2014). The figure shows the well and the three attempts that were made to bypass the magma during drilling (not to scale). The well intersected a high permeable layer above the intrusion, which showed great potential for energy production.

The KMT project aims to set up the first magma observatory (Eichelberger et al., 2018). Well IDDP-1 had confirmed the presence of superhot geothermal system (SHGS) at the interface between the hydrothermal system and the magma (Eichelberger et al., 2018; Fridleifsson et al., 2014). The KMT

objectives are to: 1) investigate the roots of the hydrothermal system to the top of the magma body; 2) Investigate and find ground-truth testing of surface-based techniques to locate magma; 3) Perturb the deep system to understand signals interpreted as volcanic “unrest”; 4) Advance drilling and completion technology, to the point that supercritical fluids can be produced from these environments; 5) Advance sensor technology, with the focus on direct monitoring of magma bodies. As 10% of Earth’s population lives within 100 km from hazardous volcanoes, any improvement in eruption forecasting is very important (Eichelberger et al., 2018); drilling at IDPP-1 demonstrated that the system is stable enough to be probed without adverse consequences, making Krafla the ideal test site. The magma encountered during drilling of the IDDP-1 showed: 1) magma is found at very shallow depths (e.g. Elders et al., 2014b); 2) the interface between the magma and the hydrothermal system is very abrupt (e.g. Mortensen et al., 2014); 3) the conductive zone between the magma and hydrothermal system is very small (Eichelberger et al., 2018); 4) On the surface, there is no evidence for any recent eruptive material matching the shallow magma (Elders et al., 2014a; Mortensen et al., 2015). With growing demand for renewable energy, exploitation of the energy potential in superheated and supercritical fluids could yield an order of magnitude higher energy output per well (e.g. Elders et al., 2014b; Fridleifsson and Elders, 2005; Fridleifsson et al., 2014; Norton and Dutrow, 2001).

Today, the most economically viable reservoirs are those that are found within active magmatic provinces, as they have been found to exhibit the greatest heat flux on Earth (e.g. Lay et al., 2008; Pollack et al., 1993). It has been estimated that 80 to 90% of magma supplied to the crust is trapped and emplaced within it, making pluton formation the most probable endpoint for much of the magma displaced (e.g. Annen et al., 2015; Bachmann et al., 2007). Magmatism, and as a result volcanism, are commonly found to be episodic. Magma ascends and stalls in the crust, releasing heat to its surroundings whilst chemically and physically evolving, producing a range of plutonic bodies (e.g., sills, dykes, laccolith, etc; Edmonds et al., 2019). At times new magma replenishment can rejuvenate the systems, and at other times magma may flow out of reservoirs and erupt (e.g. Einarsson, 1991; Sigmundsson et al., 2010). The timescales of magma supply, possible magma mixing, and recharge events can also differ greatly between reservoirs (Cooper, 2019). These eruptions lead to the emplacement of volcanic deposits that drape the landscape. Altogether, magmatism and volcanism shape the construction of geothermal reservoirs in complex manners forming a range of lithologies with distinct physical and mechanical characteristics.

1.1 Heterogeneity in volcanic rocks

Volcanic rocks can have very diverse formation and evolutionary histories (e.g. Castro and Dingwell, 2009; Druitt and Kokelaar, 2002; Farquharson et al., 2017; Heap et al., 2014b; Hornby et al., 2015; Jakobsson and Gudmundsson, 2008; Petrakova, 2012; Sigmundsson et al., 2010; Siratovich et al., 2014; Tuffen et al., 2001; Varley et al., 2010; Watton et al., 2013). The physical and mechanical properties of the emplaced rocks depends upon their specific tectonic settings of melt generation, their ascent pathways within the crust and potential eruption to the surface (e.g. Annen et al., 2015; Blundy et al., 2006; Scandone et al., 2007), the cooling rate (e.g. Jarosch et al., 2008; Yoshinobu et al., 2009) and possible post-emplacement alteration (e.g. Lévy et al., 2018; Mortensen et al., 2014; Pola et al., 2012;

Stroncik and Schmincke, 2002; Thien et al., 2015). This results in a diverse pore structure (e.g. Al-Harthi et al., 1999; Coats et al., 2018; Colombier et al., 2017; Farquharson et al., 2015; Schaefer et al., 2015), broad range permeability (e.g. Farquharson et al., 2015; Gaunt et al., 2014; Kushnir et al., 2017; Mueller et al., 2005; Vinciguerra et al., 2005) and wide range of mechanical strength (e.g. Coats et al., 2018; Heap et al., 2014d; Heap et al., 2016; Kendrick et al., 2013a; Petrakova, 2012; Pola et al., 2014; Rocchi et al., 2002; Schaefer et al., 2015; Siratovich et al., 2016; Siratovich et al., 2014; Thomas et al., 2004).

Volcanic rocks frequently contain a glass phase, formed when magma cools rapidly to quench the amorphous melt phase. Volcanic activity in subaqueous or subglacial settings may interact with water (commonly meltwater, originated from ice) forming fragmental glass that can erupt explosively (e.g. Jakobsson and Gudmundsson, 2008; Watton et al., 2013; Zierenberg et al., 1995). Volcanic glass commonly undergoes extensive alteration, resulting in the generation of clay phases, producing mostly palagonite (e.g. Johnson and Smellie, 2007; Moore, 2001; Stroncik and Schmincke, 2002; Walton and Schiffman, 2003) and also smectite and zeolites (e.g. Drief and Schiffman, 2004). The term hyaloclastite is commonly used to describe this volcanic product, where crystals and rock fragments are supported by a palagonite matrix. Within published literature, the term hyaloclastite has however been used to refer to any volcanic product that has formed due to activity in contact with water (e.g. Jakobsson and Gudmundsson, 2008; Jarosch et al., 2008) and even secondary deposition environment (e.g. Lachowycz et al., 2015; Yagi et al., 2009; Ylagan et al., 1996). The formation history of hyaloclastite can greatly influence its properties, such as clast size, clast content, matrix porosity and sedimentary structures (e.g. Alfredsson et al., 2013; Jakobsson and Gudmundsson, 2008; Jarosch et al., 2008; Lachowycz et al., 2015; Marks et al., 2015). It can therefore be hard to define hyaloclastite, as it varies greatly.

Magmatic and eruptive minerals and glass within volcanic rocks are exposed to different temperatures, pressures and thermodynamics within hydrothermal systems, compared to those of their formation. Thus, the rocks are usually in disequilibrium with the conditions and fluids within the reservoir, promoting irreversible transformations of the chemical phases (e.g. Alfredsson et al., 2013; Pola et al., 2012; Pola et al., 2014; Thien et al., 2015; Walton and Schiffman, 2003; Ylagan et al., 1996). Minerals and glasses alter to different and more stable phases in new conditions, leading to changes in the physical characteristics such as porosity, permeability and rock strength (e.g. Thien et al., 2015). Such reactions highlight the need to understand in-situ conditions and evolution of reservoir materials through time in order to successfully harness geothermal energy. Currently, subsurface geology is commonly inferred from observations of cuttings that reach the surface (e.g. Fowler and Zierenberg, 2016; Mortensen et al., 2014). As a result, physical properties at depth are estimated based on drilling parameters, such as penetration speeds, drill bit wear, weight on bit and circulation loss. In recent years, it has become more common to collect cores at depth within these reservoirs (e.g. Fowler and Zierenberg, 2016; Fowler et al., 2015; Marks et al., 2015), yielding better constraints on the physical properties of reservoir rocks and required drilling parameters.

1.1.1 The permeability of volcanic rocks

The permeability of volcanic rocks is controlled by a complex network of open voids (i.e. the rock porosity) within the rock, including vesicles, dissolved minerals, and fractures of all sizes. Many studies have linked rock porosity to permeability, noting that permeability increases nonlinearly with porosity (Fig. 1.3). More recent studies have shown that permeability is also dependent on the connectivity and geometry of the pore space (Farquharson et al., 2015; Heap et al., 2014b; Heap and Kennedy, 2016; Jouniaux et al., 2000; Kendrick et al., 2016; Klug and Cashman, 1996; Lamur et al., 2017; Mueller et al., 2005). Several studies have been conducted to address these geometric effects, by applying variations of the Kozeny-Carman (Carman, 1937; Costa, 2006; Kozeny, 1927) relationship to model the porosity-permeability relationship of volcanic rocks (e.g. Costa, 2006; Mueller et al., 2005; Saar and Manga, 1999). These studies aim to either integrate several geometric inputs, such as the connected porosity, tortuosity of the flow channel, the throat diameter of the pore space and the cross-section shape factor (Degruyter et al., 2010), or constrain the hydraulic radius of a surface area (i.e. the ratio between the cross sectional area of a channel and the boundary area that is in contact with fluid flow; Farquharson et al., 2015; Kushnir et al., 2016). Both methods rely on integrating the tortuosity of the fluid pathway, as more tortuous fluid paths interfere with the flow, reducing permeability (e.g. Degruyter et al., 2010).

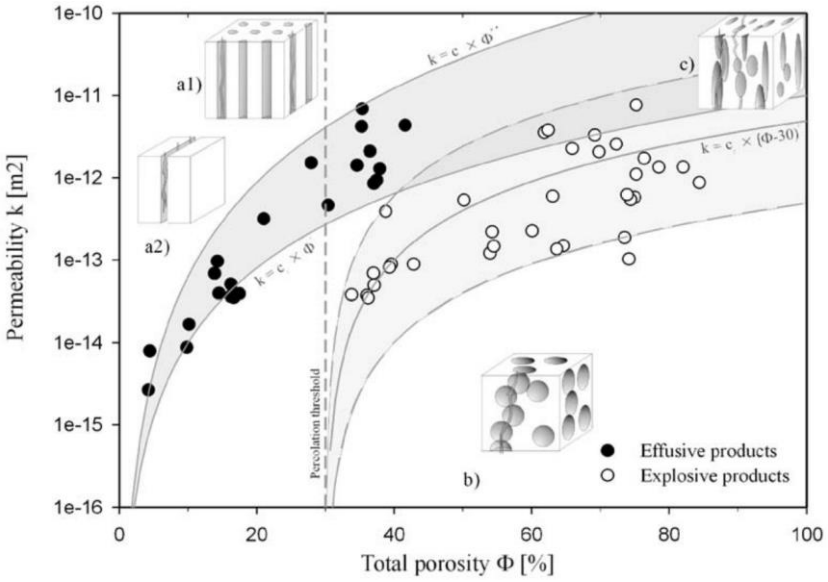

Figure 1.3: Two distinct porosity-permeability models explain the high data separation in porosity-permeability of volcanic rocks, from Mueller et al. (2005). Effusive products can most effectively be modelled using a combination of a capillary tube model and a fracture flow model (a1-2), whereas the permeability of explosive products is best fitted using a fully penetrable sphere model (b) with a zone of overlap noted at high porosity (c).

The impact of a macro-fracture has been investigated in recent experimental investigations, suggesting that a single fracture can increase the permeability by up to four orders of magnitude for low porosity rocks but the effect is less significant at elevated porosity (Heap and Kennedy, 2016; Lamur et al., 2017; Perez-Flores et al., 2017). Upscaling of these results can however be challenging due to scale-dependence of permeability, as discussed by Heap and Kennedy (2016). When scaling permeability from the laboratory (<0.2 m) to the reservoir scale (>100 m), it needs to be considered that the fracture length increases significantly, thus, increasing the tortuosity effect on the fluid flow through the

fracture. Within a rock mass, where a macro-fracture has a significantly higher impact, this effect will result in a decrease in permeability for longer fractures, causing the estimated fracture permeability of the reservoir to decrease (Heap and Kennedy, 2016). It is therefore important to consider the representative of samples carefully, as pristine rock samples can significantly underestimate the equivalent permeability within fractured reservoir, as well as samples containing a macro-fracture, which will cause the fracture permeability of the reservoir to be significantly overestimated. Moreover, it is important to consider that permeability decreases nonlinearly with increased effective pressure (confining pressure – pore pressure = effective pressure), thus with increasing burial within a geothermal system the ability for fluid to flow is reduced (see Chapter 2).

1.1.2 The natural stress field and effect by geothermal exploitation

Within hydrothermal reservoirs, rocks are subjected to both elevated pressure and temperature (e.g. Arnorsson, 1995; Bromley et al., 2013) and in volcanic settings, these pressure and temperature conditions can vary greatly over short distances, as geological processes (i.e. tectonic plate movements, magmatism and volcanism, erosion and weathering) are very active compared to the continental crust (e.g. Zoback, 2010). Exploitation of hydrothermal reservoirs will also further influence reservoir pressure and temperature (e.g. Bodvarsson, 1988; Bromley et al., 2013; Mortensen et al., 2015). To accurately determine the properties of the different reservoir lithologies, it is necessary to consider the effect of prolonged exposure to elevated pressure and temperature as well as percolating fluids. In general, in an undisturbed crust, the pressure is lithostatic and the pressure from the overlying rock increases with depth from the weight of the rocks above, with the pressure within the pores counteracting the effective pressure experienced by the rock mass. Any external forces acting on the rock can affect its pressure conditions (i.e. plate tectonics, volcanism etc) and alter the in-situ stress condition. The in-situ principal stresses are generally considered by their magnitudes from σ_1-σ_3 (where σ_1 is the greatest, σ_2 is the intermediate and σ_3 is the least principal stress, each at 90° from one another). Within shallow reservoirs, these stresses are often simplified as the vertical stress (σ_v) and the higher and lower horizontal stresses (σ_{Hmax} and σ_{hmin}). The vertical stress is assumed to be the overburden of the rock mass within the reservoir, but the magnitudes of the two horizontal stresses are a result of other local/ regional forces as a result of geological processes (Zoback, 2010).

For a range of geo-mechanical problems (i.e. circulation loss during drilling, locating permeable pathways within the reservoir, decreasing permeability of wells with time etc.), knowledge of the in-situ stresses is of fundamental importance for reservoir exploitation (e.g. Ghassemi, 2012; Zoback, 2010). Exploitation of a hydrothermal system involves extraction of fluids from the system, causing the pore pressure to drop (e.g. Bromley et al., 2013; Gudmundsson and Thorhallsson, 1986). This drop is commonly counteracted by injection into the reservoir via injection wells (e.g. Bromley et al., 2013). Pore pressure fluctuations due to extraction and/or injection will cause changes in the effective pressure, which can easily be investigated using a Mohr diagram (Fig. 1.3). The Mohr diagram allows for the representation of a plane in three-dimensional state of stress, which is acting at a given point in the stress plane ($\sigma_{(1\text{-}3)}$, τ; knowledge of σ_2 is not needed to determine the stress state). Compressive stresses are defined as positive, whereas tensile stresses are negative. The failure envelope represents the strength of the rock (determined experimentally). If the curve intersects the failure envelope, the rock breaks, forming a fracture (e.g. Zoback, 2010).

If pore pressure decreases by extraction of fluid, the stress conditions will move away from the failure envelope, to a more stable condition (depletion, Fig. 1.3), and If pore pressure increases, the stress state will move closer to the failure envelope of the material (pressurisation, Fig. 1.3). A common occurrence with injection is an increased likelihood of induced seismicity as a result of increased pore pressure (e.g. Zang et al., 2014). On the other hand, extraction and lowering of the pore pressure can cause the reservoir to compact, possibly lowering its porosity (e.g. Keiding et al., 2010). It also increases the effective pressure, which may then reach the threshold for inelastic, destructive compaction (P*), beyond which irrecoverable compaction occurs (Zhang et al., 1990). The knowledge of the mechanical properties of different lithologies can, therefore, be very important for reservoir exploitation, as some rocks are sensitive to changes occurring within the reservoir, which could lead to problems with well stability (e.g. Siratovich et al., 2016).

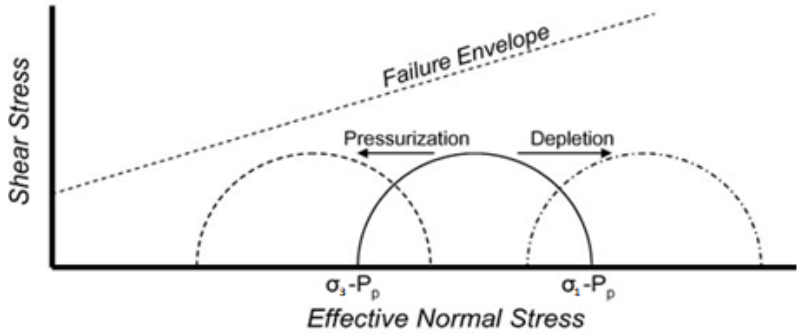

Figure 1.4: Mohr diagram showing the stress state of the greatest (σ_1) and least principal stress (σ_3) and the potential effect of changes in pore pressure (Pp). When the Pp is raised (pressurization), the effective normal stress is lowered, causing the stress state to become closer to failure. This could lead to induced seismicity. If the pore pressure is decreased within the reservoir (depletion), the stress state of the reservoir moves away from the failure envelope but may favour irrecoverable compaction.

Commonly, rock strength is observed to decrease with increasing porosity (Coats et al., 2018; Heap et al., 2014a; Heap et al., 2014d; Kendrick et al., 2013a; Loftsson and Steingrímsson, 2010; Schaefer et al., 2015). Porosity and its spatial distribution are the leading control in a rock's response to changes in stress (e.g. Griffiths et al., 2017). The stress change can be small enough to only cause reversible (elastic changes), for example the closure of pre-existing microfractures. However, if the stress exceeds the elastic limit, microfractures within the rock mass will propagate and coalesce, causing non-recoverable damage and ultimately causing the rock to fail (e.g. Brace et al., 1966; Scholz, 1968). The deformation experienced is also rate dependent, which is frequently overlooked despite evidence that lower strain rates have been correlated to lower strengths (Coats et al., 2018; Schaefer et al., 2015). Moreover, an increasing number of studies point to the weakening effect of multiple stress cycles (Heap et al., 2009; Kendrick et al., 2013a; Schaefer et al., 2015) that could be common in geothermal reservoirs during extraction or injection of fluids. These studies suggest that the weakening effect of stress cycling is more significant in initially fracture-dominated materials.

The importance of fractures for sufficient fluid flow at depth is very well known (e.g. Barton et al., 1995; Gunnarsson, 2011; Hofmann et al., 2016; Milsch et al., 2016; Perez-Flores et al., 2017). Pre-existing weaknesses including fracture networks define a material's response to stress changes (e.g. Barton and Zoback, 1992; Barton et al., 1995). Sufficient stress changes can either cause the material

to rupture and form a new macro-fracture, or cause slip within a pre-existing fracture network (e.g. Ayling et al., 1995; Faulkner and Armitage, 2013; Miller, 2015). As volcanic rocks have very diverse formation and alteration histories they may also host diverse fracture networks (Heap and Kennedy, 2016). Fractures that are hydraulically active are of great importance. Fracture orientation within the stress field will control their potential to be hydraulically active as the magnitude of the three principal stresses vary. Here, the friction coefficient becomes important, as it represents the ratio between the shear and normal stress active on a plane (Byerlee, 1978; Samuelson et al., 2008; Zoback, 2010). As Byerlee (1978) showed, the coefficient of friction in crystalline rock is between 0.6-1. Faults with high coefficient of friction (e.g. >0.6) are therefore much more likely to induce slippage along the fracture plane in a changing stress field, which may promote fluid flow (Barton et al., 1995).

1.2 Geological setting

1.2.1 Geology of Iceland

Iceland is situated at the plate boundary between the Eurasian and the North American plates, which spread apart at a rate of ~1.9mm/yr., forming the mid-Atlantic ridge. The ridge is characterised by a wide central rift valley rising above the surrounding seafloor (e.g. Demets et al., 1994; Sella et al., 2002). Iceland's vigorous volcanism has formed a plateau about 3 km higher than the mid-Atlantic rift valley to the north and south of Iceland. As a result, the Earth's crust is 3-4 times thicker in Iceland, compared to the average oceanic crust. The driving force of Iceland's volcanic activity is a hotspot which supplies vast amounts of melt close to the Earth's surface (Bjarnason, 2008; Gaherty, 2001; Wolfe et al., 1997). The mantle below Iceland has been mapped, with low-velocity seismic anomalies showing the hotspot reaching down to 400-450 km depth, 200-250 km deeper than what is commonly seen (Bjarnason, 2008).

Onshore, the Neovolcanic zone comprises four volcanic systems (Fig. 1.5) connected across central Iceland by the Mid-Iceland Belt (MIB): 1) the Reykjanes Volcanic Zone (RVZ; Reykjanes peninsula) 2) the Western Volcanic Zone (WVZ); 3) the Eastern Volcanic Zone (EVZ); 4) the Northern Volcanic Zone (NVZ). In addition, there are two volcanically active belts (Öræfajökull and Snæfellsnes; Thordarson and Larsen, 2007). These volcanic systems generally contain fissure (dyke) swarms aligned subparallel to the rift zone, and a central volcano, formed by the focal point of eruptive activity and usually containing the largest edifice within each system. Most volcanic zones have a typical lifetime of about 0.5-1.5 million years (Thordarson and Larsen, 2007). The fissure swarms commonly remain inactive for tens to thousands of years between rifting episodes (e.g. Bjornsson et al., 1977; Thordarson and Larsen, 2007; Wright et al., 2012). Within the volcanic zones, the stratigraphy is made up of volcanic deposits, mostly alternating layers of basaltic lavas and hyaloclastite formations, reflecting changing climate conditions through time, as volcanic deposits accumulate (e.g. Arnorsson, 1995; Arnorsson et al., 2008; Mortensen et al., 2014) .

The Northern Volcanic Zone (NVZ) stretches from the Vatnajökull glacier to the north coast of Iceland, hosting seven central volcanoes; 1) Tungnafellsjökull, 2) Bárðarbunga, 3) Kverkfjöll, 4) Askja, 5) Fremrinámar, 6) Krafla and 7) Þeistareykir (Hjartardottir and Einarsson, 2012). Deformation along the NVZ occurs predominantly during rifting episodes and in-between, it takes place at the more silicic central volcanoes (Hjartardottir and Einarsson, 2012; Hjartardottir et al., 2012; Sæmundsson, 1991).

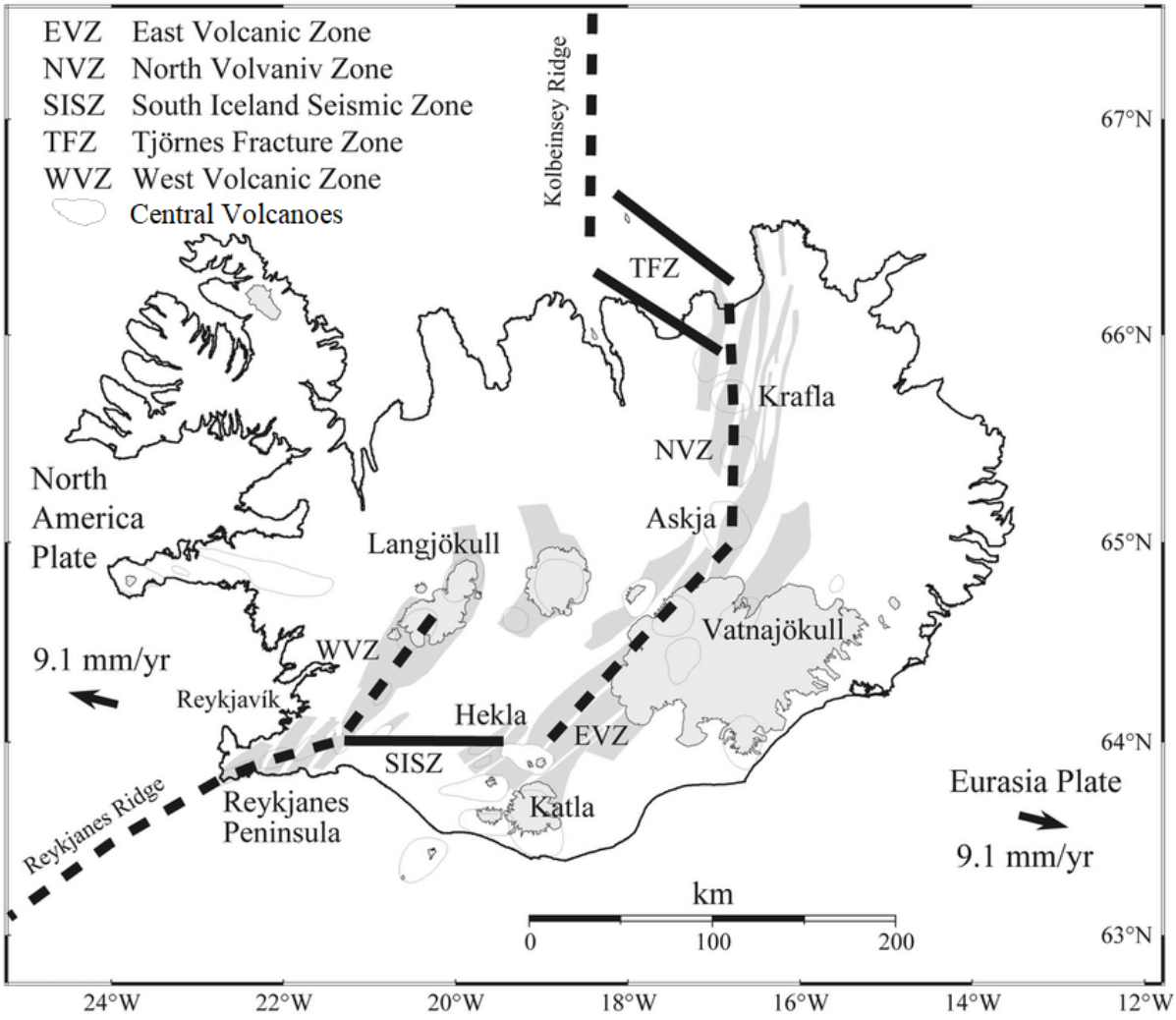

Figure 1.5: Map of Iceland, showing place names, lithosphere plates and the plate boundary structure through Iceland, modified from Einarsson et al. (2006). The divergent plate boundaries are shown with dashed lines (Reykjanes and Kolbeinsey ridges) and seismic zones and transforms are shown with thick lines (the South Iceland Seismic Zone (SISZ) and the Tjörnes Fracture Zone (TFZ)). Volcanically active regions are indicated: the Reykjanes Volcanic Zone (RVZ) at Reykjanes peninsula, the Western Volcanic Zone (WVZ), the Eastern Volcanic Zone (EVZ), the Northern Volcanic Zone (NVZ) and the). The central volcanoes are shown with thin grey lines and the fissure swarms are showed in grey.

1.2.2 Geology of Krafla volcano

Krafla central volcano is situated in the Krafla fissure swarm (Fig. 1.6), forming the Krafla volcanic system (Hjartardottir et al., 2012). The Krafla fissure swarm extends ~40 km to the south and ~50 km to the north from the volcano (Hjartardottir et al., 2012; Sæmundsson, 1991). The Krafla caldera formed about 100.000 years ago, possibly during at least two eruptive episodes. The ignimbrite found within the caldera, named "Halarauður" has been linked to the formation of the caldera. The caldera is ~8 km across north-south, but ~10 km across east-west. The oval shape is, at least partly, caused by the rifting.

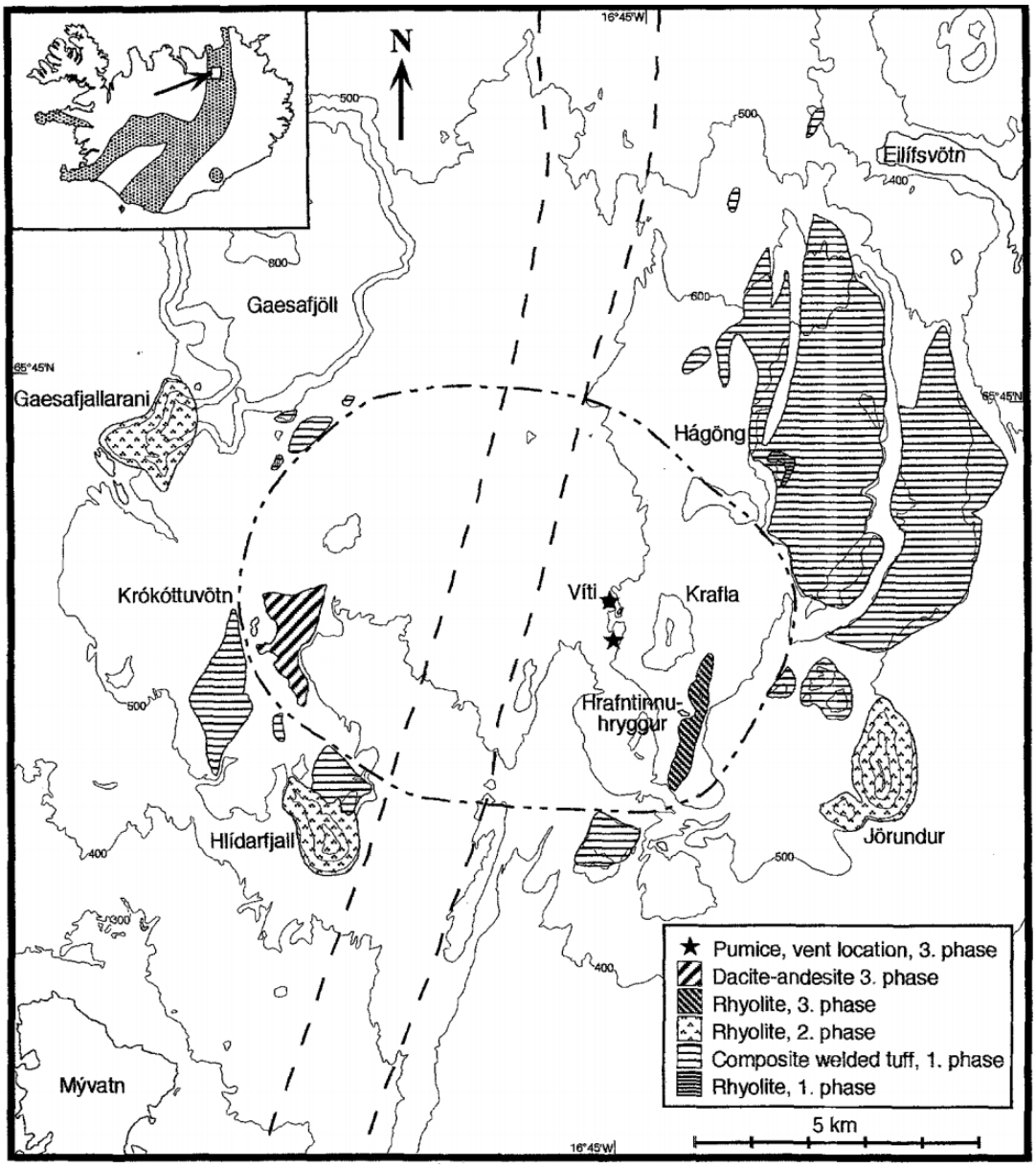

Figure 1.6: A simplified geological map of the Krafla caldera, showing the main tectonic features and occurrence of silicic volcanic rocks. The shaded area within the inset map shows the Neovolcanic zone in Iceland and the location of Krafla. The broken line shows the Krafla fissure swarm and the dot-dash line outlines the Krafla caldera. The figure is from Jonasson (1994).

Within the caldera, the stratigraphy is mostly represented by interchanging layers of eruptive material, mostly basaltic lavas, hyaloclastites and ignimbrite and later, more silicic lavas including obsidian (e.g. Jonasson, 1994; Mortensen et al., 2014; Mortensen et al., 2015). The stratigraphy has been mapped using cuttings retrieved from drilling excursions within the caldera (Mortensen et al., 2014; Mortensen et al., 2015). For the most part basaltic lavas and hyaloclastite formations are accumulated to about 1-1.3 km depth (Fig 1.7), below, more silicic intrusions, felsite and gabbro, and basaltic dyke formations become much more dominant (e.g. Arnorsson, 1995; Arnorsson et al., 2008; Mortensen et al., 2014; Mortensen et al., 2015). The hyaloclastite at the surface is thought to have formed shortly after the formation of the caldera, or early within the last glacial period (~100.000 years ago), during many consecutive eruptions. Holocene lavas have covered much of the hyaloclastite, but ridges and small

cones are still visible at the surface (Mortensen et al., 2015; Sæmundsson, 1991). Rhyolitic volcanism has been observed in Krafla (Fig. 1.6). The first phase has been linked to the formation of the caldera (~100.000 years ago), erupting a small amount of material at the surface. During the second phase, which occurred during the last glacial period, three subglacial rhyolitic ridges formed outside of the caldera rim. The third and final phase has been dated to late glacial times, where the rhyolitic volcanism activity within the caldera formed Hrafntinnuhryggur and a mixed dacite-andesite eruption occurred near Krókóttuvötn (Fig. 1.6; Jonasson, 1994).

In the Holocene, fissure eruptions have occurred every 300-1000 years within or close to Krafla caldera. Two rifting episodes have occurred within or close to the central caldera in historical times (i.e. the last 1000 years). First, the Mývatn fires occurred in 1724-1729. The eruption started with an explosive episode, forming the Víti crater. The activity was mostly characterised by dyke emplacements following the initial eruption, but in early August 1727, a large fissure opened to the surface, the first of four main eruptive fissures, the last of which opened in the summer of 1729 (Sæmundsson, 1991). Almost all of the eruptive material transported to the surface was basaltic, but fragmental rhyolitic material has also been found from the first episode when Víti formed (Jonasson, 1994; Sæmundsson, 1991). Later the Krafla fires took place, starting in December 1975 and lasting until September 1984. There was some unrest in the area leading up to the first eruptive fissure in December 1975, which lasted only for a few hours. In the coming years, most of the activity was preceded by seismic activity, as magma ascended from shallow magma bodies into the fissure swarm. The eruptions became more common in the years 1980-1984 (Einarsson, 1991; Heimisson et al., 2015; Sæmundsson, 1991). In total 17 separate periods of unrest took place, which caused 9 eruptions and a total of 0.25 km^3 of magma erupted to the surface.

Along with mapping the subsurface with cuttings retrieved during drilling excursions, alteration has been mapped, as an indication for temperature within the reservoir. Each alteration zone has an indication of the temperature conditions when the alteration took place. Commonly, the first 100-300 m of cuttings indicate a smectite zone, indicating a temperature below 200°C. At ~500-700 m depth the chlorite zone indicates a temperature of 230°C-250°C. From 700-900m depth a chlorite-epidote zone indicates a temperature of 250°C-280°C. Temperatures above 290°C can be inferred from the absence of calcite within the cuttings below ~1000 m depth within the main reservoir. Outside of the main volcanic field, these alteration zones reach much deeper as temperature is lower (Mortensen et al., 2015).

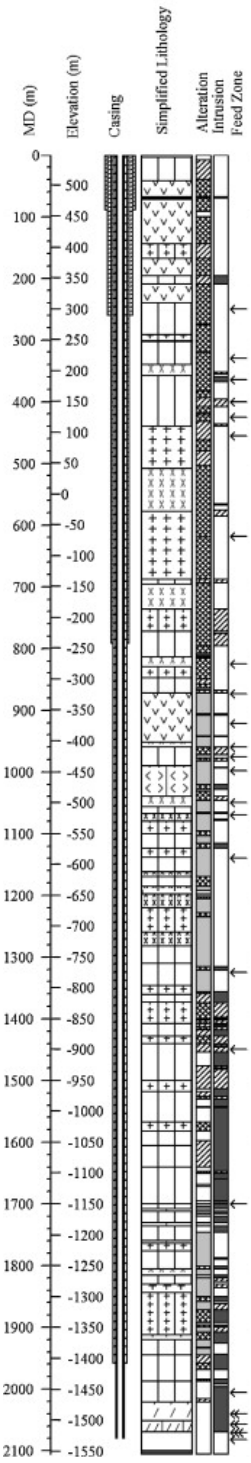

4–42 m depth, B-1: Holocene lavas with intercalated oxidized scoria and breccias consisting of mixed glassy basalt and tuff.

42–240 m depth, M-1: Consolidated and greenish altered basaltic hyaloclastite consisting of several thin layers, which are primarily aphyric, but a few of the layers contain phenocrysts of plagioclase or altered olivine.

240–872 m depth, B-2: Thick sequence of moderately altered basaltic lavas.

872–952 m depth, M-2: Light green altered hyaloclastite. The hyaloclastite consist of fine grained and medium grained basaltic tuff and is largely aphyric.

952–1362 m depth, B-3: Basaltic and basalt andesitic lava sequence.

1362–1700 m depth, Basaltic dyke complex: Sequence of dark-grey basaltic dykes with texture alternating in granularity from very fine (aphanitic) to medium grained.

1700–2000 m depth, Basaltic dykes, breccias and andesites: The sequence consists of basaltic dykes with interlayers of basaltic breccia, cryptocrystalline basalt as well as thin units of andesite.

2000–2070 m depth, Basaltic dykes, dolerites and granophyres: Below 2000 m the stratigraphy of well IDDP-1 is characterized by intrusive rocks with apparently little alteration; dark-grey, aphanitic basaltic dykes, grey coarse grained dolerite and granophyre, but white, medium and coarse grained granophyre with a few voids is prevalent below 2020 m depth.

2070–2101 m depth, No cutting retrieval: Geophysical logs reach down to 2083 m depth.

2101–2104 m depth, Rhyolitic magma: On three occasions problems were encountered leading to the drill string becoming stuck after having reached below 2100 m depth in IDDP-1 (2101 m, 2103 m and 2104 m depth). Only at the third and final occasion was circulation maintained through the drill string and cuttings of fresh fragments of obsidian were recovered revealing that the well had actually intercepted molten rock at this depth and the rhyolitic magma had been quenched by the drilling fluid.

Figure 1.7: A lithostratigraphy and a simplified stratigraphy description of well IDDP-1, from Mortensen, et al. (2014). The uppermost ~1350 m consists of basaltic lavas and hyaloclastite formations, divided into five sequences (B1-3, M1-2). Below ~1350 m, the reservoir is made up of dyke complexes, which extend to the bottom of the well at >2100 m (Mortensen et al., 2014).

1.2.3 Geothermal energy in Iceland and at Krafla Volcano

In Iceland, 29 on-land high temperature geothermal fields have been defined (Fig. 1.8), all of them are located within one of the 4 volcanic zones (Fig. 1.5). In addition, 3 offshore high temperature fields are known (e.g. Armannsson, 2016; Arnorsson, 1995). Of these 29 defined high temperature fields, 5 are being exploited for electricity production for the national power grid (Reykjanes, Svartsengi-Eldvörp, Hengill, Krafla, Þeistareykir) and to provide district heating (Svartsengi-Eldvörp and Hengill) for the nearby communities and industry (e.g. Björnsson et al., 2007; Langella et al., 2017; Zakharova and Spichak, 2012). The heat source within these fields is usually assumed to be shallow bodies of magma, that are slowly cooling, with heat convection upwards within the crust and fluid circulation (e.g. Arnorsson, 1995; Arnorsson et al., 2008). The IDDP project was initiated in the year 2000, by three energy companies (Hitaveita Suðurnesja – now HS Orka, (HS), Landsvirkjun (LV) and Orkuveita Reykjavíkur (OR) and Orkustofnun (OS; the National Energy Authority of Iceland), as a long term program by an industry-government consortium to investigate the potential of very high-temperature geothermal systems already exploited in Iceland (Fridleifsson et al., 2014).

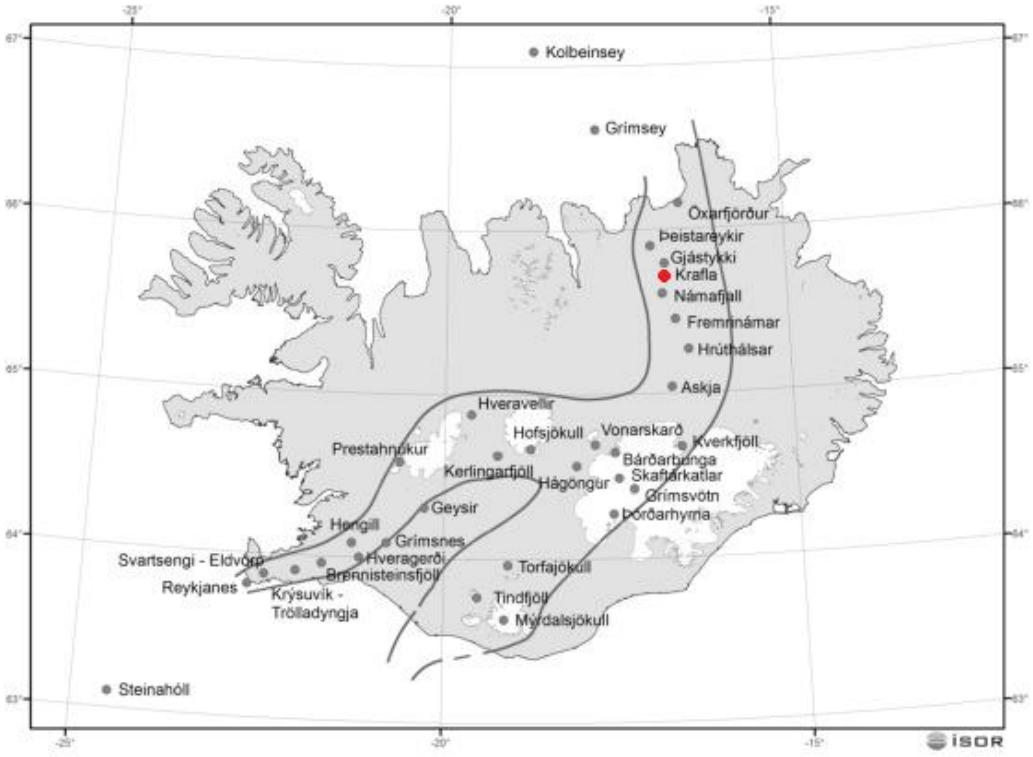

Figure 1.8: High temperature areas in Iceland marked within the Neovolcanic zone. Krafla is shown with a red dot (figure modified from Armannsson, 2016).

The hydrothermal system at Krafla volcano has been exploited since 1978 for electricity production, contributing to the national power grid. Originally, the aim was to produce 60 MW_e (2x30 MW_e turbines), but due to problems associated with the Krafla fires, where more acidic gases entered the reservoir and caused corrosion problems within wells and equipment, the power plant did not reach its target production until a second turbine was installed in 1998 (Guðmundsson, 2001). As exploration in Krafla has expanded through time, the characteristics of the reservoir have become clearer. Today, the well field has been divided into five sub-areas, based on their characteristics and location. Within

two of these areas, the reservoir is also divided into the upper and lower sections, as they exhibit different behaviour. Today, most wells in production reach to a depth of ~2 km or deeper through directionally drilled wells (Fig. 1.9), aimed at possible high permeability zones (Mortensen et al., 2015).

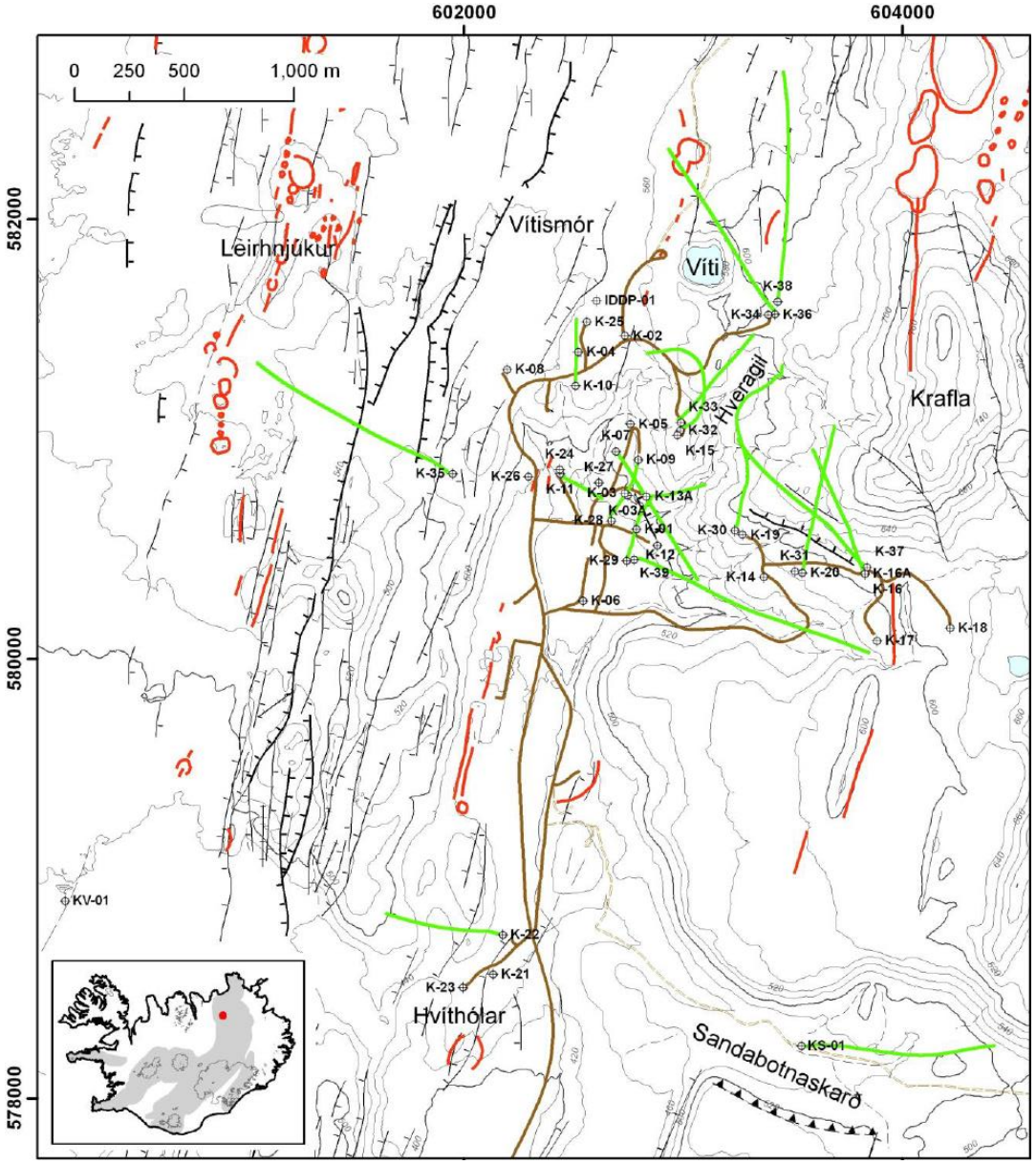

Figure 1.9: Locations of wells within the Krafla geothermal reservoir. The green lines indicate the directionally drilled well locations (Figure is from Mortensen et al. 2015). Inset shows the location of Krafla in Iceland.

1.3 Motivation and aims for the present study

The hydrothermal reservoir at Krafla has been exploited for over 40 years. A common experience with wells drilled within the reservoir is that they diminish rapidly in capacity with time. This is usually assumed to be due to corrosion and scaling within the well which clogs the fluid pathways and reduces the permeability, causing the well head pressure to decrease. Both pressure fluctuations and overall pressure decrease have been measured within a reservoir as a result of production (Mortensen et al., 2015). For increased well permeability, thermal stimulation has been used, directly after drilling, to stimulate wells in the past, sometimes with good results (e.g. Axelsson et al., 2006; Stefánsson et al., 1982). The thermal stimulation process is considered to be a very cost effective and attractive method for stimulation, but one of the least understood methods in active geothermal energy extraction (Axelsson et al., 2006). In addition, drilling within the hydrothermal reservoir at Krafla has showed that Krafla has the potential to be at the frontier of geothermal energy production and volcanic research via the use of superheated fluids for energy, as two wells have penetrated magma. Well KJ-39 penetrated magma at close to 3 km depth, and the well was subsequently plugged with cement at the bottom (Mortensen et al., 2015). IDDP-1 penetrated magma at even shallower depth, at 2.1 km, where the magma could not be bypassed (Elders et al., 2014b). The conductive zone at IDDP-1, close to magma, showed great potential for production (Eichelberger et al., 2018; Ingason et al., 2014). The opportunities at Krafla, from enhancing permeability within the hydrothermal reservoir already exploited, to further extending into new frontiers with up to magmatic temperatures (>900°C), offer great potential for improved reservoir exploitation and volcanic forecasting. Such ventures may facilitate even greater efficiency in the extraction of geothermal energy.

The objective of this thesis is to constrain the physical (i.e. porosity, permeability, thermal properties) and mechanical (e.g., tensile and compressive strength, Young's modulus) properties of the rocks found within the Krafla geothermal reservoir. The aim is to gain knowledge of the rock behaviour under various conditions, such as pressure and temperature, to seek ways to increase the permeability of the reservoir to enhance productivity of the exploited geothermal wells and to understand how these rocks might be affected by elevated temperatures. The thesis is split into three parts:

- **Chapter 2:** To constrain the permeable properties of both intact and fractured reservoir rocks found within the Krafla caldera and define how thermal stimulation can impact the permeability.
- **Chapter 3:** To constrain the mechanical properties of the reservoir rocks in response to pressure changes**.**
- **Chapter 4:** To further investigate the evolution of hyaloclastite within an active caldera, where the surface hyaloclastite is progressively buried with time, affecting its properties**.**

To do this, samples of the different lithologies were sampled at Krafla caldera to study in the Volcanology and Geothermal Research Laboratory at the University of Liverpool. Landsvirkjun, the National Power Company of Iceland also provided a number of core samples. The experiments were planned to gain knowledge of the different lithologies as they were subjected to changes in pressure and how that might affect their properties. The effect of temperature change was also investigated to gain knowledge of the thermal response of the different lithologies, as drilling excursions involve injection of cold water for circulation and commonly thermal stimulation is performed after drilling, so

knowledge of the thermal response of the different lithologies is vital to know how such processes will impact a reservoir. As most of the samples used were collected at the surface, knowledge of the in-situ rock properties in the reservoir could only be simulated. Thus, additional samples of hyaloclastite were made available by Landsvirkjun, who provided hyaloclastite cored at a range of different depths to be studied and compared to the surface material. This provided insight into the evolution of the initially porous surficial hyaloclastite within the reservoir as it was subjected to heat, pressure and percolating fluids.

Due to Iceland's unique geological history and the range of depositional environments of the eruptive material, the need to understand rock properties is urgent but neglected in many cases. Previous studies have either focused on low temperature reservoirs (e.g. Guillou-Frottier et al., 2013) or within reservoirs of very different geological history (e.g. Siratovich et al., 2014; Siratovich et al., 2016). The results of this thesis will therefore contribute towards a better understanding of rock properties within Icelandic geothermal systems. The mechanical dataset obtained will further contribute to current collaborative efforts to constrain magma reservoir conditions targeted by the Krafla Magma Drilling Project (Eichelberger et al., 2018), which aims to increase our understanding and ability to detect magma residence, as well as to pioneer the efficient and safe utilisation of this high thermal anomaly for increased geothermal production.

1.4 Status of manuscripts and co-author contribution

Chapter 2 - **Improving fluid flow in geothermal reservoirs by thermal and mechanical stimulation: The case of Krafla volcano, Iceland**

Authors: *G. H. Eggertsson[1], Y. Lavallée[1], J. E. Kendrick[1], S. H. Markússon[2].*

Affiliations:

[1]Department of Earth, Ocean and Ecological Sciences, University of Liverpool, 4 Brownlow Street, Liverpool, United Kingdom, L69 3GP.

[2]Landsvirkjun, Háaleitisbraut 68, 103 Reykjavík, Iceland.

Status: *Published in the Journal of Volcanology and Geothermal Research.*

Date submitted: *3rd of November 2017.*

Date accepted: 9th of April 2018.

Available online: *11th of April 2018.*

Authors Contributions: *All authors contributed towards conceptualising the project and contributed and revised the final manuscript.*

Guðjón H. Eggertsson: Primary investigator, collected samples from Krafla, conceptualised the final project, performed all the measurements and drafted the manuscript and figures.

Yan Lavallée: Helped with sample collecting, helped conceptualise the project, supervised the work and revised the manuscript and figures.

Jackie E. Kendrick: Verified the datasets and revised the manuscript and figures.

Sigurður M. Markússon: Revised the manuscript and figures.

Chapter 3 – **Mechanical behaviour of geothermal reservoir rocks at Krafla, Iceland**

Authors: *G. H. Eggertsson[1], Y. Lavallée[1], P. A. Wallace[1], J. Weaver[1], J. E. Kendrick[1], S. H. Markússon[2].*

Affiliations:

[1]Department of Earth, Ocean and Ecological Sciences, University of Liverpool, 4 Brownlow Street, Liverpool, United Kingdom, L69 3GP.

[2]Landsvirkjun, Háaleitisbraut 68, 103 Reykjavík, Iceland.

Status: in preparation for submission.

Date submitted: N/A

Date accepted: N/A

Available online: N/A

Authors Contributions: *All authors contributed to and revised the final manuscript.*

Guðjón H. Eggertsson: Primary investigator, collected samples from Krafla, conceptualised the final project, performed all the measurements and drafted the manuscript and figures.

Yan Lavallée: Helped with sample collecting, helped conceptualise the project, supervised the work and revised the manuscript and figures.

Paul A. Wallace: Participated with the thin section work and revised the manuscript and figures.

Josh Weaver: Participated in some of the triaxial experiments and revised the manuscript and figures.

Jackie E. Kendrick: Revised the manuscript and figures

Sigurður M. Markússon: Revised the manuscript and figures

Chapter 4 – **Compaction of hyaloclastite from the active geothermal system at Krafla volcano, Iceland**

Authors: *G. H. Eggertsson[1], J. E. Kendrick[1], P. A. Wallace[1], J. Weaver[1], J. E. P. Utley[1], J. D. Bedford[1], M. J. Allen[1], S. H. Markússon[2], R. H. Worden[1], D. R. Faulkner[1] and Y. Lavallée[1].*

Affiliations:

[1]Department of Earth, Ocean and Ecological Sciences, University of Liverpool, 4 Brownlow Street, Liverpool, United Kingdom, L69 3GP.

[2]Landsvirkjun, Háaleitisbraut 68, 103 Reykjavík, Iceland.

Status: Submitted to *Geofluids* special issue "*Structural controls on basin- and crustal-scale fluid flow and resulting mineral reactions*".

Date submitted: 20th of October 2019.

Date accepted: N/A

Available online: N/A

Authors Contributions: *All authors contributed to and revised the final manuscript.*

Guðjón H. Eggertsson: Primary investigator, collected samples from Krafla, conceptualised the final project, performed all the measurements and drafted the manuscript and figures.

Jackie E. Kendrick: Verified the datasets, revised the manuscript and figures.

Paul A. Wallace: Participated with the thin section work and revised the manuscript and figures.

Josh Weaver: Participated in some of the triaxial experiments and revised the manuscript and figures.

J. E. P. Utley: Performed the QEMScan measurements and revised the manuscript and figures.

J. D. Bedford: Advised on the triaxial experimental work and revised the manuscript and figures.

M. J. Allen: Performed the low permeability measurements and revised the manuscript and figures.

Sigurður M. Markússon: Revised the manuscript and figures.

R. H. Worden: Revised the manuscript and figures.

D. R. Faulkner: Revised the manuscript and figures.

Yan Lavallée: Helped conceptualise the project, supervised the work and revised the manuscript and figures.

1.4.1 Additional projects

In addition to the three papers presented in this thesis, contributions have been made to other projects and studies that have either been published in peer-reviewed papers along with two short papers presented at conferences and which appear in conference volumes. Below these contributions, short-conference papers are listed.

Peer-reviewed papers

Lamur, A., Kendrick, J.E., **Eggertsson, G.H.**, Wall, R.J., Ashworth, J.D., Lavallee, Y., 2017, The permeability of fractured rocks in pressurised volcanic and geothermal systems. *Scientific Reports 7*.

Lavallée, Y., **Eggertsson, G.H.**, Utley, J.E.P., Kendrick, K.E., Tripodis, N.A., Lamur, A., Wallevik, S.Ó., Karlsdóttir, S.N., Alexandersson, K.F., Přikryl, J., von Aulock, F.W., Coats, R., Worden, R.H. and Markússon, S.H., Thermo-mechanical degradation of hardened well cement casing due to geothermal activity at the wellhead: a case of the Icelandic Deep Drilling Project (IDDP). Being revised for *Geothermics*.

Weaver. J, **Eggertsson. G.H.**, Utley, J.E.P., Wallace, P.A., Lamur, A., Kendrick. J.E., Tuffen. H., Markússon, S.H. and Lavallée. Y., Thermal liability of hyaloclastite in the Krafla geothermal reservoir, Iceland: the impact of phyllosilicates on permeability and rock strength. Submitted to *Geofluids* special issue *"Structural controls on basin- and crustal-scale fluid flow and resulting mineral reactions".*

Wallevik, S.Ó., Alexandersson, K.F., Přikryl, J., **Eggertsson, G.H.**, Y., L., Utley, J.E.P., Worden, R.H., Karlsdóttir, S.N. Mechanical, microstructural and chemical properties of geothermal well cement casings from the IDDP-1 well, Iceland. In preparation for *Geothermics*.

Conference papers

Eggertsson, G.H., Lavallée, Y., Kendrick, J.E., Lamur, A., Markússon, S., 2016. Enhancing permeability by multiple fractures in the Krafla geothermal reservoir, Iceland. Presented at the *European Geothermal Congress, Strasbourg*.

Eggertsson G. H., Lavallée Y., Kendrick J. E., 2018. Impact of thermo-mechanical stimulation on the reservoir rocks of the geothermal system at Krafla, Iceland. Presented at the *Stanford Geothermal Workshop 43rd annual*, *Stanford. [included here as appendix I]*

Chapter 2:

Improving fluid flow in geothermal reservoirs by thermal and mechanical stimulation: The case of Krafla volcano, Iceland

Paper abstract

The magmatic-hydrothermal system at Krafla Volcano, North-East Iceland, is an important source of fluids exploited for geothermal energy. Here, we employ laboratory measurements to constrain the porosity and permeability of the main lithologies forming the reservoir and investigate the impacts of different thermal and mechanical stimulation practices to improve fluid flow.

Six main rock types were identified and sampled: three basalts (a dense and a porous lava, and a surficial dyke); a hyaloclastite; an obsidian; an ignimbrite; a felsite; and a gabbro. Permeability measurements were made in a hydrostatic cell using the steady-state flow method at a range of confining pressures (1-100 MPa). The measurements show that permeability generally increases with porosity, but that permeability may vary significantly for a given porosity, depending on the presence of pore connectivity and micro-fractures. We note that an increase in effective pressure results in a decrease in permeability due to closure of pre-existing cracks, abundant in some rocks. When unloading, samples fail to recover pre-loading permeability, as cracks do not necessarily entirely reopen. To further examine the hysteresis imposed by crack closure, we cyclically loaded/ unloaded a felsite sample ten times by varying pore pressure which resulted in a further nonlinear decreases in permeability with each pressurisation cycle; thus an understanding of the pressurisation path may be a requirement to constrain fluid flow variations in geothermal systems.

To test the effects of thermal stimulation on fluid flow, samples of dense basalt and felsite were thermally stressed by heating to 450 °C and cooling at different rates (in air, in water and at a controlled rate of <5 °C.min^{-1}). The results show that the permeability of originally highly fractured rocks is not affected by thermal stressing, but originally unfractured rocks show a nonlinear increase in permeability with each thermal stressing cycle, especially with the largest thermal shock imposed by quenching in water; thus thermal stimulation may not be expected to result in a similar magnitude of permeability creation along the length of a borehole.

Finally, following the permeability measurements on intact rocks, the Brazilian tensile testing method was employed to impart one and two (orthogonal) macro-fractures, and permeability was measured after each step. The creation of one macro-fracture strongly enhanced the permeability of the rock (especially dense rocks), resulting in a narrower range of permeability (as a function of porosity) for the fractured rocks. Imparting a second fracture had trivial additional impact on the permeability of the rock. Yet, the presence of fine fragments and possible minor offset of fracture interfaces was found to obstruct fracture closure, which resulted in higher permeability irrespective of effective pressure;

thus, hydraulic fracturing may locally increase fluid flow, especially when employing proppants to obstruct fracture closure and ensure a stable permeable network in a reservoir.

We discuss the implications of the findings for a first order constraint on the permeability of the reservoir rock and the potential of thermal and mechanical stimulation methods on energy production in geothermal systems nested in active volcanic fields.

2.1 Introduction

2.1.1 Fluid flow in reservoirs

Fluid flow in geomaterials has been the subject of numerous studies since the pioneering efforts of Henry Darcy (Darcy, 1856). These studies have highlighted the central importance of fluid flow in many environments, namely: water aquifers (e.g. Strehlow et al., 2015), petroleum and gas reservoirs (e.g. Jansen, 2011), volcanoes (e.g. Edmonds and Herd, 2007), and hydrothermal systems utilised for geothermal energy (e.g. Darling and Armannsson, 1989) – the subject of this study.

Hydrothermal systems are widespread on Earth and whilst they have been utilised for their thermal output in many cultures (e.g. Carlino et al., 2012; Gallois, 2007), they have long been recognised to be a source of devastating volcanic hazards (e.g. Gudmundsson et al., 2008; Hansell and Oppenheimer, 2004). Within active hydrothermal systems, the porous and fracture networks of the reservoir rocks may store high-pressure and temperature fluids that can be extracted for geothermal energy production (Gudmundsson, 1995) – a procedure established in 1904 by Italian scientist Piero Ginori Conti (Tiwari and Ghosal, 2005), and increasingly practiced in our efforts to deliver clean, renewable energy. The storage capacity of a reservoir is directly related to the porosity of the rock and the compressibility of the fluids (dependent on their chemistry), and our ability to extract these fluids requires a high degree of pore connectivity (e.g. Siratovich et al., 2014). Hence, permeability within exploited geothermal fields has an important control on both productivity and the sustainability of fluid flow within the reservoir. The development of permeability (whether natural or anthropogenic) has a great impact on the success, magnitude, and sustainability of energy production (Mock et al., 1997; Zimmermann et al., 2009).

The architecture of the porous network of rocks and, as a result permeability, varies widely in nature (e.g. Ashwell et al., 2015; Brace, 1980; Cant et al., 2018; Eichelberger et al., 1986; Farquharson et al., 2015; Heap et al., 2014a; Heap and Kennedy, 2016; Heap et al., 2014c; Heap et al., 2016; Jouniaux et al., 2000; Kendrick et al., 2016; Kendrick et al., 2013b; Klug and Cashman, 1996; Kushnir et al., 2016; Lamur et al., 2017; Mueller et al., 2005; Okumura and Sasaki, 2014; Saar and Manga, 1999; Schaefer et al., 2015; Stimac et al., 2004). This is especially the case for volcanic rocks, as they have undergone complex petrogenetic and deformation histories during their formation (Farquharson et al., 2015; Kendrick et al., 2013b; Klug and Cashman, 1996; Schaefer et al., 2015). For instance, during explosions, the pores which store the gas that triggers fragmentation are frozen into the lavas as they erupt; in contrast, the pore geometry of effusive lavas reflect a complex history of deformation, which results from bubble growth, coalescence, collapse and fracturing. Dense volcanic rocks are generally found to contain flattened and/ or irregular (concave) pores and multiple micro-fractures, whereas highly vesicular volcanic rocks tend to have sub-rounded (convex) pores. As a result, explosive products have

been described to hold a different permeability-porosity relationship than effusive products (Mueller et al., 2005). In addition, it has been suggested that there is a porosity change point (ranging between 14-~20 %) in microstructural control on effusive volcanic rock permeability, due to changes in relative tortuosity and pore throat size of the variably constructed porous networks of dense and porous rocks (Farquharson et al., 2015).

At depth, volcanic rocks may have different properties. Volcanic rocks buried by subsequent eruptive products – as is commonly the case in caldera systems (the setting of the geothermal system in this study) – tend to compact, closing micro-fractures (Kolzenburg et al., 2012), and if stress is sufficient, deformation may modify the architecture of the porous network (e.g. Heap et al., 2015a). Both micro-fracture closure (e.g. Lamur et al., 2017; Tanikawa and Shimamoto, 2009) and shear-enhanced compaction (Heap et al., 2015a) generally decrease the permeability of rocks buried at depth. When directly emplaced in the crust, intrusive volcanics tend to have low contents of vesicles and micro-fractures, and their permeability is equally low (Murphy et al., 1981), at least, at a small scale (Brace et al., 1968); yet, at a large scale, cooling contraction can trigger the development of columnar joints (Degraff and Aydin, 1993; Kantha, 1981), providing preferential fluid pathways.

Geothermal exploitation relies heavily on the presence of fractures to optimise fluid flow and energy generation. During drilling operations, a number of methods have been applied to enhance the extent of permeable fractures (e.g. Aqui and Zarrouk, 2011), whether through hydraulic fracturing (e.g. Legarth et al., 2005; McClure and Horne, 2014; Miller, 2015; Murphy et al., 1981; Tomac and Gutierrez, 2017; Zang et al., 2014; Zimmermann et al., 2011) or thermal stimulation (e.g. Grant et al., 2013; Siratovich et al., 2015b). In high-temperature, high-enthalpy geothermal reservoirs, where the rock may exhibit ductile behaviour (e.g. Violay et al., 2012), it is commonly presumed that fractures would not remain open nor preferentially oriented for long periods of time (e.g. Scott et al., 2015). This may be the case if temperature is sufficient, such that the diffusivity of the main rock forming minerals and melt (if present), favours fracture healing (e.g. Farquharson et al., 2017; Lamur et al., 2019; Tuffen et al., 2003) or viscous deformation of the porous network (Kendrick et al., 2013b; Kushnir et al., 2017). However, such rapid closure of permeability can be overcome if the rock remains fractured by keeping stress sufficiently high (e.g. Lavallée et al., 2013b), by building pore overpressure (e.g. Pearson, 1981) or by keeping temperature low (Lavallée et al., 2008), thus thermally contracting the rock (e.g. Siratovich et al., 2015b). Understanding the permeability of reservoir rocks, the sustainability of conditions and the longevity of production is key to characterising the potential exploitability of hydrothermal reservoirs for geothermal energy. Laboratory experimentation can help provide necessary constraints for material behaviour in simulated geothermal reservoir conditions (Ghassemi, 2012). For example, the presence of macroscopic fractures may significantly increase the permeability of rocks, especially of dense rocks (Eggertsson et al., 2016; Heap and Kennedy, 2016; Heap et al., 2015b; Lamur et al., 2017; Nara et al., 2012).

2.1.2 Geological setting of the Krafla geothermal system

Krafla is a caldera volcano, located in North-East Iceland (Figure 2.1a). The volcanic field hosts a partly filled caldera of about 8 x 10 km (Sæmundsson, 1991; Figure 2.1b) and is intersected by a 90 km long fissure swarm trending NNE (Hjartardottir et al., 2012). The caldera hosts an active hydrothermal

system, approximately 10 km^2 in size. In the Holocene, fissure eruptions recurring every 300-1000 years characterised the volcanic activity (Sæmundsson, 1991). In 1724-1729, the Mývatn fires occurred west of Krafla; initiating with an explosion at Víti crater, which exposed at the surface gabbroic and felsitic lithics originating at depth in the system. The most recent eruption was the Krafla fires, which initiated in 1975 and resulted in intermediate episodes of the outpouring of basaltic lava for 9 years (Einarsson, 1991). Magmatic activity associated with the eruption impacted the chemical composition of the fluids within the reservoir (Guðmundsson, 2001; Ármannsson, 1989) and led to increased hydrothermal activity (Einarsson, 1978, 1991; Sæmundsson, 1991).

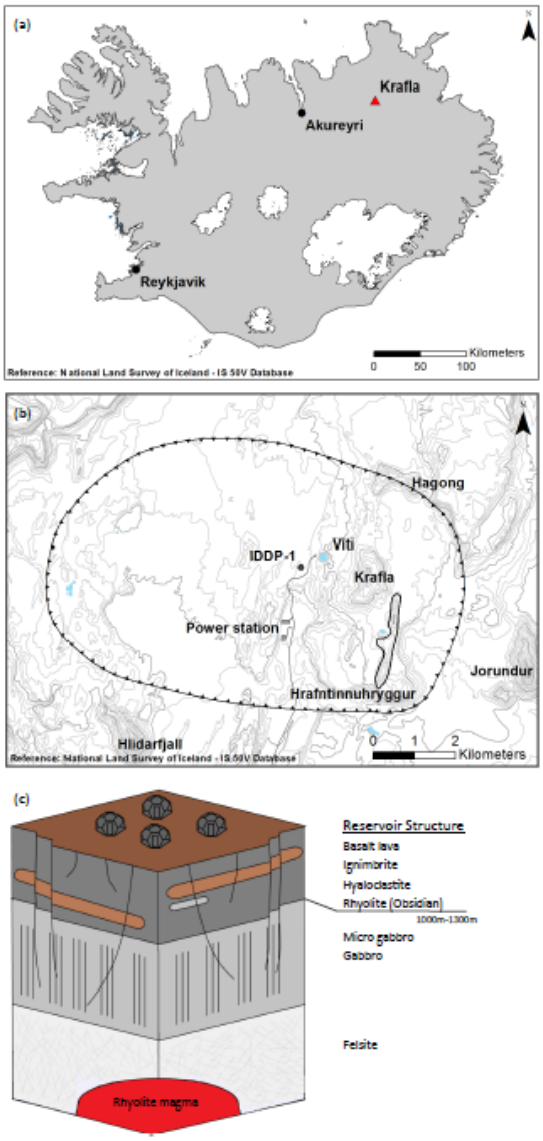

Figure 2.1: Krafla volcano, location, main features and lithology. (a) Location of the Krafla volcanic field in North-East Iceland. (b) Overview of the Krafla caldera, delimited by the line with tick marks (after Sæmundsson, 1991). The map shows the location of key features, in particular the power station, the Víti crater, the drill site of IDDP-1 and Hraftinnuhryggur (a large obsidian ridge). (c) Schematic of the lithologies comprising the Krafla geothermal reservoir. The uppermost 1000 - 1300 m of the reservoir are primarily made up of extrusive rocks, including lavas, ignimbrite and hyaloclastite. At greater depth, the reservoir is dominated by intrusive volcanics, gabbro and felsite (Mortensen et al., 2015). In a part of the system, rhyolitic magma was encountered at a depth of 2.1 km (Elders et al., 2014b).

In 1974, the government of Iceland initiated the construction of a geothermal power plant within the caldera. The aim was to install two turbines to produce 60MW_e, but due to problems associated with the Krafla fires eruption, the power plant only used one turbine until 1999; now that both turbines operate, the power plant readily produces 60 MW_e (Guðmundsson, 2001). In 2009 the Krafla geothermal field became site of the Iceland deep drilling project (IDDP-1), with the aim to source deep, high-enthalpy, supercritical geothermal fluids at a depth of 4-5 km (Fridleifsson et al., 2014). This attempt terminated abruptly as the drill string penetrated an active rhyolitic magma body at a depth of 2.1 km (Elders et al., 2014b). During flow tests of this, the World's hottest producing geothermal well, near-magmatic fluid entering the well head at a temperature exceeding 450 °C resulted in the transport of dry superheated steam at high pressures (40–140 bar), which due to its corrosive nature severely damaged the equipment and production ceased soon thereafter (Elders et al., 2014b). Yet, this unique opportunity demonstrated the possibility of producing 35 MWe from a single well (Ingason et al., 2014), and helped define parts of the geothermal system for the first time, constraining the pressure (Elders et al., 2011) and temperature (Axelsson et al., 2014; Elders et al., 2011) conditions in the encountered rhyolite body. Volatile concentrations measured in glass shards recovered during drilling in magma were used to define a pressure of ~30-50 MPa (Zierenberg et al., 2013), which is lower than that expected from lithostatic pressure (ca. 50-70 MPa; considering a depth of 2.1 km and assuming a range of rock densities between 2.5-3.3 $kg.m^{-3}$), but above hydrostatic pressure (~21 MPa) for this depth (Elders et al., 2011). This pressure discrepancy suggests that fluid pressure at the encountered magma body may be affected by connectivity across the hydrothermal system (e.g. Fournier, 1999).

Examination of drilling products (cores and cuttings) has provided a view of the rocks and structures hosting the reservoir fluids in the Krafla geothermal system. The observations suggest that the upper 1000-1300 m of the reservoir, where temperatures are ca. 100-300 ˚C, primarily consists of variably indurated and welded ignimbrite, intact as well as fractured basaltic lavas and variably compacted hyaloclastite. At depths below 1000-1300 m, where temperature may reach ca. 350 ˚C, the reservoir is made up of intrusive volcanics, primarily gabbro and felsite, which both show variable degrees of fracture damage (Bodvarsson et al., 1984; Mortensen et al., 2014; Sæmundsson, 1991). The last rock encountered before reaching the near aphyric magma body during IDDP-1 was a felsite sill (argued to be the crystallised, mushy, magmatic aureole) which totalled ~80 m in thickness (Mortensen et al., 2014). This magmatic aureole is characterised by a sharp temperature increase from ~400 to ~900 ˚C (e.g. Axelsson et al., 2014; Elders et al., 2014b; Mortensen et al., 2014). Thus, 40 years of extensive drilling operations in and around the Krafla caldera has provided us with invaluable information that helped reconstruct the reservoir rock (Figure 2.1c). This study aims to constrain the permeability of these rocks and assess how different thermal and mechanical stimulation methods may improve fluid flow in the hydrothermal system, and ultimately inform decisions to improve geothermal productivity in high-enthalpy systems.

2.2 Materials and Methods

2.2.1 Rock samples

During a field survey in Autumn 2015, and through information gathered from previous drilling exercises, six main rock types were identified and sampled to carry out this study (see Supplementary Data – Appendix II): three basalts (a lava with 11 to 27 % porosity, a basalt dyke with 31-36% porosity, and a porous lava with 34 to 60 % porosity); one hyaloclastite (35-45 % porosity); one obsidian (1-5 % porosity); one ignimbrite (14-17 % porosity); one felsite (9-18% porosity) and one gabbro (11-15 % porosity). The samples host a spectrum of pore micro-structures (Figure 2.2), which we anticipated would result in equally diverse permeability properties. The samples were loose blocks (therefore not orientated), collected from surface outcrops without hammering to prevent adding fracture damage and compromising the porosity and permeability values determined here; the felsite and micro-gabbro's (which form the roof of the magma reservoir; Mortensen et al., 2014) were erupted explosively through, and scattered around, Víti crater during the Mývatn fires (Sæmundsson, 1991).

2.2.2 Experimental methods

Here, we aim to constrain the natural range of permeability of reservoir rocks and investigate how to enhance fluid flow by testing the effects of thermal and mechanical stimulation methods; including the impact of pressure oscillations, thermal stressing and fracturing. This was done in several steps: first, we measured the porosity and permeability of all rock samples as collected; second, we subjected them to the thermal or mechanical stimulation methods (see below); and finally, we measured the permeability anew.

In this study over 120 core samples were prepared from large blocks of the aforementioned six rock types, and tested to constrain the range of porosity and permeability of each: As loose samples of blocks were collected from outcrops with no strong fabrics, cores were prepared in no particular orientation, yet parallel to one another within a given block. To examine the influence of a macro-fracture on the permeability of rocks core samples with a diameter of 26 mm and a thickness of ~13 mm were prepared; to investigate the impact of pressure fluctuations on permeability, cylindrical samples of felsite with a diameter and thickness of 26 mm were tested; for the investigation of thermal stressing impact on permeability, cylindrical samples of felsite and basalt with diameter of 25 mm and length of 50 mm were prepared and tested. The samples were kept in a drying oven at 75 ˚C after preparation, then left to cool in a desiccator before determinations of the porosity and permeability. The permeability dataset, obtained through the above experimental program, was complemented by additional porosity/ permeability measurements on 50 mm long by 25 mm diameter core samples (see Supplementary Data – Appendix II), which will be used in a future mechanical study of Krafla rocks (Eggertsson et al., chapter 3).

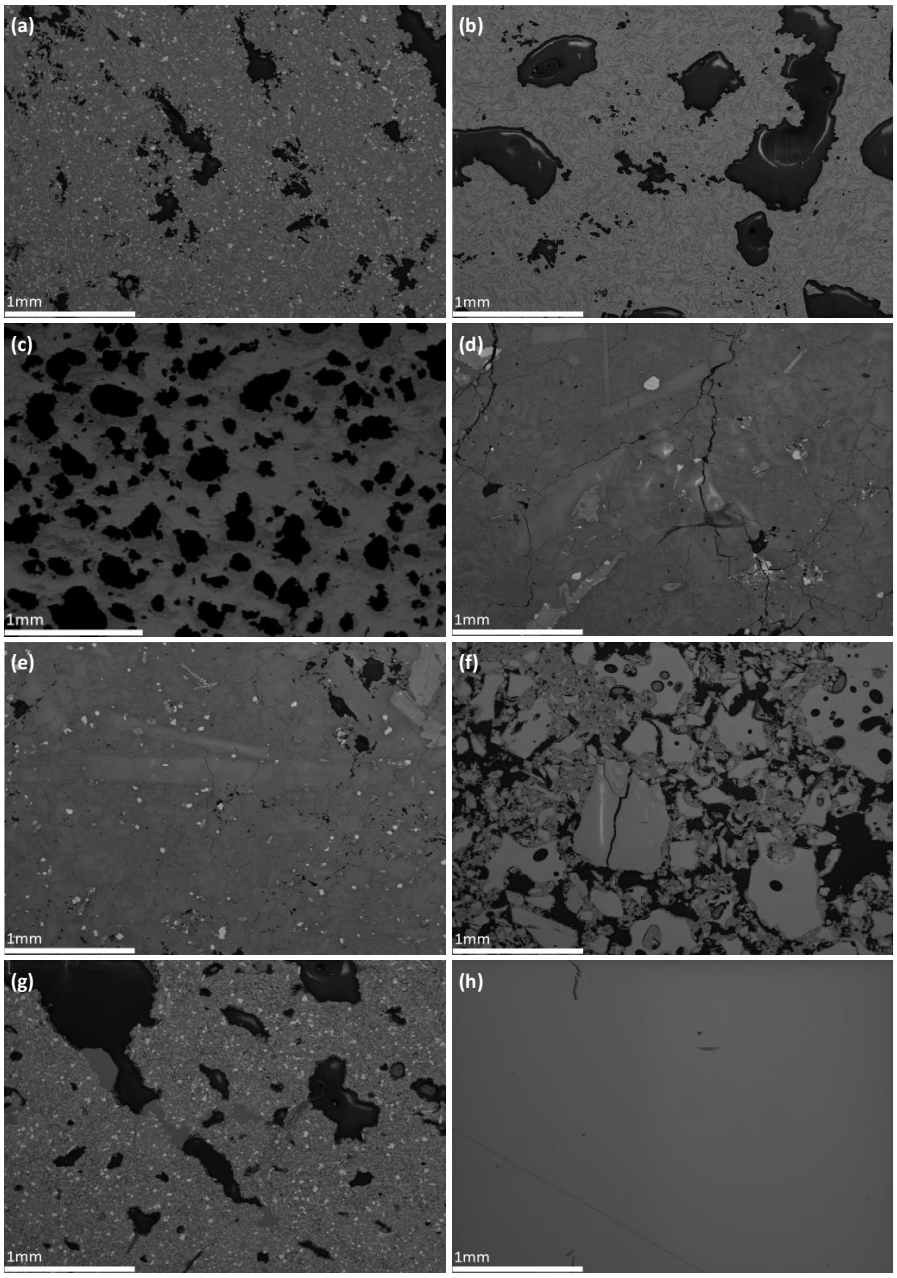

Figure 2.2: Backscattered electron (BSE) images (obtained by scanning electron microscope (SEM)) of the main Krafla reservoir lithologies. (a) Microcrystalline basalt with 11 % porosity, consisting of irregular vesicles with a range of sizes (< 1 mm), tortuosity and connectivity; micro-fractures are sparsely present but too narrow to be visible at this scale. (b) Microcrystalline basalt with 45 % porosity, comprising a bimodal porous network made of large and generally rounded, though slightly irregular, vesicles (<2 mm) and small irregularly distributed vesicles; micro-fractures are sparsely present but too narrow to be visible at this scale. (c) Basalt dyke sample with 32 % porosity, predominantly made of relatively evenly distributed, sub-rounded vesicles (100-400 microns); the rock contains a trivial amount of very narrow micro-fractures. (d) Felsite with 11.5 % porosity, consisting of very few small and irregular vesicles, sometimes connected by micro-fractures, up to 10-20µm wide. (e) Gabbro with 12 % porosity, made up of a connected network of many small, irregular-shape vesicles, and poorly developed micro-fractures. (f) Hyaloclastite with 40 % porosity, made up of irregular-shape pores between a highly fragmental, angular glass and crystalline assemblage. Micro-fractures as wide as 20 µm are visible in larger fragments. (g) Ignimbrite with 15 % porosity, comprising generally elongate and sub-rounded vesicles, and a lack of micro-fractures visible at any scale. (h) Dense obsidian with scarce micro-vesicles (<0.01 %) and no obvious micro-fractures.

2.2.2.1 Porosity and Permeability

The connected porosity of the cores was determined using an AccuPyc 1340 Helium pycnometer from Micromeritics. The device measures the sample skeletal volume (i.e. the volume of the solid rock as well as isolated pores which cannot be accessed by helium gas) in chambers of 100 cm^3 and 35 cm^3 (depending on the size of the sample), which provides a volume determination accuracy for the sample of ±0.1 %. The measurement, together with the sample weight, constrains the relative sample density (including isolated pore space), and as we know the volume of the initial sample core, we can determine the fraction of connected pores.

The permeability of the cores was measured in a hydrostatic pressure cell from Sanchez Technologies (Figure 2.3a) using the steady-state flow method. A water-saturated core was placed inside a rubber jacket and loaded in the pressure vessel, making sure that the pore pressure line was water saturated. The sample assembly was then slowly pressurised using silicon oil to the desired confining pressures (5-100 MPa), spanning the conditions of the Krafla geothermal reservoir. As the sample was pressurised, the volume of water displaced by the sample compaction was monitored with a volumometer to track changes in the porosity (from the original porosity, measured by He-pycnometry) of the sample at various confining pressure. [The accuracy of the volumometer on the two Stigma 300 pumps (from Sanchez Technologies; now Core Lab) is 0.002 ml, which, when measuring fluid volume for the smallest sample volume of 6.9 cm^3, results in an accuracy of porosity determination of 0.05 %.] Once equilibrated at the first confining pressure increment (e.g., 5 MPa) the rock permeability was measured using water, by imposing a pore pressure gradient of 1.5 MPa across the sample (2 MPa upstream and 0.5 MPa downstream) at an average pore pressure of 1.25 MPa, and by monitoring the flow rate at the sample exit; the permeability was only determined when the flow rate had stabilised. To assess the need for the use of Klinkenberg or Forchheimer corrections, the flow rate was varied by changing the pressure gradient and to check whether obtained permeability values changed; for the pressure gradient of interest, no such corrections were needed here. Once the permeability measurement was completed (after 20 to 600 minutes), the confining pressure was increased to the next increment (e.g., 10 MPa), whilst monitoring pore volume changes [generally, the pore volume decrease would stabilise (within resolution of the volumometer) after 1-10 min]; then the permeability was measured anew.

To further constrain the elastic limits of the weak, porous hyaloclastite, we constrained the effective pressure threshold for inelastic, destructive compaction (defined as P* of the rock), beyond which, an accelerated, irrecoverable compaction occurs (Zhang et al., 1990). This was done by loading a water-saturated sample in the permeameter. The confining pressure and pore pressure were increased slowly (to keep the effective pressure below 5 MPa) to 53 and 50 MPa, respectively. Then, the pore pressure was reduced (and thus the effective pressure was increased) at a rate of 0.1 $MPa.min^{-1}$ and the volume of water within the sample was monitored. P* was defined as point of negative inflection following a linear decrease in pore volume during effective pressure loading.

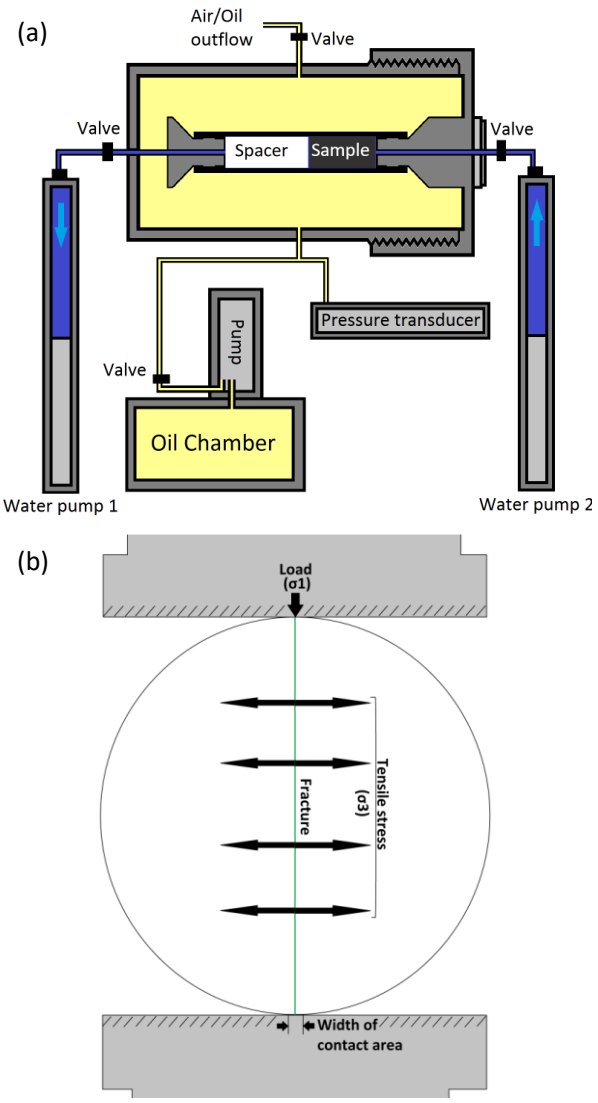

Figure 2.3: Experimental setup of the permeameter and Brazilian disc tests. (a) Schematic of the setup (hydrostatic cell and pumps) used to determine the permeability of rocks. The permeability was measured using water (blue) by imposing a pressure gradient of 1.5 MPa across the sample at an average pore pressure of 1.25 MPa (upstream: 2 MPa; downstream: 0.5 MPa) for a range of confining pressures (5-100 MPa) exerted by silicon oil (in yellow). (b) Illustration of the sample assembly to determine the tensile strength using the indirect Brazilian testing method. Here, a disc of 2:1 ratio (26 mm diameter by 13 mm thickness) is diametrically loaded at a constant displacement rate of 3 µm.s^{-1} between the pistons of an Instron press, and the load is continuously recorded.

2.2.2.2 Pressure fluctuations

We tested the effects of pore pressure fluctuations over 10 cycles, whilst keeping the confining pressure constant to simulate the impact of well pressure fluctuations associated with water injection during drilling operations. This was performed on felsite samples which we loaded to 39.5 MPa confining pressure and 1.5 MPa pore pressure (= 38 MPa effective pressure, assuming a simple effective pressure law). An effective pressure of 38 MPa may be representative of conditions at ca. 2 km depth, near the hydrothermal-magmatic system interface (Mortensen et al., 2015). We then measured the permeability at these conditions by imposing a pressure gradient of 1 MPa across the sample (2 MPa upstream and 1 MPa downstream). Once the permeability was measured, the pore

pressure was increased to 3.5 MPa and the permeability was measured by applying a pressure gradient of 1 MPa (4 MPa upstream and 3 MPa downstream). When the permeability had been measured at the lower effective pressure (higher pore pressure), the pore pressure was lowered back down to 1.5 MPa and the same procedure repeated, in total 9 times. The effective pressure change between each stage was therefore 1.5 MPa (from 38 MPa to 36.5 MPa effective pressure and back).

2.2.2.3 Thermal stimulation

The impact of thermal stimulation was tested on the samples of basalt (10.9-12.1 % porosity) and felsite (9.4-10.3 % porosity). The porosity and permeability of 3 cores of each sample was first measured as discussed above. The samples were then heated to 450 °C at 5°C.min^{-1} in a box furnace and left for 1 hour to dwell. After that, one sample of each rock type was cooled in a furnace, with a set cooling rate of 5 ˚C.min^{-1}; one sample of each rock was removed from the furnace and left to cool at ambient conditions on a benchtop; and finally, one sample of each rock type was removed from the furnace and quenched in a water-filled bucket at ambient temperature. Once cooled (estimated to be sufficient to cool the whole sample after 30 min – 12 hours, depending on the cooling method), the samples were then dried, and their porosity and permeability were measured again. This procedure was repeated, and the porosity and permeability were measured again after five and fifteen cycles. The cooling rates were chosen to represent different cooling rates experienced at different distances from boreholes during drilling activities and thermal stimulation procedures.

2.2.2.4 Fracturing

To induce a radial macro-fracture through the samples, the Brazilian tensile testing method was employed (Figure 2.3b). A cylindrical sample was loaded diametrically in a 5969 Instron uniaxial press at a displacement rate of 3 µm.s^{-1} until a through-going fracture was produced. To ensure that the samples would not disintegrate during indirect tensile fracturing, the samples were carefully wrapped in electrical tape around the circumference (thus the mechanical data are not of publishable quality). After sample failure, the tape was carefully removed, and the sample loaded into the pressure vessel for another series of permeability determinations.

For six basalt samples, a second set of fractures was then imparted, perpendicular to the first fracture in the samples. This time, however, the sample was left in the rubber jacket during loading in the press to ensure coherence. After sample failure, the permeability was measured once again under the same range of conditions as detailed above.

2.3 Results

2.3.1 Storage capacity of intact rocks

The porosity of a rock is a measure of the storage capacity for fluids and varies as a function of effective pressure (Wong and Baud, 2012). Here, we combine He-pycnometry measurements at atmospheric pressure (i.e. effective pressure of 0 MPa) and fluid volume changes measured by the volumometer in each pump during pressurisation and depressurisation in the hydrostatic pressure vessel, to constrain the evolution of porosity upon confinement.

The lithologies tested exhibit a wide range of porosities; especially the three basalt samples, which contain between 11 and 60 vol. % porosity. The porosity evolution as a function of effective pressure could only be measured for four rock types (Figure 2.4), as the obsidian and the ignimbrite had permeabilities too low to be determined using our setup in its current configuration (which cannot accurately constrain permeability lower than ~10^{-18} m^2). In all cases, the samples show a nonlinear decrease in pore volume with effective pressure. We note that the spread of porosity within each sample set is not particularly sensitive to effective pressure, suggesting that the nonlinear decrease in porosity with effective pressure is similar for a given rock type. For the most porous samples, the porosity decrease is slightly more pronounced (Figure 2.4b,e), which may be accentuated if the effective pressure exceeds P*, resulting in crushing of the rock and compaction (e.g., hyaloclastite; inset figure 2.4e).

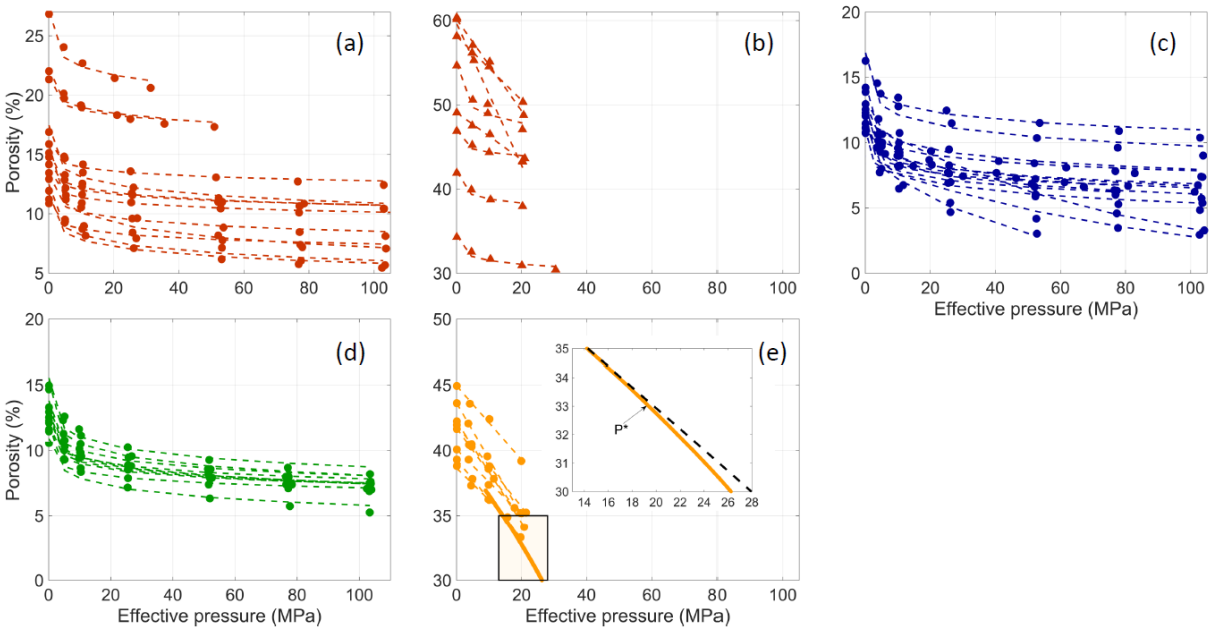

Figure 2.4: Porosity evolution with effective pressure for intact rocks. (a) dense basalt (shown in figure 2.2a; 10 samples tested), (b) porous basalt (shown in figure 2.2b; 6 samples), (c) felsite (14 samples), (d) gabbro (10 samples), and (e) hyaloclastite (8 samples) as a function of effective pressure. Here, the initial porosity measurement is made by He-pycnometry, with subsequent measurements extrapolated by monitoring volume gain in the pumps (hence volume loss in the samples) during permeability measurements. The figure shows a nonlinear decrease in porosity with effective pressure, indicative of micro-fracture closure. Across the lithologies, porosity decreases most rapidly as effective pressure is increased up to ~10 MPa. Note that the scale of each graph differs. The inset in (e) shows the inelastic (destructive) compaction beyond P^*, where the rock strength is not sufficient withhold the increased pressure and starts to collapse.

2.3.2 Permeability of intact rocks

The permeability of rocks varies as a function of porosity (e.g. Mueller et al., 2005), fracture density (e.g. Heap and Kennedy, 2016; Koudina et al., 1998) and effective pressure (e.g. Alam et al., 2014; Walsh, 1981). Here, we present permeability measurements on 60 intact samples; the basalt ($1.9x10^{-16}$ m^2 – $2.5x10^{-13}$ m^2), felsite ($1.8x10^{-15}$ m^2 – $1.1x10^{-13}$ m^2), gabbro ($7.2x10^{-16}$ m^2 – $1.0x10^{-14}$ m^2) and hyaloclastite ($6.0x10^{-14}$ m^2 – $1.8x10^{-13}$ m^2) samples show a range of permeabilities (Figure 2.5). The data show that sample length (used here) has no effect on the permeability of a rock (see Supplementary

Data – Appendix II). The basalts displayed the widest range of permeabilities (Figure 2.5a, b), as might be expected from their variable initial porosities (Figures 2.2a-c, 2.4a, b). [Note that the basalt dyke was not measured under such conditions.] The densest basalt shows little change in permeability with increased pressure (Figure 2.5a). The basalt samples with the highest porosities (>34 vol. % porosity; figure 2.5b) show a small decrease of permeability with confining pressure (up to 20-25 MPa); lower than may be anticipated due to the porosity decrease witnessed upon pressurisation (Figure 2.4b). The felsite and gabbro samples exhibit relatively larger decreases in permeability (Figure 2.5c,d) in response to effective pressure than the basalts (Figure 2.5a), owing to the highly fractured nature of these rocks. Yet, despite a fragmental origin of the hyaloclastite (Figure 2.5e), it only exhibited moderate decrease in permeability within the low effective pressure range tested (before the samples could not sustain the effective pressure); however, the samples compacted inelastically above an effective pressure of 18 MPa (inset figure 2.4e), which resulted in a significantly lower permeability.

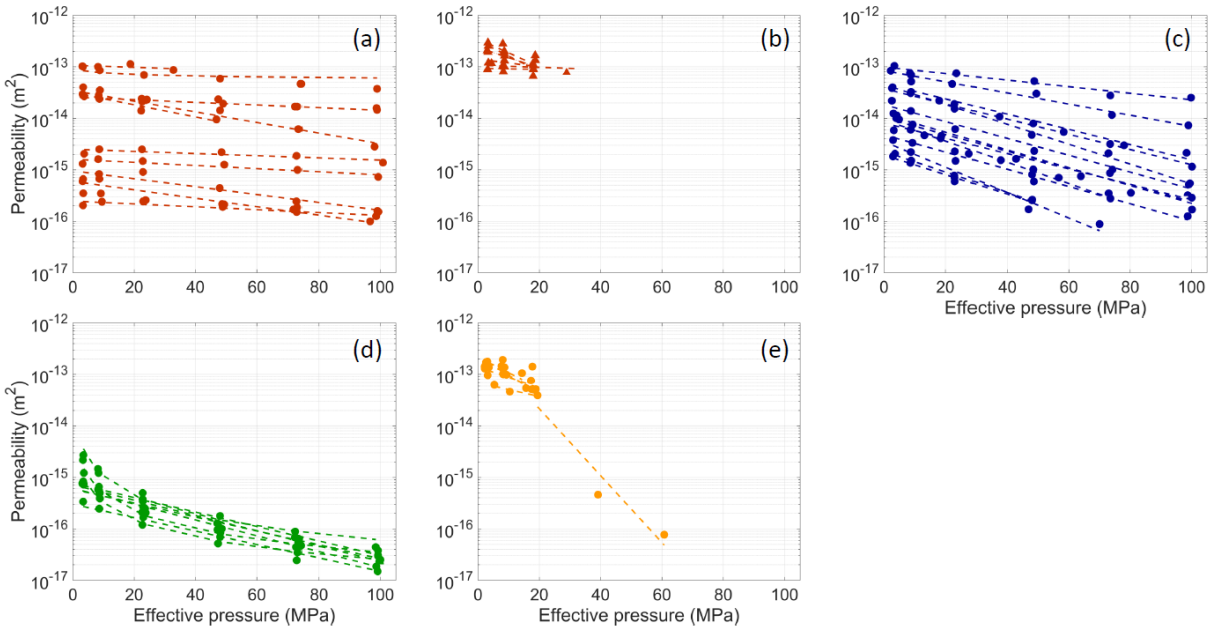

Figure 2.5: Intact rock permeability evolution with effective pressure of (a) dense basalt (10 samples tested), (b) porous basalt (6 samples), (c) felsite (14 samples tested), (d) gabbro (10 samples tested), and (e) hyaloclastite (8 samples tested). The general nonlinear decrease in permeability with effective pressure is attributed to the compaction and closure of micro-fractures as observed by the porosity volume decrease in figure 2.4.

2.3.3 Impact of pressure fluctuations

During a well operation, changes in pore pressure are inevitable, from injection during drilling to functional operation at different pressures. These changes can be considered minor, but their resulting influence on the rock permeability remains poorly tested. Here, we investigate the impact on the permeability of pressurising and depressurising highly fractured felsite samples. When decreasing the pore pressure applied to a sample (at a set confinement), we note a slight increase in the rock porosity and permeability (Figure 2.6a); yet, not as significant as the magnitude of porosity and permeability decrease monitored during pressurisation. Thus, pressurisation and depressurisation of porous rocks leads to hysteresis of its permeable structure on the timescales investigated here.

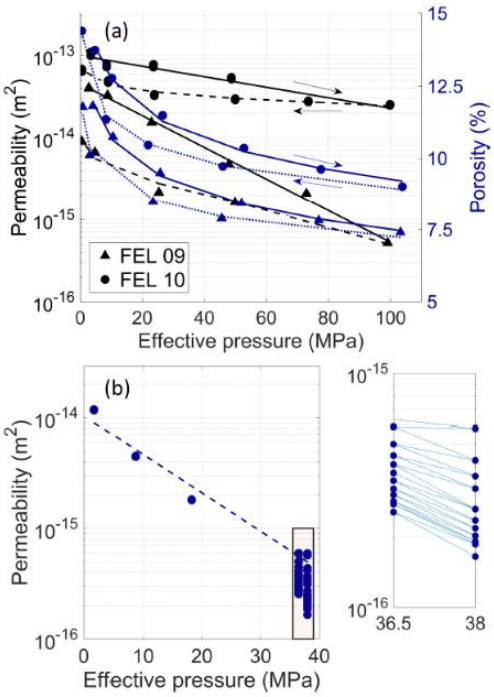

Figure 2.6: Effect of permeability due to changes in effective pressure. Variations of: (a) Permeability and porosity of felsite resulting from pore pressure (and thus effective pressure) loading/ unloading cycles to 100 MPa. The figure shows a degree of hysteresis; as effective pressure is decreased the sample does not recover the initial (i.e. lower pressure) permeability and porosity of the rock. (b) Permeability evolution of felsite during pore pressure (hence, effective pressure) oscillations of 1.5 MPa. The data (zoomed-in inset in b) shows that each unloading cycle never fully recovers permeability efficiency, and the permeability lowers further with each loading cycle due to further closure of permeable pathways.

The hysteresis of a rock porous structure to pressure fluctuations were investigated further by testing the impact of 10 pressurisation/ depressurisation cycles on the felsite by first pressurising the sample to the target confining pressure of 38 MPa (left for 30 min to equilibrate each time the pressure was changed), and fluctuating the pore pressure by 1.5 MPa (Figure 2.6b). Interestingly, we note that each pressurisation cycle decreases the permeability of the rocks, which never fully recover during depressurisation (Figure 2.6b). The impact is most pronounced in the first few cycles but persists throughout all 10 cycles.

2.3.4 Impact of thermal stimulation

During well drilling and operation, the reservoir temperature fluctuates. To test the effect of temperature changes, we subjected felsite and basalt to thermal stress cycles by cooling from 450 °C to ambient temperature by cooling in a furnace (under controlled conditions), in air (on a benchtop) as well as in water (at ambient temperature, to quench). The data shows that the porosity and permeability of the felsite was not affected by thermal stressing, even after fifteen heating/cooling cycles (Table 2.1; Figure 2.7). On the other hand, the porosity of the basalt was relatively unchanged (Table 2.1), while the permeability of the basalt increased by over one order of magnitude after the first five cycles; the most drastic impact being imposed by quenching in water (Figure 2.7).

Table 2.1 Porosity of volcanic rocks subjected to thermal stressing cycles.

	Porosity (%)			
Number of cycles	**0**	**1**	**5**	**15**
FEL_TRI_29	10.3	10.5	10.3	10.5
FEL_TRI_23	9.4	9.3	9.4	9.3
FEL_PP_02	9.8	9.8	9.9	9.9
BAS_TRI_43	11.5	11.5	11.4	11.4
BAS_TRI_51	12.1	12.2	12.1	12.0
BAS_TRI_63	10.9	11.1	10.9	11.1

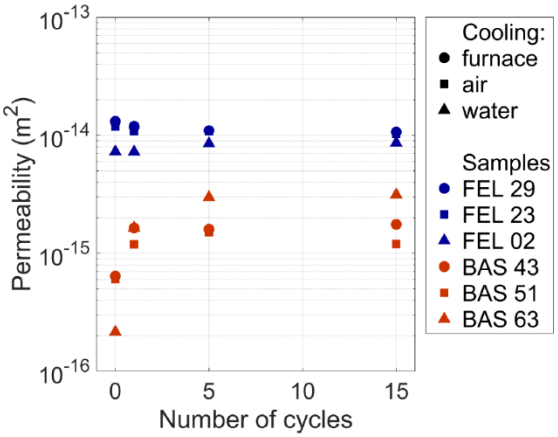

Figure 2.7: Influence of thermal stressing (up to 450 ˚C) cycles on the permeability of basalt (BAS) and felsite (FEL) cooled under different conditions. The data show that the permeability of the felsite is insensitive to thermal fluctuations, presumably as the original sample contains multiple micro-fractures (see figure 2.2). In contrast, the permeability of the basalt nonlinearly increases with thermal cycles (especially the first five cycles). We note that permeability is highest in samples cooled by water (triangles), compared to cooling in ambient air or under controlled conditions in the furnace (i.e. at <5 ˚C.min^{-1}).

2.3.5 Impact of one macro-fracture

The effect of a macro-fracture on the permeability of a sample has been the focus of recent studies (Heap and Kennedy, 2016; Lamur et al., 2017; Nara et al., 2011); here we expand this dataset by testing the impact of macro-fractures on several lithologies. Of the lithologies tested here, the hyaloclastite did not withstand a fracture, but rather compacted during Brazilian tensile testing, and therefore the permeability of fractured hyaloclastite could not be measured. Similarly, of the felsite cores tested, only a few developed clean fractures during mechanical testing, therefore reducing the number of fractured samples measured for permeability. The basaltic dyke was not subjected to this testing method (as we had insufficient material).

For the dense basalt and felsite, for which intact samples showed a wide range of permeabilities, the presence of a fracture narrowed the range of permeabilities to relatively high values (Figure 2.8a, c). In contrast, the permeability of the porous basalt was not affected by the addition of a macro-fracture (Figure 2.8b). For all other samples, imparting a fracture increased permeability by as much as 2-5 orders of magnitude (Figure 2.8d-f).

Effective pressure showed variable influences on the permeability (Figure 2.5) of these macro-fractured rocks; yet, permeability decrease was generally greatest in the early stages of confinement, and for most samples led to a nonlinear decrease of 1-2 orders of magnitude of permeability (Figures 2.8 and 2.9). The sensitivity of permeability of fractured samples to confinement was heightened as compared to their intact counterparts (Figures 2.5 and 2.8). Within one lithology (basalt) however, the sensitivity to confinement was variable (Figure 2.9); yet, these macro-fractures are irregular, and bordered by minor fractures and fragments (Figure 2.10).

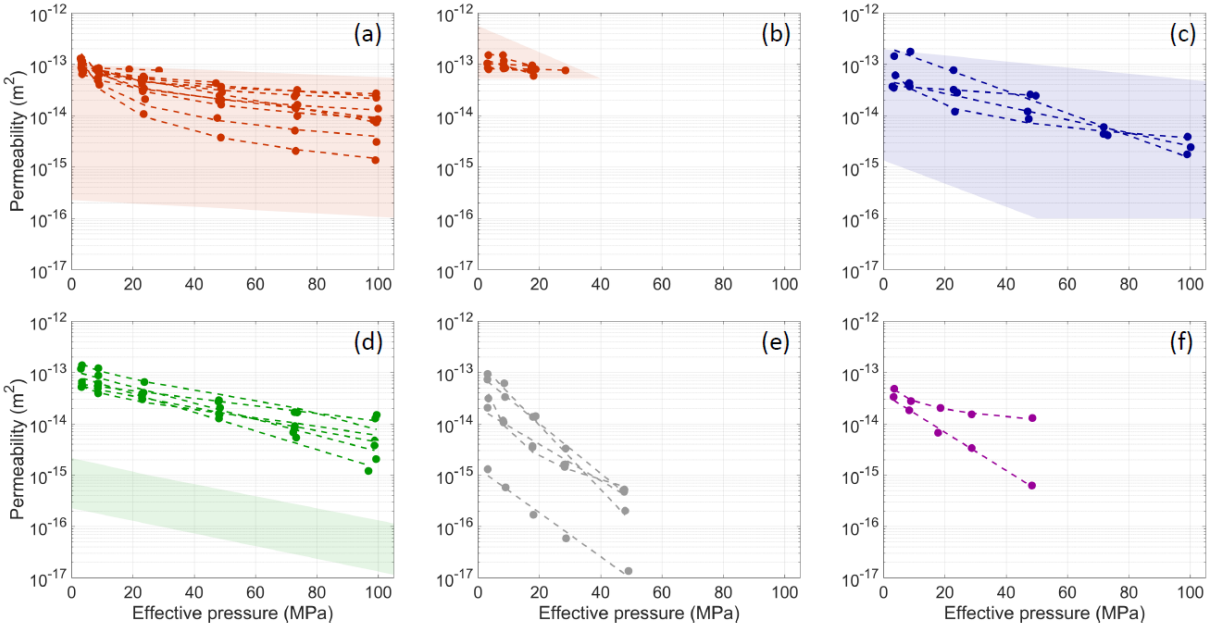

Figure 2.8: Permeability evolution with effective pressure of macro-fractured rocks (a) dense basalt (10 samples), (b) porous basalt (5 samples), (c) felsite (4 samples), (d) gabbro (6 samples tested), (e) Ignimbrite (5 samples), and (f) obsidian (2 samples). The shaded areas show the range of permeability of intact samples before they were fractured (from figure 2.5), showing the variable effect of fractures on permeability. Note that the permeability of the intact ignimbrite and obsidian was below the detection limit for our apparatus (which was developed for permeable samples).

2.3.6 Impact of two macro-fractures

The basalts, being a key rock type in Iceland and the most mechanically consistent rock of the lithologies at Krafla, were used to test the impact of two orthogonal macro-fractures on the permeable porous network, as they display a wide range of initial porosities and permeabilities. The tests were systematically conducted on six samples, ranging between 10.9 and 21.3 vol. % porosity.

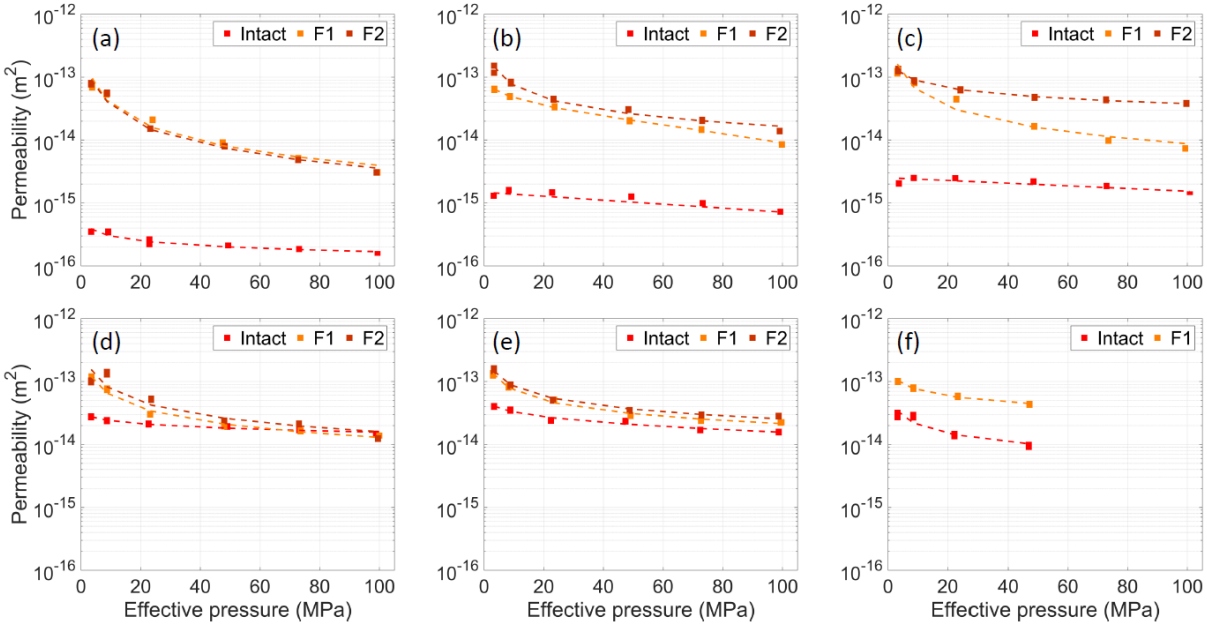

Figure 2.9: Permeability variations with effective pressure for intact and experimentally fractured samples , and the same samples with one fracture (F1) and two fractures (F2), imparted experimentally for basalts with a range of initial porosities from (a) 10.9 %, (b) 12.9 %, (c) 13.5 %, (d) 14.8 %, (e) 15.9 % to (f) 21.3 %. The data show a 0.5 to >2 order of magnitude increase in permeability due to fracturing, which is more significant at low porosity. Increasing effective pressure closes the fracture and the permeability nonlinearly decreases, trending towards that of the intact rock. This convergence is not always possible, presumably as in imperfect contact or dislodged fragments may obstruct fracture closure (See figure 2.10).

The generation of a second, orthogonal fracture increased the permeability of the rocks further for samples across the range of porosities tested. The most porous sample (Figure 2.9f) was unable to sustain the fracture and crumbled. The permeability increase induced by the second fracture was not as significant as the first fracture (Figures 2.8-9), despite creating more fracture surface area and increasing porosity. This observation remains valid over the range of effective pressures tested; the interesting exception to this is the sample with 13.5 % porosity, for which the second fracture seems not to close adequately with an increase in effective pressure, resulting in a permeability nearly an order of magnitude higher than the single-fractured sample at 100 MPa effective pressure. For all other samples with 1 or 2 fractures, upon confinement, the permeability trends towards that of the intact rock. This convergence is not always possible and appears less readily attainable in the lower porosity samples (Figure 2.9a-c), which have the lowest initial permeability values and for which the permeability is most affected by fracturing.

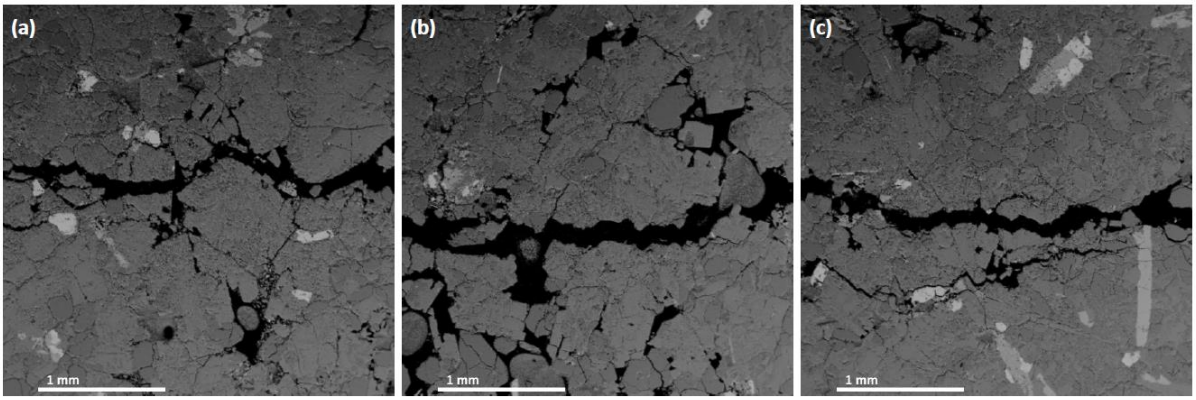

Figure 2.10: Backscattered electron (BSE) images (obtained by scanning electron microscope (SEM)) of fractures generated in the felsite (average 11.5 % porosity). The images show that failure was accommodated by a macro-fracture, hosting small rock fragments and bordered by fine, branching subparallel fractures, with slight variability within one lithology.

2.4 Discussion and implications

The findings presented here enhance our understanding of the impacts of thermal and mechanical stimulation practices. The data shows that pore pressure fluctuations at pressures lower than the local confining pressure may not be an effective way to increase the permeability of a reservoir; yet, we surmise that if this pore pressure variation takes place at pressures nearing or exceeding the local stress – a condition favouring tensile fracture propagation (see section 2.4.1), then the effect may be quite contrasting (e.g. Rozhko et al., 2007). Thermal stimulation demonstrated variable influence on the resultant permeable porous network. Here, we noted that rocks void of micro-fractures were more liable to thermal stressing than micro-fractured rocks. This may be because, when present in a rock, micro-fractures may simply open during cooling contraction of the solid phase, without building large tensile stresses; in contrast, crack-poor rocks would build up large tensile stresses during cooling contraction, which may result in cracking, and thus enhanced fluid flow. The observed change in permeability of about one order of magnitude is moderate compared to Siratovich et al. (2015a), which showed a permeability change by three orders of magnitude for the dense andesite of the Rotokawa geothermal field. Thus, the permeability of hydrothermal reservoirs may be subject to changes in the lifetime of fluid extraction if it results in temperature changes, especially if rapidly heating and cooling dense unfractured lithologies. Yet ultimately, it is the generation of fractures, whether microscopic or macroscopic in nature, which controls permeability in the reservoirs, and arguably when fractures are mechanically impeded from adequate closure that they present the most persistent fluid pathways.

2.4.1 On the permeability of intact and fractured volcanic rocks

Detailed knowledge of the storage capacity and permeability of reservoir rocks is crucial to improve the utilisation of geothermal resources and to maximise energy production. The experimental work carried out here sheds light on the efficiency of fluid flow through the permeable porous network in the Krafla geothermal reservoir. The reservoir consists of a succession of mafic lavas, ignimbrites and hyaloclastites at shallow depth (<1 km) and at greater depth (>1 km), of cross-cutting mafic, intermediate and felsic intrusions (Mortensen et al., 2015). All the rocks display a range of porosities and permeabilities, and correspondingly, differing responses to effective pressure. The rocks found at

shallow depths are highly variable: the basaltic rocks have a wide range of porosities and permeabilities, and the densest lithologies remain strong when pressurised (or, in natural terms, buried); whereas the porous basalt and hyaloclastite can only experience relatively low confinement without undergoing compaction (at P*). The intrusive rocks originating at depth were observed to be highly fractured, which led to high permeability (and higher dependence of permeability on effective pressure), despite their low porosities. The basaltic dyke however has low permeability, despite relatively high porosity (32-34 vol. % porosity; Figure 2.11), due to a predominantly isolated pore structure (Figure 2.2c). Within the reservoir, we expect that other dykes may be denser and less permeable.

When compiled together, the permeability of the intact rocks increases nonlinearly with porosity (Figure 2.11), as previously described (e.g. Ashwell et al., 2015; Brace, 1980; Eichelberger et al., 1986; Farquharson et al., 2015; Heap et al., 2014a; Heap and Kennedy, 2016; Heap et al., 2014c; Heap et al., 2016; Jouniaux et al., 2000; Kendrick et al., 2016; Kendrick et al., 2013b; Klug and Cashman, 1996; Kushnir et al., 2016; Lamur et al., 2017; Mueller et al., 2005; Okumura and Sasaki, 2014; Saar and Manga, 1999; Schaefer et al., 2015; Stimac et al., 2004). [It should be noted that previously published data collected at slightly different effective pressures (e.g. Tanikawa and Shimamoto, 2009) may increase scatter.] As permeability-porosity measurements of a variety of volcanic rocks accrue (e.g. Farquharson et al., 2015; Lamur et al., 2017; Mueller et al., 2005), a picture is rapidly emerging which depicts a wide range of permeabilities at all porosities (e.g., at ~10 % and ~35 % in figure 2.11); here, we advance that the absence of a petrogenetic link between rocks with different porosities and permeabilities (owing to distinct petrological and deformational histories) may preclude the necessity to invoke a change point dividing two permeability regimes – fracture- vs vesicle-controlled – (even if statistically determined by the current dataset) and that a simple power-law regression may be an equally adequate approximation to be used in simulations, until a genetic link is established.

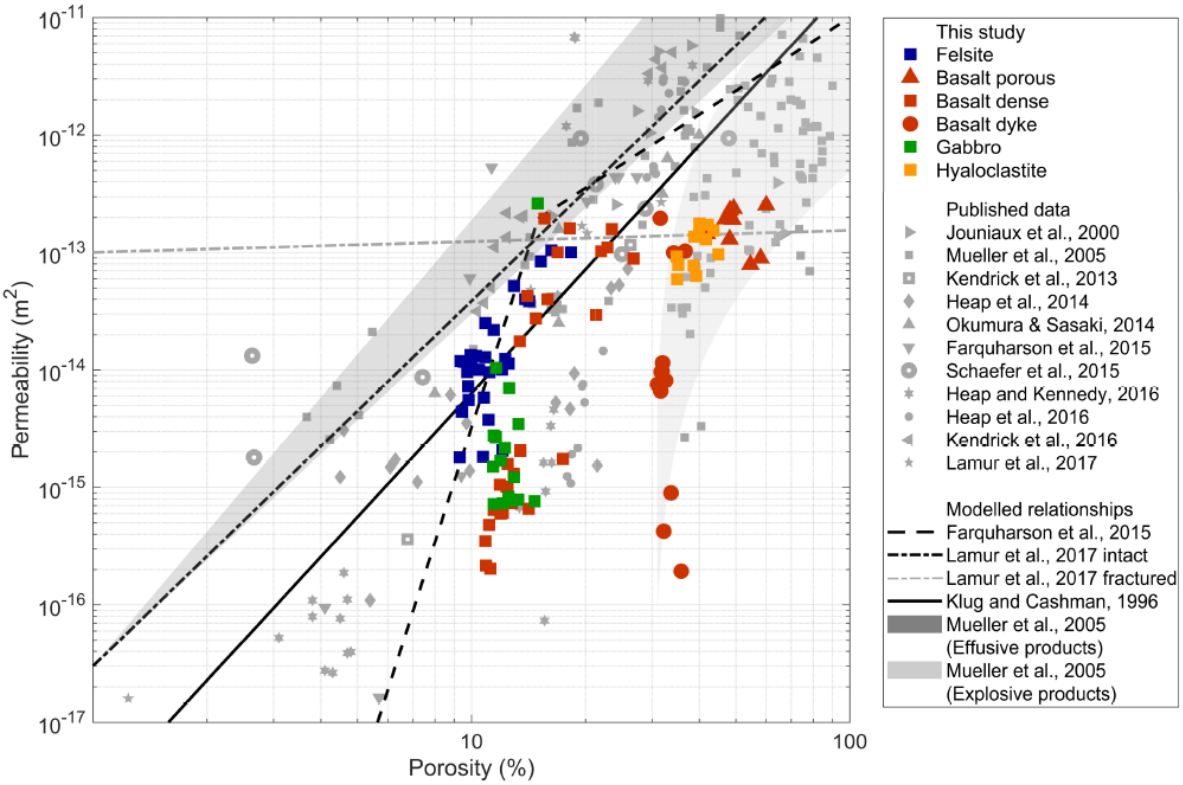

Figure 2.11: Permeability as a function of porosity, showing the extensive variability of the lithologies examined (Permeability measured at P_{eff}=3,75 MPa) . Data from this study correlate well with previously published data (measured at a range of effective pressures, which increases scatter further). Comparing the data to models to describe the porosity-permeability relationship, we note that the model for explosive products from Mueller et al. (2005) correlates very well with samples collected form a dyke. For the lower porosity samples, the model proposed by Farquharson et al., (2015) shows a better correlation than other models proposed, with a rapid increase in permeability over relatively narrow range of porosity, although above the inflection point the trend does not correlate well. Rather, it appears that the relationship for fractured rocks from Lamur et al. (2017) appropriately describes the upper limit of permeability observed here.

The addition of a macro-fracture increases the permeability of porous volcanic rocks. Recent experimental investigations (Heap and Kennedy, 2016; Lamur et al., 2017) have proposed models to constrain the impact of fractures on permeability as a function of effective pressure, demonstrating that in the presence of one fracture, the permeability-porosity relationship follows a power law dependence (Lamur et al., 2017); here, our dataset appears to abide to such a power-law relationship (Figure 2.12). The permeability-porosity relationship of fractured volcanics further appears to limit the permeability of all porous rocks (>15 vol. % porosity) present at Krafla (Figure 2.11).

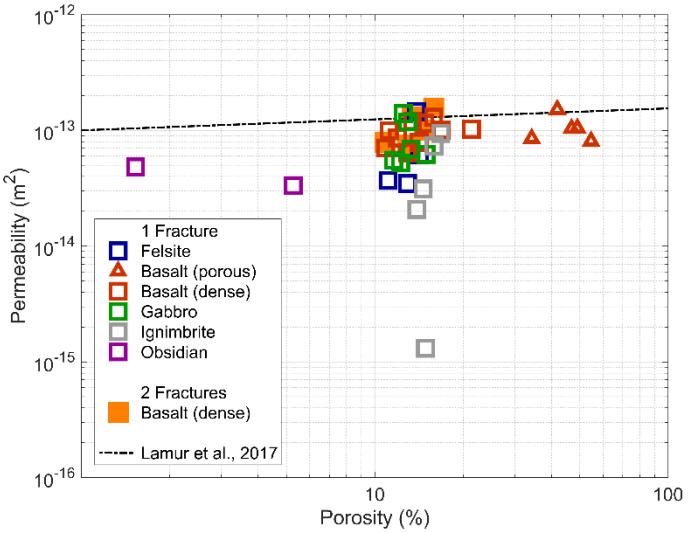

Figure 2.12: The connected porous networks of the fractured samples shows a very narrow variability of permeability across all lithologies , typically, less than 1 order of magnitude (P_{eff}=3.75 MPa) across a wide range of starting porosities. The data is compared to the relationship for fractured rock permeability described in Lamur et al. (2017) for the correct effective pressure. This relationship appropriately to describe the dataset with both 1 and 2 macro fractures, as well as appearing to describe the upper permeability limit of our intact samples (Figure 2.11).

The data presented here further suggest that the obstruction of fractures by particles locally fragmented and offset between fracture planes may prevent complete fracture closure (Figure 2.10). This influence is more likely as more fractures are introduced, and results in persistence of high permeability even at high effective pressures. Perez-Flores et al. (2017) showed that the effect of fracture offset on permeability varies between lithologies, but at a certain offset length, the effect on permeability reached a maximum, which for fresh basalt, was around two orders of magnitude of permeability. With time, offset fractures also withhold a higher permeability, by keeping the fracture network open even if pressure changes (Hofmann et al., 2016), as we observe. Fracture closure and fracture network response to changes in effective pressure have also been shown to be controlled by the mechanical properties of a rocktype, as stronger rocks may prevent efficient fracture closure, whereas weak rocks may deform and shut fractures (Milsch et al., 2016). Slurries containing sand particles with the purpose of obstructing fracture closure have been used to optimise reservoir permeability and fluid extraction (Brinton et al., 2011), and our findings corroborate these practices. We further suggest that strategic thermo-mechanical stressing to impart fractures which orthogonally intersect local or regional fractures may be an equally efficient way to increase the permeability of a reservoir and thus, its resultant energy output. The outcome of this practice may likely be enhanced if the fracture produced is strategically aligned at low angles to the principal stress (in an anisotropic stress field) to favour slight displacement/ misalignment of the fracture interfaces, which may leave gaps in the rock to permit extensive fluid flow. This effect may be central to the efficiency of thermo-mechanically derived fractures as pathways to increase connectivity in the reservoir.

2.4.2 Permeability of the Krafla hydrothermal reservoir

Today at Krafla, geothermal energy production focuses on fluid extraction at shallow depth up to about 2-3 km (Mortensen et al., 2015); yet, deeper fluid extraction is often contemplated in our pursuit of higher energy production (Fridleifsson et al., 2014). In doing so, efforts must be made to avoid intersecting the shallow magma reservoir located at a depth of 2.1 km (Elders et al., 2014b). Geochemical investigation of the glass fragments recovered during drilling into the magma reservoir suggests that volatile concentration is in equilibrium with a temperature of 800-950 ˚C (Axelsson et al., 2014; Elders et al., 2011) and a pressure of 30-50 MPa (Elders et al., 2011). At Krafla, a depth of 2.1 km corresponds to a lithostatic pressure of approximately 65 MPa, if we assume a rock density of 3,100 kg/m^3 for the predominantly basaltic chemistry of these volcanics; thus, the discrepancy between the estimated equilibrium and the approximation of the lithostatic load suggests that fluid connectivity in the hydrothermal system may be efficiently decrease local magmatic pressure to below lithostatic. Thus, we can assume that at any given depth in the Krafla hydrothermal reservoir, the effective pressure can be approximated by subtracting the hydrostatic pressure (i.e. the pore pressure in our experiments) from the lithostatic pressure (i.e. the confining pressure in our experiments). Therefore, a depth of 2-3 km may correspond to effective pressures of 40-50 MPa (in agreement with equilibrium conditions for the glass; (Elders et al., 2011). The study shows that the storage capacity and permeability of the reservoir rocks nonlinearly increases by decreasing the effective pressure exerted in the system, so fluid extraction may be optimised by ensuring high pressure of fluid injected into the hydrothermal system to keep fractures open as wide as permits (whilst remaining stable and not creating undesired hydraulic fractures).

During IDDP-1, drilling activities suffered from a loss in fluids shortly before intersecting the magma reservoir at 2.1 km (Palsson et al., 2014). This 50-m thick zone of fluid loss coincided with encountering felsite – a crystalline rock believed to represent the crystallised aureole that surrounds the magma reservoir (Mortensen et al., 2014). No large samples of felsite were retrieved by the drilling activities, but samples can be collected from the phreatomagmatic deposits that surround the Víti crater (Sæmundsson, 1991). In this study, we examined gabbro and felsite blocks from this phreatomagmatic event, and we found that both samples are highly micro-fractured (Figure 2.2d, e), which results in high permeability (and fracture compressibility with effective pressure). Phreatomagmatic eruptions are known to be highly explosive (Austin-Erickson et al., 2008) and we postulate that the high fracture density observed in the samples tested here is congruent with their eruption and with a damaged source region. Deep-seated fragmentation at depths of ca. 2.1 km, perhaps even due to emplacement of the rhyolitic magma, may thus be at the origin of this felsitic zone with high-fracture density that led to important fluid loss during IDDP-1. If such is the case, the high permeability of fractured magmatic aureoles – commonly believed not to have open fractures due to their propensity to flow and heal (e.g. Scott et al., 2015) – may be key in ensuring fluid connectivity between the Earth's surface and the magma reservoir. This permeable architecture may naturally prevent the accumulation of excess volatile concentration, dissolved in the magma, making it not particularly buoyant and hence unlikely to erupt during drilling operations.

The laboratory measurements performed on samples primarily collected from surficial outcrops at Krafla, offer a first order constraint on the storage capacity and permeability of the reservoir rock

present at Krafla volcano. Yet, much remains to be investigated to obtain a complete picture of fluid flow in this hydrothermal system: from complexity arising from the effects of high-temperatures (Kushnir et al., 2017; Violay et al., 2017) to the influence exerted by devolatilisation (e.g. Heap et al., 2013), dissolution (Gislason and Arnorsson, 1993), clogging by fine fragments (e.g. Farquharson et al., 2017; Kendrick et al., 2016) and secondary mineral precipitation (e.g. Curewitz and Karson, 1997). Such descriptions are the subject of ongoing work as part of the international IDDP and KMT projects.

2.5 Conclusions

This experimental study describes the permeability and storage capacity of the lithologies found within the Krafla reservoir. We find that each lithology exhibits a wide range of porosity and permeability; both of which are found to decrease nonlinearly with effective pressure – an effect which is more pronounced in samples with significant presence of fractures. We tested the influence of pressure oscillations, thermal stressing and fracturing on fluid flow in these rocks. We found that pressurisation/ depressurisation cycles leads to the progressive shutting of micro-fractures, which result in an overall permeability decrease of the rocks, though our experiments fluctuated pore pressure at values significantly lower than confinement, and we postulate that the effect may be reversed if pore pressure locally exceeded confining pressure. Thermal stimulation (especially when thermal shocks are caused by water) results in an increase of the permeability of rocks which are originally devoid of significant micro-fractures; however, fractured rocks remain largely unaffected by thermal stressing. Imparting a single macro-fracture increases the permeability of a rock at low effective pressure, but as confinement increases, the fracture begins to close and permeability trends towards that of the intact rock; imparting a second orthogonal fracture offers only a slightly higher increase in permeability of the rocks, but increases the possibility of offset along the fractures and thus the persistence of high permeability under confinement. Where the fracture was slightly offset, or where fine fragments lodged themselves in the fracture, obstruction from closure at high effective pressure resulted in high, relatively pressure-independent permeabilities. The data suggests that when thermo-mechanically stimulating a reservoir, efforts should be made to generate fractures orthogonal to primary local faults and fractures, or at low angle to principal stresses in order to increase gap opening at their intersections and favour fluid flow in the hydrothermal system. These findings support the use of proppants, such as non-reactive granular materials, to open fractures and ensure efficient fluid flow in production wells.

2.6 Acknowledgements

This study has been partially financed by research funds from Landsvirkjun National Power Company of Iceland as well as a scholarship from the Institute for Risk and Uncertainty at the University of Liverpool and the European Research Council Starting Grant on Strain Localisation in Magma (SLiM, no. 306488). We wish to thank Dr. M.J. Heap and an anonymous reviewer for constructive comments as well as A. Lamur for fruitful discussions.

Chapter 3:

Mechanical behaviour of geothermal reservoir rocks at Krafla, Iceland

Paper abstract

Knowledge of rock properties within reservoirs are important to predict their potential for production and assess the engineering concerns that might arise during exploitation. Well stimulation practices, tailored from a good knowledge of rock properties, are commonly employed to optimise production, especially from new wells. With the geothermal sector shifting its target towards reservoirs with higher temperatures and pressures to source supercritical fluids (e.g., the Iceland Deep Drilling Project, IDDP), knowledge of the rocks behaviour at conditions extant in such poorly explored environments becomes even more important. The first well of the Iceland Deep Drilling Project was drilled in 2009 within the Krafla caldera, located in North-East Iceland. The drilling had to be terminated at a depth of 2.1 km as the drill penetrated magma that could not be bypassed. The rocks above, however, showed great potentials for exploitation.

To better constrain the mechanical properties and thermal response of the Krafla reservoir rocks during cold water injection (during drilling and stimulation), six different rock types were sampled, based on knowledge off the main lithologies [three basalts: lava (10-27% porosity); a basalt dyke (31-34% porosity) and high porous lava (40-60 % porosity), hyaloclastite (35-45% porosity), obsidian (0.2-5% porosity), ignimbrite (13-18% porosity), intrusive felsite (10-16% porosity) and a micro-gabbro (10-16% porosity)]. The samples were loose blocks (therefore not orientated), collected from the surface or surface outcrops without hammering to prevent adding fracture damage. The porosity of all samples was measured using a helium pycnometer. The results of the mechanical tests [uniaxial compressive strength (UCS) test, triaxial compressive test and indirect tensile strength using the Brazilian disc method (unconfined tensile strength - UTS)] show that the rock strength is inversely proportional to the porosity and is strongly affected by the microstructure of each rock. With increased confinement, the rocks display different failure criteria and rocks with higher porosities (>15% vol. pores) displayed pore collapse at relatively low effective pressure, considering the pressure condition of the Krafla reservoir. The felsite, which displayed low UCS and UTS, however, showed more strengthening with confinement than expected as a result of substantial closure of an extensive network of opened micro-fractures, which interlock with confinement.

Investigation of the thermal behaviour of felsite and basalt shows a slight increase in thermal expansivity with rising temperature within both rocks. The felsite contains quartz, which can be seen as a peak in expansivity when it crosses the α-β transition at 573°C. Modelling the thermal stress induced by instantaneous temperature changes, using the measured expansion coefficient and rock properties, shows that the induced thermal stress increases with confinement (i.e. burial depth), as the rocks Young's modulus correspondingly increases with confinement. The findings give insight into the mechanical and thermal properties of the reservoir rocks and increase our understanding of their

behaviour within the geothermal reservoir, ultimately allowing for a better and safer exploitation strategy.

3.1 Introduction

Heat loss from the Earth's interior is most significant within volcanically active areas (e.g. Pollack et al., 1993). The associated geothermal energy within some of these systems has been harnessed by extracting hot groundwater for space heating or electricity production (e.g. Bodvarsson et al., 1984; Krupp and Seward, 1987). However, for the utilization to be economical, the natural fluid flow within the reservoir needs to be sufficient to maintain production (e.g. Darling and Armannsson, 1989). During the different phases of reservoir exploitation, such as drilling, stimulation, production and injection, a good knowledge of rock behaviour is required to improve reservoir management (e.g. Ghassemi, 2012; Gunnarsson, 2011). Inducing fractures, either mechanically (e.g. Legarth et al., 2005; McClure and Horne, 2014; Zimmermann et al., 2011) or thermally (e.g. Grant et al., 2013), can increase permeability (e.g. Eggertsson et al., 2018b; Heap and Kennedy, 2016; Kushnir et al., 2018; Lamur et al., 2017) and cause circulation loss during drilling (e.g. Lamur et al., 2017; Mortensen et al., 2014) and increase subsequent fluid extraction (e.g. Grant et al., 2013; Siratovich et al., 2015a; Stefánsson et al., 1982). However, a reduction in reservoir fluid pressure (e.g., due to extensive extraction) increases the effective pressure acting on the fractured rocks (where effective pressures = confining pressure – pore pressure), leading to compaction and fracture closure, which can decrease permeability (Eggertsson et al., 2018b). Conversely an increase in reservoir fluid pressure (e.g., due to injection), can induce seismicity (e.g. Gunnarsson, 2011; Zang et al., 2014), fracture widening and associated permeability increase (e.g. Eggertsson et al., 2018b; Lamur et al., 2017). Thus, a good knowledge of rock properties is required to understand the impact of geothermal exploitation on the system's response.

Thermal stimulation procedures are common in high temperature reservoirs (>230°C; e.g. Sanyal, 2005) as thermal gradients capable of fracturing the host rocks can be achieved through the introduction of cold fluids (e.g. David et al., 1999; Stefánsson et al., 1982). This method is easy and cost-effective after drilling activities are complete (Stefánsson et al., 1982). The impact imposed by the presence of fractures on the permeability of rocks can be significant (e.g. Eggertsson et al., 2018b; Heap and Kennedy, 2016; Lamur et al., 2017). In very high-temperature regions of hydrothermal reservoirs (e.g., >450 °C), such as those increasingly sought out for high-enthalpy fluids, the rock can exhibit pseudo-plastic behaviour (e.g. Violay et al., 2012) such that it is commonly assumed that fractures will not remain effectively open for long periods of time (e.g. Scott et al., 2015). To overcome this, the rock may be kept fragmental if stress is sufficiently high (e.g. Lavallée et al., 2013a) or the temperature kept low enough to slow diffusion (preventing fracture healing; e.g. Lamur et al., 2019) and ensure a dominantly brittle response (e.g. Tomac and Gutierrez, 2017; Violay et al., 2012). Four primary factors have been suggested to contribute to fracture formation during thermal stimulation: 1) a difference in thermal expansion of rock-forming minerals (e.g. Browning et al., 2016; Siratovich et al., 2015a); 2) development of a strong temperature gradient; 3) bursting of fluid inclusions (e.g. Lin, 2002); and 4) mineral decomposition and devolatilization (e.g. Cooper and Simmons, 1977; Heap et al., 2012; Simmons and Cooper, 1978). The volumetric change associated with heating or cooling has not been shown to correlate with the degree of fracturing, but the cracks generated may provide needed

space for mineral precipitation (Cooper and Simmons, 1977). At elevated effective pressures within the reservoir, thermal expansion may, however, be counteracted by the natural boundary conditions, as fractures close under elevated pressures (e.g. Eggertsson et al., 2018b; Lamur, 2018), therefore potentially limiting the impact of thermal stimulation (e.g. Siratovich et al., 2015b).

Laboratory experiments designed to measure and investigate rock mass properties have long been performed, with empirical tools to bridge the gap between the lab scale experiments and the borehole or even reservoir scale, such as the Hoek-Brown failure criterion (Hoek et al., 2002). To constrain the instantaneous thermoelastic stress change associated with heating or cooling of a rock mass, the equation by Timonsheno and Goodier (1970) is commonly used:

$$\sigma_t = \frac{\alpha E \Delta T}{(1-\nu)} \tag{3.1}$$

which relates the development of induced tensile stress σ_t to the ratio between the product of the thermal expansion coefficient α, the Young's modulus E, the temperature change ΔT, and the difference between 1 and the Poisson's ratio ν. For eq. 3.1 to be valid, the assumption is made that the plane that experiences temperature change is initially in thermal equilibrium and no external stresses are acting on it, therefore all stress change experienced is tensile. The rocks in a reservoir are loaded by their overburden, therefore the assumption that cooling will solely induce tensile stresses is incorrect, as it may simply serve to lower the principal stresses (Zoback, 2010). Therefore, any consideration of rock state and whether it may rupture during thermal stimulation must combine knowledge of principle stress magnitudes along with a detailed account of stress change profile associated with temperature changes.

The thermo-mechanical response of reservoir rock to changes in temperature and pressure is central to the drilling and subsequent utilization of wells. During drilling, cold mud or water is usually used to clear out any cuttings and other material within the well; as a result, the rocks proximal to the well cool and accumulate stress. The thermo-mechanical response of rock strongly depends on its constituents. Within the field of rock mechanics, efforts have focused on civil engineering and mining problems, which have led to a thorough description of sedimentary rocks (e.g. Alam et al., 2014; Baud et al., 2000; Benson et al., 2005; Bourbie and Zinszner, 1985; Gueguen and Fortin, 2013; Ju et al., 2013; Wu et al., 2000) as well as intrusive igneous rocks (e.g. Alam et al., 2014; David et al., 1999; Keshavarz et al., 2010; Lim et al., 2012; Takarli et al., 2008). These include the characterization of rock behaviour under different conditions, such as variable stress fields (e.g. Fialko and Rubin, 1997; Gruber, 2018; Hashida and Takahashi, 1993; Heap et al., 2015b; Lamur, 2018; Li and Wong, 2013) confining pressures (e.g. Heap et al., 2011), temperatures (e.g. Heard, 1960; Vishal et al., 2011) and water saturation (e.g. Bauer et al., 1981). The mechanical properties derived from laboratory testing have further been related to the minerology and microstructure of rocks (e.g. Heap et al., 2014d; Heap et al., 2016; Kendrick et al., 2012; Siratovich et al., 2016; Siratovich et al., 2015a). Volcanic rocks, with their wildly variable range of constituents (i.e., variable crystallinities, porosities, glass content, and degrees of coherence), and thus physical, mechanical, chemical and rheological properties, have only recently become the focus of studies (e.g. Baud et al., 2014; Bubeck et al., 2017; Coats et al., 2018; Fakhimi and Gharahbagh, 2011; Griffiths et al., 2017; Heap et al., 2011; Heap et al., 2015a; Heap et al., 2015b; Kendrick et al., 2013a; Schaefer et al., 2015; Schöpfer et al., 2009; Siratovich et al., 2016). The

understanding of their thermo-mechanical response is incomplete owing to their complex heterogeneous nature.

In this study, a new experimental dataset for the mechanical properties of the different lithologies found within the hydrothermal reservoir of Krafla volcano is presented, with the aim to 1) investigate the strength of the different lithologies; 2) constraint if and when the lithologies behave in a brittle or ductile manner; 3) measure the thermal expansion coefficient of felsite and basalt. The mechanical and thermal properties obtained are then used to model the induced thermal stress for rocks subjected to cold fluids during drilling and thermal stimulation, and to inform future geothermal activities at Krafla.

3.1.1 Geological setting

The Krafla hydrothermal system is situated within the partly-filled caldera of Krafla volcano, which last erupted in 1975-1984 in what is known as the Krafla fires (Einarsson, 1991). The caldera is about 8 km x 10 km in diameter (Sæmundsson, 1991) with a 90-km long fissure swarm trending in a 5°-15° NNE orientation (Hjartardottir et al., 2012). The active hydrothermal system is thought to extend over an area of about 10 km^2, located in the southeast part of the caldera (Sæmundsson, 1991). Observations of surface geology and drilling products (cuttings and cores) have provided extensive knowledge of the rocks and structures within the reservoir. The uppermost 1.3 km of the reservoir, in which temperature is about 100-300 °C, is primarily made up of basaltic lavas and hyaloclastite sequences, with welded ignimbrite and rhyolitic obsidian contributing to a lesser extent. Below 1.3 km depth, where temperature is higher, the reservoir is made up of intrusive igneous rocks, such as gabbro and felsite (Bodvarsson et al., 1984; Mortensen et al., 2014; Mortensen et al., 2015; Sæmundsson, 1991).

Shortly after beginning of the construction of the geothermal power plant in 1975, the Krafla fires started, which, due to repeated magmatic intrusions into the roots of the hydrothermal system, had a long-lasting impact on the chemical composition of fluids within the reservoir (Guðmundsson, 2001; Ármannsson, 1989). The aim was to construct a power plant, consisting of two 30MW_e turbines, but due to the problems following the eruption, the power plant only used one turbine until 1999, when the second one was put in operation to reach 60 MW_e production target (Guðmundsson, 2001).

In 2009, Krafla was chosen to be the site for the first well of the Iceland Deep Drilling Project (IDDP-1). The aim of IDDP project is to source deep, high-enthalpy, supercritical geothermal fluids at a depth of 4-5 km (Fridleifsson et al., 2014). In their attempt at Krafla, IDDP unintentionally penetrated a rhyolitic magma body at a depth of 2.1 km (Elders et al., 2014b). This led to important challenges; in particular, drilling in superhot, near-magmatic rocks resulted in complete loss of fluid circulation (subsicuently no cuttings were retrieved), likely resulting from extensive thermal cracking induced by the strong undercooling of the system (Lamur et al., 2018). Yet, despite this challenge and despite falling short of tapping in supercritical fluids, the well was allowed to flow, revealing the World's hottest producing geothermal well sourcing dry superheated steam from near-magmatic conditions, with temperature exceeding 450 °C, high pressures of 40–140 bar (Elders et al., 2014b), and 5-10x higher power output compared to conventional wells (Ingason et al., 2014). Due to the corrosive nature of these fluids, the equipment and casings were damaged, and the well was plugged and abandoned (Elders et al., 2014b). The retrieval of near-magmatic cuttings further helped to constrain the pressure (Elders et al., 2011)

and temperature (Axelsson et al., 2014; Elders et al., 2011) conditions in the magmatic body. Volatile concentrations measured in glass shards recovered during drilling were used to define a pressure of 30-50 MPa (Zierenberg et al., 2013), which is lower than that expected from lithostatic pressure (ca. 50-60 MPa; considering a depth of 2.1 km and assuming a range of rock densities between 2.5-3.0 ton.m^{-3}) but above hydrostatic pressure for this depth (Elders et al., 2011). This pressure discrepancy suggests that the conditions of the magma may be partially influenced by the hydrothermal system owing to a well-connected permeable network (e.g. Fournier, 1999). In addition, drilling through the rock-magma interface revealed abrupt temperature changes from ~450 to 850 °C over a distance of 30 m, corresponding to a steep thermal gradient of 15 °C.m^{-1} (Eichelberger et al., 2018). If such hot rocks are to become the focus of higher energy extraction practices, it is imperative that we seek to better constrain their thermo-mechanical properties.

3.2 Materials and methodology

3.2.1 Material

At Krafla, six main lithologies have been identified within the reservoir of the active hydrothermal systems, based on investigations of surface mapping and examination of drilling products (Mortensen et al., 2014; Mortensen et al., 2015). In this study, samples from the surface were collected from blocks in outcrops that were later cored for samples; these include three basalts (lava with 10-27 % porosity, a basalt dyke with 31-34% porosity and highly porous lava with 40-60 % porosity), a hyaloclastite (35-45% porosity), an obsidian (0.2-5% porosity), an ignimbrite (13-18% porosity), an intrusive felsite (10-16% porosity) and a micro-gabbro (10-16% porosity). The felsite and micro-gabbro clasts are found as scattered ejecta at the surface as they were entrained from depth and erupted explosively at Víti crater at the start of the Mývatn fires in 1724 (Sæmundsson, 1991). The other blocks were collected from surface exposures without hammering, to ensure tests are carried out on representative rocks.

3.2.1.1 Microstructural analysis

The samples used show a wide range of microstructure, and porosity variability. Their properties, in relation to their effect on the permeability has previously been discussed and described in Eggertsson et al. (2018b; chapter 2 of this thesis). For this study, a representative thin section was prepared from all lithologies, with fluorescent dyed epoxy. The backscatter electronic (BSE) images were acquired using a Philips XL 30 tungsten filament scanning electronic microscope (SEM).

3.2.2 Experimental methods

This study aims to describe the uniaxial compressive strength (UCS), the Young's modulus (E), and the unconfined tensile strength (UTS) of the main lithologies at Krafla; we further investigated the compressive strength of the basalts and felsite under confinement, the thermal expansion coefficients (α) of the basalt and the felsite. All measurements were conducted in the Experimental Volcanology and Geothermal Research laboratory at the University of Liverpool.

3.2.2.1 Sample preparation

To perform these measurements, three types of cores were prepared. First, to measure the compressive strength (uniaxially and triaxially), of 170 cylindrical cores with a diameter of 25-26 mm and length of 50-52 mm (i.e., an aspect ratio of 2:1) were made. Secondly, 250 discs with a diameter

of 25-26 mm and thickness of 12-13 mm (i.e., an aspect ratio of 1:2) were made to measure the rock tensile strength using the Brazilian testing method. Finally, small cylindric samples with a diameter of 6.0 mm and a length of 5.0 mm were prepared to determine the thermal expansivity of the basalt and felsite. After preparation, all sample cores were stored overnight in a drying oven at 75°C, before being left to cool in a desiccator before testing.

Once cooled, the connected porosity of the cores for UCS, triaxial and UTS tests was measured using an AccuPyc 1340 helium pycnometer from Micromeritics. The device requires input of the sample weight and measures the skeletal volume of the sample (i.e., the solid including the isolated pores within it) to calculate the density. For the largest samples used in UCS and triaxial tests, a chamber of 100 cm^3 was utilised, whereas a chamber of 35 cm^3 was used for the smaller samples for UTS measurements. The accuracy for the sample volume determination and density determination is ±0.1%. Comparing the cores' geometric volume (V_c) with the skeletal volume (V_s), we can calculate the samples connected porosity via $(V_c-V_s)/V_c$.

3.2.2.2 Unconfined tensile strength

The UTS tests were performed in a 5969 Instron uniaxial press equipped with a 50 kN static load cell (with a resolution of 50 N) and an actuator (testing range of 0.001-600 $mm.min^{-1}$). Prior to testing, the pistons of the press were loaded against one another to a maximum load of 50 kN, whilst monitoring the displacement associated with the compliance of the machine; the load compliance was later subtracted from the mechanical data obtained for the various rock to accurately constrain the rock properties (see Gruber, 2018). To determine the tensile strength of the rocks, the Brazilian testing method was employed (e.g. Griffith, 1920; Hornby et al., 2019; Li and Wong, 2013), in which cores were placed sideways between the pistons of the press and loaded diametrically at a displacement rate of 3 $\mu m.s^{-1}$ until failure, which was accompanied by a stress drop.

3.2.2.3 Uniaxial compressive strength

The UCS tests were performed using an 8800 Instron uniaxial press equipped with a 100 kN load cell (with a resolution of 100 N) and an actuator (testing range of 0.001-600 $mm.min^{-1}$) (see Coats et al., 2018 for detail of the apparatus). Here again, compliance tests were performed (up to 100 kN) in order to correct for machine compliance during the rock measurements. Cylindrical samples were placed upright between the pistons of the press and axially loaded at a strain rate of 10-5 s^{-1}, until failure, which was accompanied by a stress drop. For 60 tests, the Young's modulus was calculated from the measured stress-strain curves.

3.2.2.4 Triaxial press

The compressive rock strength, under confinement, was tested for three basalt rocks, grouped based on their porosities (with 11.0-15.0%, 19.5-22.0%, and 46.5-48.5% porosity groups) and one felsite (with 9.9-10.1% porosity). The experiments were performed using a TRX100-300 triaxial press developed by Sanchez technologies. The apparatus controls the experimental conditions (up to 300 MPa of axial load and 100 MPa of pore pressure and confinement) using four Stigma 300 pumps and various fluids: the radial confinement was applied using pumped argon, the axial deformation was controlled using oil in another pump along with a 1.5 kbar gas booster (pressure ratio of 1:150) from Maximator, whilst the

pore pressure was controlled by two pumps using water as a medium. The Stigma 300 pumps have a volume of 300 cm^3 capable of applying flow rates of 110 $cm^3.min^{-1}$, with a resolution of 0.0001 mm^3 and a volume determination accuracy of 0.1%, and a volume control accuracy of 0.1% of the set flow rate; the pumps operate up to 1 kbar with a resolution of 1 mbar, a pressure determination accuracy of 0.1%, and a pressure control accuracy of 0.02%. In these tests a core specimen was loaded upright in the middle of a sample assembly made up of alumina cylindrical spacers of 25 mm diameters, (see Fig. 3.1), centrally drilled with a 3 mm diameter hole to let pore fluid through, all of which was jacketed in a Viton sleeve. Prior to testing on rock samples, the machine compliance was constrained by loading a sample assembly containing a sample of steel (for which the elastic properties had been accurately constrained *a priori*) to 300 MPa. Subtracting the steel predicted deformation during loading, we were able to quantify the machine compliance as a function of applied axial stress. To test rock samples, a core was placed in the sample assembly and inserted in the press. A small amount of confining pressure was then applied (2 MPa), whilst water was supplied to the sample assembly to set the pore pressure at 1 MPa, after which the assembly was allowed to wait until the pumps saw no more volume change (all volume within the samples had been pressurised to 1 MPa). Then, the confining pressure (Pc) was increased to a desired testing value (5-30 MPa), whilst axially loading the core by an additional 2 MPa (i.e., higher than confinement), to ensure the confinement does not force the pistons to recede, causing slack in the assembly; during this phase, the samples compacted slightly (as cracks closed; e.g. Wong and Baud, 2012) and we monitored the volume of water expelled due to this compaction. Together, the confining pressure and the pore pressure ensured we achieved effective pressures of 5-30 MPa, as experienced within the Krafla geothermal system. Axial deformation was finally applied at a strain rate of 10^{-5} s^{-1}, whilst monitoring the resultant load through time. The test was ended upon the substantial stress drop associated with sample rupture, after which the Young's modulus was calculated for all samples.

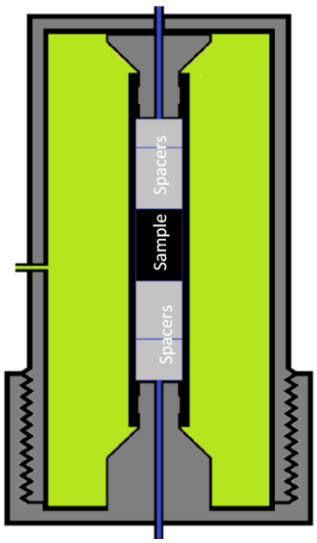

Figure 3.1: Schematic figure of the pressure vessel of the Sanchez triaxial press and the sample assembly. The volume change occurring within the sample is recorded by monitoring the volume change within the water pump, whilst keeping 1 MPa pore pressure within the sample. Once the sample is compressed and compacted, water is moved from the sample and into the pump. Axial load is applied to the assembly and always kept at a pressure of 2 MPa higher than the confining pressure, applied by argon.

3.2.2.5 Thermal analysis

The thermal expansion coefficient (α) was measured using a Netzsch TMA 402 F1 Hyperion Thermomechanical Analyser (TMA; see Coats et al., 2018; Siratovich et al., 2015b for detail about apparatus). In these tests, small cylindrical samples (6 x 5 mm) were axially loaded between two pistons encased in a furnace. The sample was set to heat at 5 °C.min^{-1} to 850 °C and cooled at the same rate whilst applying a constant load of 1.0000 N (equivalent to 11.6 MPa) and monitoring length change at an accuracy of ±0.125 nm. The expansion coefficient (α) was calculated as the ratio of length change (dL) over the sample length (L), divided by the temperature change (dT) experienced following $\alpha = dL/LdT$.

3.3 Results

3.3.1 Microstructural description of rock samples

Microstructure examination was made to distinguish and set apart any pre-existing anisotropy within the different lithologies. The different basalts demonstrate a wide range of porosities and representative samples were chosen due to their contrasting properties. The dense microcrystalline basalt lava, with 11% porosity (Fig. 3.2a), contains irregular shaped vesicles, with mostly small vesicles but few up to 1 mm in diameter and they are found to be unevenly distributed throughout the sample. The basalt dyke (Fig. 3.2b), withholding 33% porosity, exhibits a very evenly distributed network of sub rounded micro-vesicle, ranging in size from 100-400 µm. The microcrystalline basalt, withholding a porosity of 45% (Fig. 3.2c), contains large irregular vesicles (<2 mm) somewhat evenly distributed throughout the rock. Within the basalts, no microfractures were visible at this scale (Fig. 3.2a-c).

The felsite, containing 11.5% porosity (Fig. 3.2d), with a very dense network of micro-fractures at different size, up to 20 µm wide and irregular shaped vesicles (100-500 µm). No preferable orientation is observed within the micro-fracture network. The gabbro, with 12% porosity (Fig. 3.2e), has fewer microfractures (up to 20 µm in size), compared to the felsite, and they display no preferred orientation. The vesicles are irregularly shaped throughout the groundmass (100-500 µm in size). The hyaloclastite, containing a porosity of 35% (Fig. 3.2f), which is both made up of irregular shaped pores, between fragmental angular glass and crystalline matrix, where microfractures are observed to be both between fragments and through them, up to 20 µm in size. The ignimbrite contains 15% porosity (Fig. 3.2g), where no microfractures were visible at this scale. The pores are irregularly shaped and are usually smaller than 2 mm in diameter, but few larger once were observed. The obsidian contained very low porosity (< 1% porosity; Fig. 3.2h), where small vesicles (<100 µm) and one microfracture (5 µm) was observed.

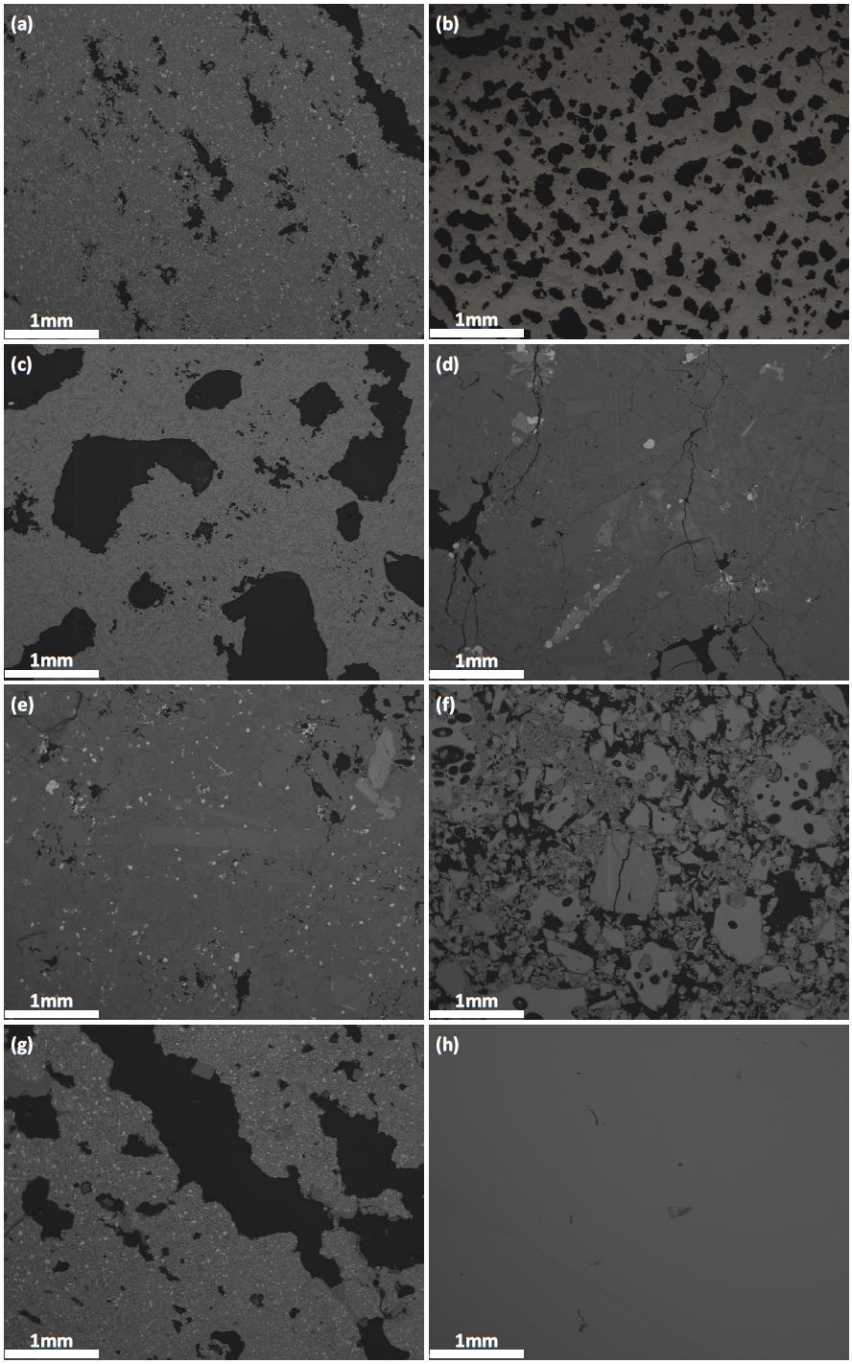

Figure 3.2: Backscattered electron (BSE) images of the six different rock types sampled from Krafla (obtained by scanning electron microscope (SEM)). (a) Microcrystalline basalt with 11% porosity with mostly small vesicles (<1 mm) and no visible microfractures in this scale. (b) Basaltic dyke sample with 33% porosity, predominantly made of relatively evenly distributed, sub rounded vesicles (100-400 µm) and no visible micro-fractures at this scale. (c) Microcrystalline basalt with 45% porosity, made of large irregular vesicles (usually <2mm) with no microfractures visible at this scale. (d) Felsite with 11.5% porosity, consisting mostly of a microfracture network, up to 10-20 µm wide and few small vesicles (100-500 µm). (e) Gabbro with 12% porosity, made up of small pores (100-500 µm) and a microfracture network (10-20 µm wide). (f) Hyaloclastite with 39% porosity made up of both irregular-shaped pores between fragmental angular glass and crystalline matrix. Microfractures are visible and are as wide as 20 µm. (g) Ignimbrite with 15% porosity, where no microfractures are visible at any scale, but pores are usually large (<2 mm). (h) Dense obsidian with very low porosity (<1% porosity), where one 5-µm wide micro-fracture was visible.

3.3.2 Mechanical response of the different lithologies

The tensile strength of the different lithologies was determined by using the Brazilian disc method (e.g. Griffith, 1920; Li and Wong, 2013), where displacement in the radial direction of the sample is displayed against the tensile stress developed under this geometrical arrangement (Fig. 3.3a-h). The failure occurs via fracture nucleation in the middle of the sample, which laterally propagates outwards towards the piston of the press (e.g. Griffith, 1920; Li and Wong, 2013). Example of representative stress-axial deformation curves for each of the different lithologies is shown in Figure 3.3a-h. The dense basalt lava (Fig. 3.3a), basalt dyke (Fig. 3.3b), gabbro (Fig. 3.3e), ignimbrite (Fig. 3.3g) and obsidian (Fig. 3.3h) all display a clear stress drop. The high porosity basaltic lava stress-displacement has several small stress changes before the fracture has penetrated through the sample (Fig. 3.3c), which was due to small rupture events between pores in areas of samples near the pistons, as well as failure between pores, where the fracture propagated through the sample. The felsite (Fig. 3.3d) and hyaloclastite (Fig. 3.3f) exhibited very low strength, and no distinctive peak was observed during failure within both rock types, but a tensile fracture became visible.

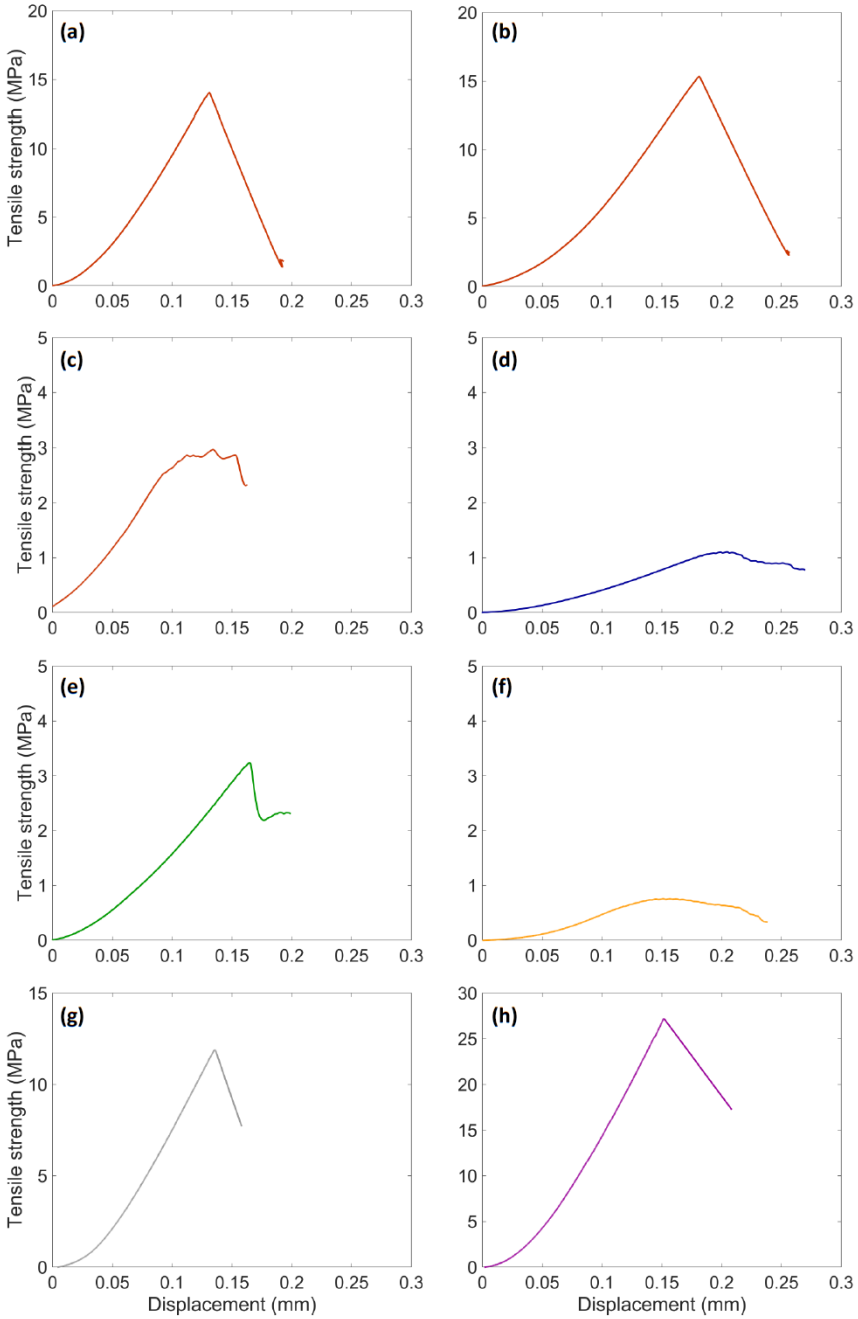

Figure 3.3: Examples of stress-axial displacement curves for each of the different rock types. a) Basalt with low porosity, b) Basaltic dyke, c) Basalt with high porosity, d) Felsite, e) Gabbro, f) Hyaloclastite, g) Ignimbrite and h) Obsidian.

The lithologies exhibit difference in their compressive strength and brittle response (Fig. 3.4a-h), once exposed to elevated loading pressure. The brittle failure process has commonly been split into four stages (e.g. Brace et al., 1966; Coats et al., 2018; Heap et al., 2014d; Scholz, 1968); 1) during the initial build-up of stress, the original microcracks aligned perpendicular to the loading axis (σ_1) closed, forming the initial convex segment on the stress-strain curve. 2) once the stress-strain becomes linear, the stress build-up is considered to be mostly recoverable elastic deformation. 3) the next stage is the strain hardening, which marks the onset of micro-fracturing and un-recoverable damage. This can be seen as a deviation from the linear portion of the curve. 4) Finally, the peak strength is reached and

followed by a stress drop, when the fracture propagates through the sample. This behaviour can be seen in representative curves for each lithology, deforming in the brittle regime (Fig. 3.4a-h). The dense basalt lava (Fig. 3.4a), basalt dyke (Fig. 3.4b), felsite (Fig. 3.4d), gabbro (Fig. 3.4e), and obsidian (Fig. 3.4h) all display a clear stress drop. The high porosity basaltic lava (Fig. 3.4c), hyaloclastite (Fig. 3.4f) and ignimbrite (Fig. 3.4g) example curves all exhibit some small stress-strain changes before the clear stress drop. This, we associate with fracture formation within the rock samples, before the fracture has penetrated through the sample.

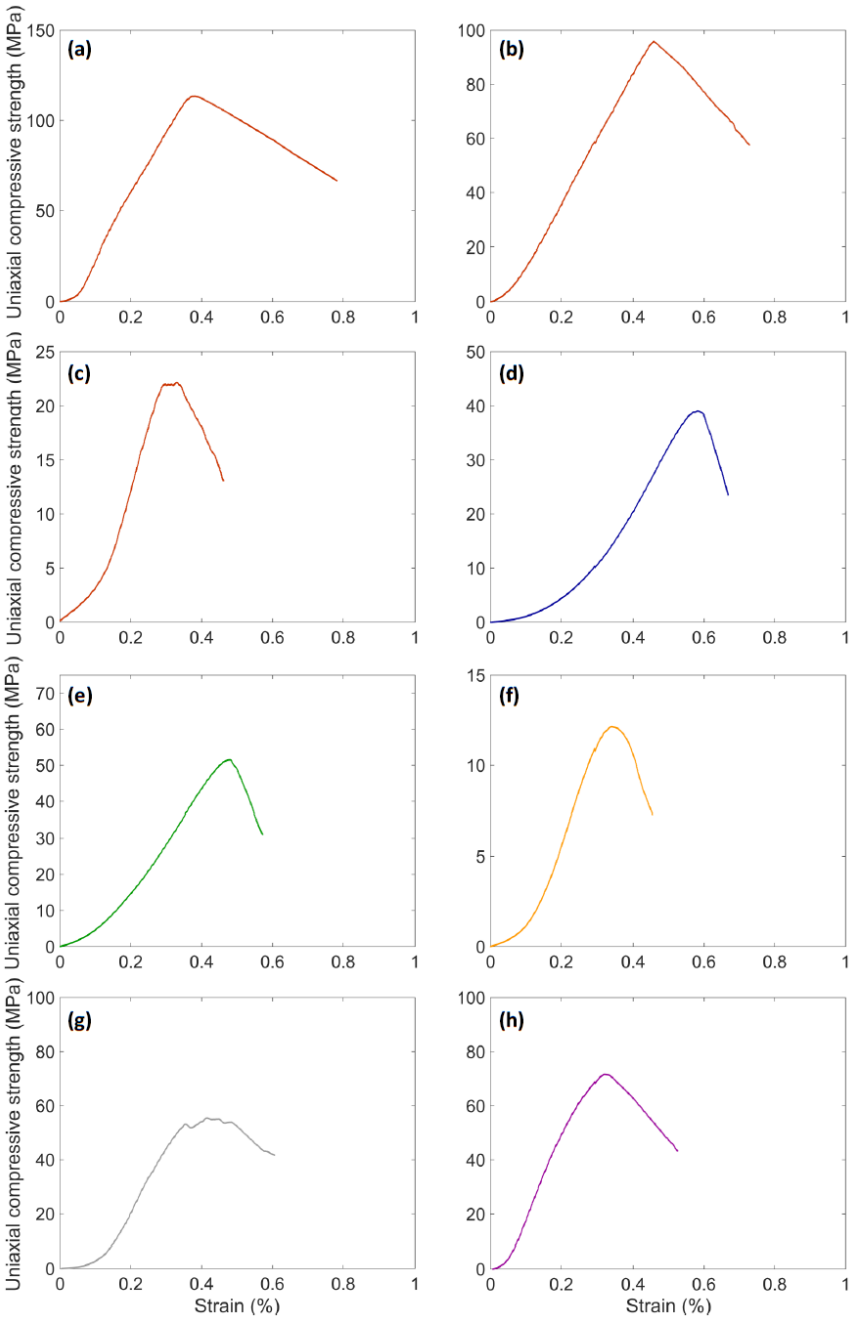

Figure 3.4: Examples of stress-strain curves for each of the different rock types: a) Basalt with low porosity, b) Basalt dyke, c) Basalt with high porosity, d) Felsite, e) Gabbro, f) Hyaloclastite, g) Ignimbrite and h) Obsidian.

3.3.3 Influence of effective pressure on rock strength and failure mode

To constrain the influence of effective pressure on the mechanical properties of rocks at Krafla, we tested three basalts (with small porosity ranges of 11.0-15.0 vol.%, 19.5-22.0 vol.% and 46.5-48.5 vol.%) and a felsite (with 9.9-10.1 vol.% porosity), which were chosen owing to their importance in the system and their contrasting microstructures (see section 3.3.1). For those samples that deform in a brittle manner, the mechanical data displayed four stages (i.e., segments in the stress-strain curves) leading to brittle failure, which was also reflected in the data of volume of water displaced from the samples subjected to loading (i.e. porosity change; Fig. 3.5 a-h; e.g. Brace et al., 1966; Coats et al., 2018; Scholz, 1968): 1) during the initial convex portion of the stress-strain build-up, when microfractures are closing, porosity of the sample is increasingly reduced; 2) Once the stress-strain becomes linear, the porosity reduces linearly with load; 3) When strain hardening begin, owing to the onset of microfractures, the porosity decrease with load slows down; until 4) the peak stress is reached. For the samples deforming under brittle conditions, the microfractures forming during the strain hardening will start to link up, allowing more water to infill the pores that are opening, until failure occurs. For those samples that deform under ductile conditions the sample will keep compacting, causing the porosity to decrease beyond the peak stress.

The mechanical data shows that the basalt and felsite, with low porosity (<15% vol. pores) exhibit an increased strength with effective pressure in the brittle field. During testing of low porosity samples, initial compaction reduces the porosity (closing of pre-existing microfractures) of the rock. Following compaction, loading continues along a linear stress-strain relationship until dilation is experienced, where porosity increases again (nucleation and growth of new microfractures). The mechanical data show a stress drop following the peak stress, indicating a brittle failure. The higher porosity samples (>15% vol. pores) show mostly ductile deformation modes, even at low effective pressure. In these cases, stress drops are mild following rupture, and often, the accumulated differential stress increases with strain. With an increase in effective pressure, the strength reduces. As materials deform in the ductile field, the pore structure collapses, leading to a decrease in porosity.

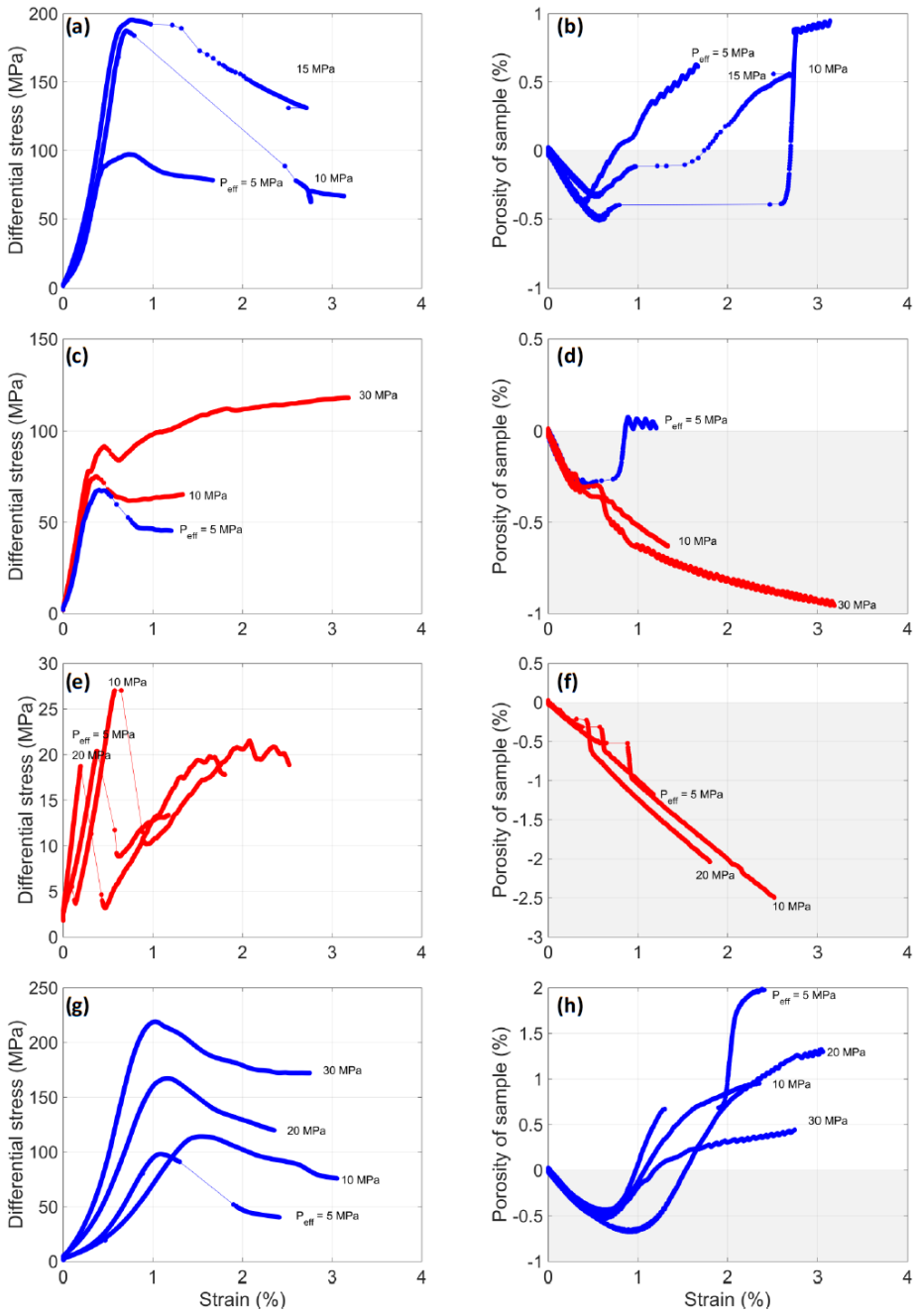

Figure 3.5: Stress-strain curves and measured porosity change under different triaxial conditions. a) Stress-strain curves at different confining pressure for basalt with 11-15% porosity. b) Measured porosity change (i.e. water displaced) during loading of basalt with 11-15% porosity at different confining pressures. c) Stress-strain curves at different confining pressure for basalt with 19.5-22% porosity. d) Measured porosity change (i.e. water displaced) during loading of basalt with 19.5-22% porosity at different confining pressures. e) Stress-strain curves at different confining pressure for basalt with 46.5-48.5% porosity. f) Measured porosity change (i.e. water displaced) during loading of basalt with 46.5-48.5% porosity at different confining pressures. g) Stress-strain curves at different confining pressure for felsite with 9.9-10.1% porosity. h) Measured porosity change (i.e. water displaced) during loading of felsite with 9.9-10.1% porosity at different confining pressures.

3.3.4 Thermal expansivity and heat capacity analyses

The thermal expansion coefficients (α) of the basalt and felsite samples were measured using a TMA (Fig. 3.6; table 3.1). The basalts showed slight increases in thermal expansivity up to 250 °C, beyond which α remained rather stable around $6x10^{-6}$ -$7x10^{-6}$ $°C^{-1}$. The felsite showed a slight increase in thermal expansivity with rising temperature, with a large peak at 573 °C, where the α-β transition of quartz present in the rock is crossed (e.g. Dolino et al., 1983; Fukuhara and Sampei, 2001), before decreasing back, up to 850 °C (Table 3.1).

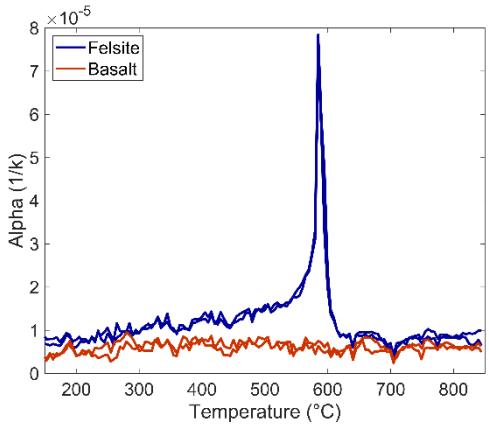

Figure 3.6: Thermal expansivity of felsite and basalt (felsite in blue and basalt in red). Both rocks show constant expansivity, apart for the felsite pronounced peak at around 550-600 ˚C due to crossing of the α-β quartz transition.

Table 3.1 Mean linear thermal expansion coefficient values for basalt and felsite at different temperature intervals.

Temperature interval (°C)	Basalt	Felsite
150-200	$4.82x10^{-6}$	$7.57x10^{-6}$
200-250	$4.93x10^{-6}$	$8.25x10^{-6}$
250-300	$6.37x10^{-6}$	$9.30x10^{-6}$
300-350	$6.54x10^{-6}$	$1.13x10^{-5}$
350-400	$6.71x10^{-6}$	$1.11x10^{-5}$
400-450	$6.30x10^{-6}$	$1.22x10^{-5}$
450-500	$7.00x10^{-6}$	$1.40x10^{-5}$
500-550	$6.42x10^{-6}$	$1.62x10^{-5}$
550-600	$6.26x10^{-6}$	$3.40x10^{5}$-*
600-650	$5.25x10^{-6}$	$9.61x10^{-6}$
650-700	$6.23x10^{-6}$	$8.23x10^{-6}$
700-750	$5.44x10^{-6}$	$7.28x10^{-6}$
750-800	$6.45x10^{-6}$	$8.60x10^{-6}$
800-850	$5.97x10^{-6}$	$8.37x10^{-6}$
Average expansion	$6.05x10^{-6}$	$1.19x10^{-5}$

*Crosses the α-β transition in quartz.

3.4 Discussion

3.4.1 Influence of porosity on rock strength and Young's modulus

During different phases of reservoir exploitation (such as by drilling, producing, completion with possibly adding injection back into the reservoir at some point), a good knowledge of rock behaviour will improve reservoir management (e.g. Ghassemi, 2012; Gunnarsson, 2011). Induced fractures, either mechanically (e.g. Legarth et al., 2005; McClure and Horne, 2014; Zimmermann et al., 2011) or thermally (e.g. Grant et al., 2013), can increase permeability (e.g. Eggertsson et al., 2018b; Heap and Kennedy, 2016; Kushnir et al., 2018; Lamur et al., 2017) and cause circulation loss (e.g. Fridleifsson et al., 2017; Lamur et al., 2017). Furthermore, a reduction in reservoir fluid pressure (e.g., due to extensive extraction) can trigger rock compaction and fracture closure, which commonly decreases permeability (e.g. Eggertsson et al., 2018b; Lamur et al., 2017; Perez-Flores et al., 2017; Walsh, 1981); whereas an increase in reservoir fluid pressure (e.g., due to injection), can cause induced seismicity (e.g. Gunnarsson, 2011; Zang et al., 2014), fracture widening and associated permeability increase (e.g. Eggertsson et al., 2018b; Lamur et al., 2017).

The mechanical tests conducted on the main Krafla lithologies have shown that: 1) the rock strength decreases with increased porosity (e.g. Baud et al., 2014; Bubeck et al., 2017; Griffiths et al., 2017; Heap et al., 2014a; Schaefer et al., 2015), however we note that the strength of low-porosity rocks can vary greatly depending on their microstructure (Fig. 3.7a-b); 2) The UCS is about 5-10x higher than the rocks UTS (Fig. 3.7a-b; e.g. Palchik and Hatzor, 2004); 3) the Young's modulus is strength dependent (Fig. 3.7c-d; e.g. Heap et al., 2014b); 4) within the brittle field, an increased confining pressure results in strengthening (e.g. Heap et al., 2015b; Paterson and Wong, 2005; Siratovich et al., 2016). The strengthening of felsite, with confining pressure is particularly interesting, as its UCS and UTS are considerably lower than off low density basalt, with similar porosities (Fig. 3.7a-b; Fig. 3.5a,c). However, under confinement (Fig. 3.5g), the strength of the felsite increases, as microfractures are closed, due to increased confinement.

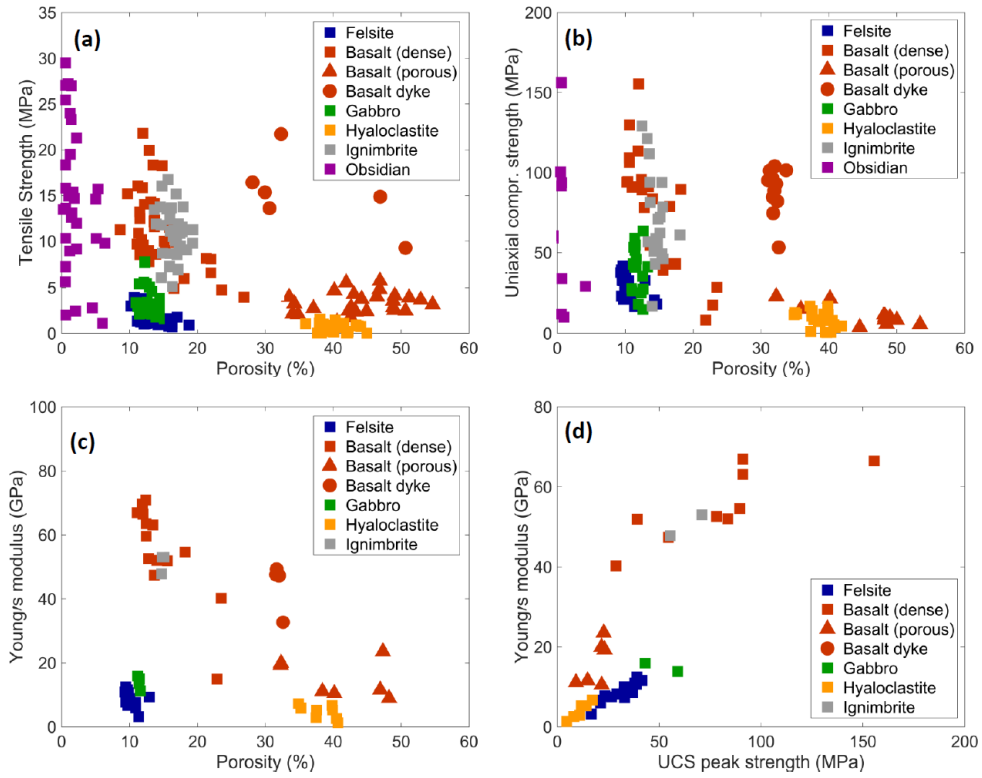

Figure 3.7: Results from uniaxial testing. a) Uniaxial tensile strength (UTS) as a function of porosity for different lithologies within the Krafla reservoir. b) Uniaxial compressive strength (UCS) as a function of porosity for different lithologies within the Krafla reservoir. c) Calculated values of Young's modulus for samples of different lithologies within the Krafla reservoir. d) Comparison between calculated Young's modulus values and their UCS.

The measured UCS of the samples can be compared to a modelled strength (Fig. 3.8), using the pore-emanating crack model by Sammis and Ashby (1986), with the assumption that the porous fraction of the sample is made up of round pores with no microfractures. The modelled strength seems to agree well with that measured in the laboratory for the basalt, as it only contained very minor micro-fractures. The highly porous basalt containing large pores (Fig. 3.2c), show a good fit with the modelled UCS where samples contain pores up to 1 mm diameter. The basalt dyke samples, however, hold a much denser pore network with rounded pores, smaller in size compared to other basalt (Fig. 3.2b), even though the porosity difference is not great. The dense basalt and ignimbrite indicate that pore size and structure have a high impact on the strength of the samples (Fig. 3.2a). The effect of micro-fractures is demonstrated with the strength of felsite and gabbro, where both samples contain small pores but significant micro-fracture network (Fig. 3.2d-e), causing a great decrease in rock strength, compared to the modelled strength, based on pore size (Fig. 3.8). The same is true with the obsidian, where a micro-fracture was visible, indicating that they might be present within the samples, therefore affecting their strength (Fig3.7b; Fig. 3.8). The hyaloclastite contains both big pores and microfractures (Fig. 3.2f), which explains its low strength.

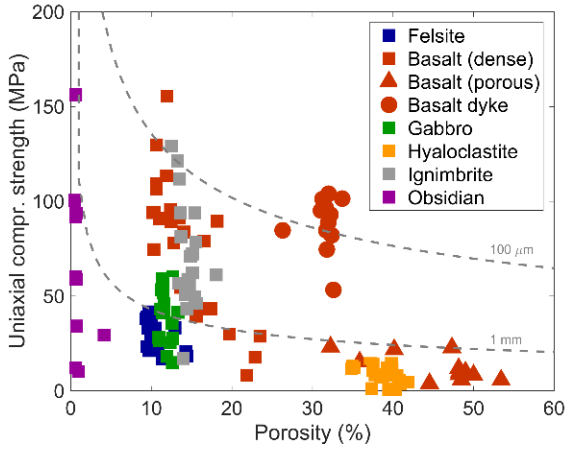

Figure 3.8: Uniaxial compressive strength (UCS) results overlapped with modelled isopore lines, predicting the UCS, based on the pore-emanating crack model by Sammis and Ashby (1986). The assumption is made that the porosity is purely based on rounded pores and the samples do not contain any micro-fractures.

3.4.2 Failure criteria for the reservoir rocks

Understanding the rock's mechanical properties at increased effective pressure is valuable for estimating rock behaviour at depth. To analyse how the different Krafla reservoir rocks, behave, rock samples were chosen with different properties. The triaxial data has been plotted in principal stress space (σ_1 as a function of σ_3) with the sample failure criteria (Fig. 3.9a). The failure criteria is based on the Hoek-Brown failure criteria for intact rock (Hoek and Brown, 1980; Hoek et al., 2002), which plots the failure criteria in two dimensions using the effective principal stresses (induced stress – pore pressure), with the minor principal stress on the X-axis and the major principal stress on the Y-axis. The failure curve is defined by eq. 3.2:

$$\sigma_1 = \sigma_3 + \sigma_c(m_i \frac{\sigma_3}{\sigma_c} + 1)^{0.5} \quad (3.2)$$

where σ_1 is the differential stress, σ_3 is the effective confining pressure, σ_c is the UCS (when $\sigma_3 = 0$), and m_i is the curve fitting parameter estimated based on the triaxial experimental results. It should be noted that the failure criteria cannot consider samples, for which the minor principal stress is higher than 50% of the UCS value.

From the constructed failure criteria (Fig. 3.9 a-b) we note that in general, lower porosity samples tend to be stronger and display a longer failure envelop. However, the difference in strength is somewhat affected by microstructure (pore size and degree of micro-fracturing) as the very weak felsite shows a failure envelop at rather higher differential stress value, as discussed earlier (e.g. Bubeck et al., 2017; Griffiths et al., 2017).

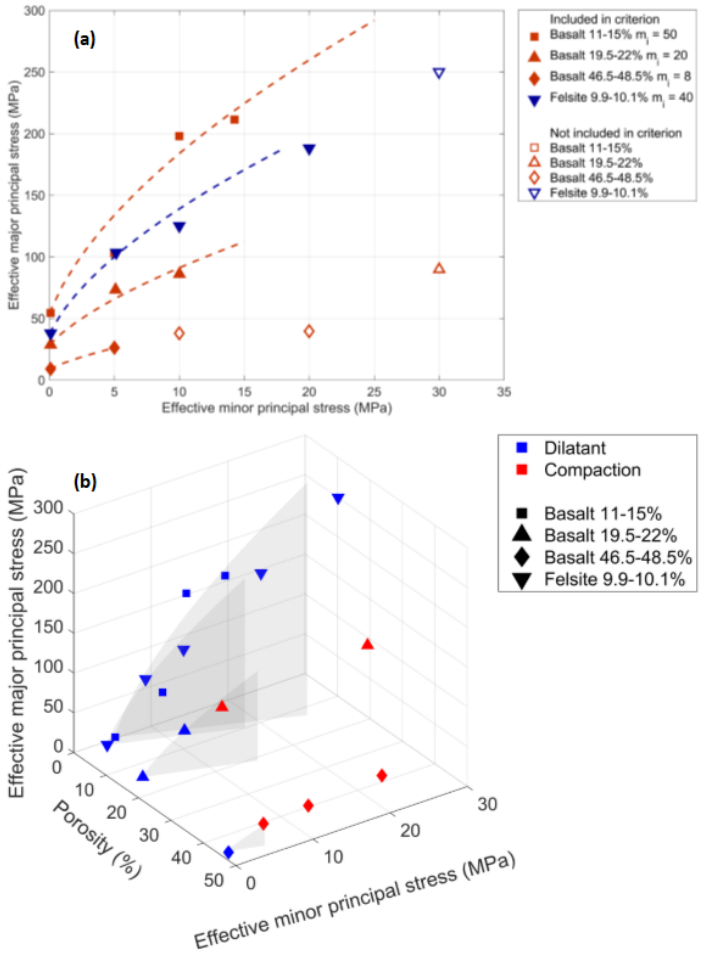

*Figure 3.9: Hoek-Brown failure criterion plotted for different lithologies from Krafla. a) Filled symbols indicate data used to construct the failure criterion (σ3<0.5*UCS value) and open symbols represent data where the confining pressure was too high to use for the failure criterion (σ3>0.5*UCS value). b) The same data but plotted in respect to their porosity.*

Based on Anderson's faulting theory (Anderson, 1951) and the focal mechanism calculated from earthquakes at Krafla (Schuler et al., 2016) at shallow depth the horizontal stress is the highest principal stress within the reservoir, but with greater depth, it is vertical and the loading stress is approximated at 30 MPa.km^{-1} (assuming an average rock density of 3 ton.m^{-3}), whilst the hydrostatic pressure increase by 10 MPa.km^{-1} (density of water 1 ton.m^{-3}), leading to an effective horizontal pressure increase within the reservoir of 20 MPa.km^{-1} (e.g. Elders et al., 2011). As the production is within the top 1-2.5 km of the reservoir this would therefore indicate that failures occurring within the reservoir is brittle for low porosity rocks (<~20% porosity), when temperature effects are neglected. Rocks dilate during rupture in the brittle field (Fig. 3.5 b,d,h). The fracture that forms has been showed to increase permeability within volcanic rocks (e.g. Eggertsson et al., 2018b; Heap and Kennedy, 2016; Lamur et al., 2017), causing positive feedbacks on reservoir productivity. The high porosity basalt indicated a ductile response to increased pressure and crushing of the pore space, therefore decreasing porosity and possibly altering rock strength (Bedford et al., 2018). Reduction in porosity within the reservoir is also likely to have negative effect on its productivity (Eggertsson et al., 2018b).

3.4.3 Induced thermal stress

As thermal stimulation is a common practice in Iceland during well completion (e.g. Axelsson et al., 2006; Flores et al., 2005), knowledge of the stress changes occurring when a well is being stimulated can help constrain the temperature change needed to induce a stress change to enhance the fluid flow (e.g. Grant et al., 2013; Siratovich et al., 2015a). To constrain the induced thermal stress change occurring, knowledge of the thermal and physical properties of the rocks are needed. By utilising eq. 3.1, thermal stress can be modelled (Fig. 3.10 a-d).

The thermal expansivity of felsite and basalt can be seen in Fig. 3.6 and table 3.1. The basalt displays a stable thermal expansivity with temperature, whereas the felsite shows a slight increase in thermal expansivity with temperature [especially as it crosses the α-β quartz transition, resulting in high thermal expansion for a narrow range at 573°C; (e.g. Dolino et al., 1983; Glover et al., 1995)]. From eq. 3.1, we note that when the Young's modulus is high, a smaller temperature change is needed to induce higher thermal stress within the rock mass. For the dense basalt (Fig. 3.10a), the change in Young's modulus as the rock is confined reduces the temperature change needed to induce higher stresses, in comparison to higher porosity basalts (Fig. 3.10b-c); therefore, we see that stronger rocks are more affected by the temperature change they are exposed to. If compared to the UTS results in Fig. 3.7a, we note that a temperature change in the range of 35-60°C would be sufficient to exceed the tensile strength (of the order of 25 MPa), assuming that all principal stresses are zero and all stress change during cooling occurs in tension. Within the Krafla reservoir, these rocks might experience temperature change that can exceed 300 °C, such that when the rock is cooled, the induced thermal stress can exceed 100 MPa. With further confinement, these rocks would need less temperature change to reach higher tensile stresses.

When the more micro-fractured felsite (Fig. 3.10d) is compared to the basalts (Fig. 3.10a-c), we note that the Young's modulus is less affected by confinement, causing the temperature change needed to induce sufficient stress for failure to be higher. The felsite is however much weaker, compared to the dense basalt (Fig. 3.7a-b) and would need to undergo a smaller temperature change to exceed its tensile strength (assuming all principal stresses are zero and all the induced stress were tensile). The rock however experiences the same behaviour, that with increased confinement, less temperature change is needed to induce stress within it.

For thermal stimulation to be effective, induced tensile fractures at the well face need to open (Eggertsson et al., 2018b; Heap and Kennedy, 2016; Siratovich et al., 2015a). Induced tensile fractures often fail to increase permeability as the fractures do not propagate outwards unless the pressure exceeds the minimum principal stress (e.g. Weng et al., 2011), requiring further fracture stimulation to enhance the fluid flow. For the fracture to propagate, the pressure within the fracture needs to exceed the rock strength (e.g. Camacho and Ortiz, 1996; Nordgren, 1972; Warpinski and Teufel, 1987). The heavily micro-fractured felsite could, however, cause different changes to occur during thermal stimulation. As the cooling will cause a contraction and induced thermal stress within the rock mass, the microfractures will expand and open up, increasing permeability as showed by Eggertsson et al. (2018b). So, even though the thermal contraction is not high enough to cause the rock to fail and form a tensile fracture, the cooling might still open up the fluid pathways within the rock, causing the cold

fluids to flow further from the well, thereby enhancing the impact of thermal stimulation, increasing the likelihood of a successful stimulation.

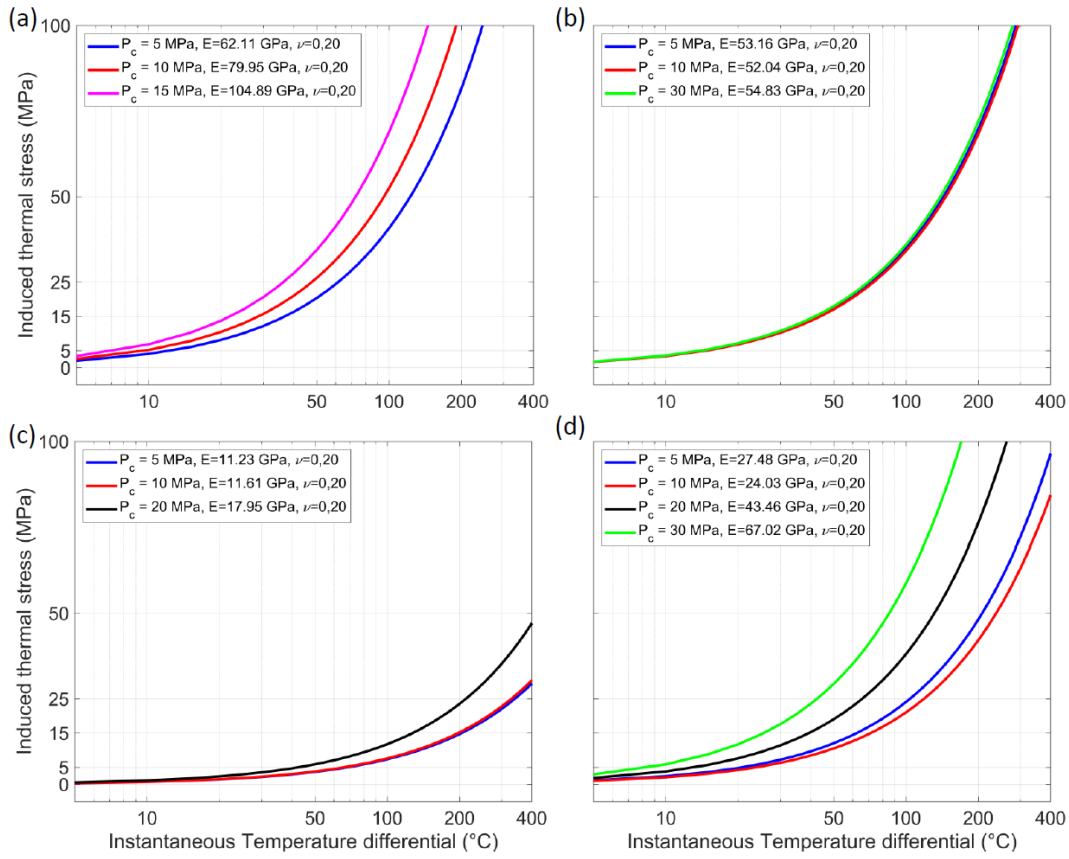

Figure 3.10: Modelled tensile stress induced by temperature changed during thermal stimulation of rocks with different Young's modulus, for variously porous rocks: a) basalt with 11-15% porosity, b) basalt with 19.5-22% porosity, c) basalt with 46.5-48.5% porosity, and d) Felsite with 9.9-10.1% porosity. Note that the Poison's was not measured but assumed to be 0.20.

3.4.4 Application of results to geothermal exploitation

The findings presented here improve our understanding of the mechanical properties (Fig. 3.7a-b) of the reservoir rocks found within the reservoir at Krafla and furthermore, they give insight into the impact of drilling, thermal stimulation and evolution of the reservoir. During burial or lowering of pore pressure within the reservoir (i.e. resulting in an increase in effective pressure), the rock strength increases, resulting in an increase in Young's modulus (Fig. 3.10). Thermal stress modelling shows that this rock strengthening will correspondingly increase the induced thermal stress caused by any temperature change occurring within the reservoir. As the induced thermal stress is nonlinear with temperature (Fig. 3.10) and the failure envelope of the different rocks is equally non-linear (Fig. 3.9a), the data suggest that there may be an optimal set of conditions, under which, rock failure during thermal stimulation best enhance permeability within the reservoir. This "threshold" may have been exceeded during drilling of both wells in the IDDP project, when the superhot parts of the reservoirs were reached [IDDP-1 (Palsson et al., 2014); IDDP-2 (Friðleifsson et al., 2017)], as both wells were drilled with great circulation loss (Friðleifsson et al., 2017; Palsson et al., 2014).

The induced thermal stresses experienced within different rock types may promote secondary fracture formation, as different lithologies may respond differently to temperature changes. The UTS was generally very low for basalt and felsite (Fig. 3.7a) and modelled induced thermal stress for these rocks was generally exceeded within <100 °C temperature change (Fig. 3.10), well within the expected reservoir temperature change occurring during thermal stimulation of high temperature geothermal reservoirs (e.g. Axelsson et al., 2014; Elders et al., 2014b; Sanyal, 2005).

3.5 Conclusion

This chapter focuses on the mechanical properties of the main rock types found within the Krafla geothermal system and the thermal expansivity of basalt and felsite to model thermally induced stresses associated with thermal stimulation practices. We find that the lithologies exhibits a wide range of porosity, reflected in there UCS and UTS, which are inversely proportional to the porosity and strongly affected by the abundance of microcracks. The UCS is generally 5-10x higher than the UTS. The porous lithologies (>15% porosity) may undergo transition to a dominantly ductile deformation mode, accompanied by significant compaction at relatively low effective pressures (i.e., depth within the reservoir); such deformation result in a decrease in porosity with strain. We find that the samples collected from a basalt dyke exhibits high strength, for their given porosity, owing to the sole presence of small round vesicles, without micro-fractures. The presence of micro-fractures within the felsite result in very low UCS (<50 MPa) and UTS (<5 MPa), but once under confinement, the felsite displays similar strengths as the basalt with similar porosity, as both rock types increase in strength with confinement. This we relate to the micro-structure, which under confinement, interlocks the fracture network, causing the rock strength to increase greatly with confinement. The thermal expansivity of the basalt and felsite both show slight increase in thermal expansivity with temperature, but as the felsite contains quartz, a peak is observed when the quartz crosses the α-β transition. The induced thermal stresses modelled for the basalt and felsite show that with increased rock strength (e.g., as the Young's modulus increases with confinement), the induced thermal stress increases. The data suggest that thermal stimulation could be more successful for deep drilling project (e.g., IDDP), as deep hot wells of dense rocks (4-5 km deep) might be more sensitive to thermal stimulation than conventional wells (2-3 km deep). For shallower reservoirs (1-3 km deep), which have experienced decrease in reservoir pore pressure due prolonged exploitation, the resultant increase in effective pressure may increase the suitability for thermal stimulation. Thus, the data shows that although complex and varied, an understanding of volcanic rock properties in geothermal systems may increase our understanding of reservoir behaviour through time and when stimulated.

3.6 Acknowledgements

This study has been supported by Landsvirkjun National Power Company of Iceland and financially supported by Landsvirkjun's Energy Research fund. Y. Lavallée acknowledges grants NÝR-17 – 2015, NÝR-16 – 2016 and NÝR-20 – 2017, as well as a scholarship from the Institute for Risk and Uncertainty at the University of Liverpool and a Starting Grant on Strain Localisation in Magma (SLiM, no. 306488) from the European Research Council (ERC).

Chapter 4:

Compaction of hyaloclastite from the active geothermal system at Krafla volcano, Iceland

Paper abstract

Hyaloclastites commonly form high-quality reservoir rock in volcanic geothermal provinces. Here, we investigated the effects of confinement due to burial from prolonged eruptive activity on the evolution of surficial and subsurface (from 70, 556, 732 m depths) hyaloclastites at Krafla volcano, Iceland. Upon loading in a hydrostatic cell, the porosity and permeability of the surficial hyaloclastite decreased linearly with effective pressure, as cracks closed upon elastic (non-destructive) compaction up to 22-24 MPa (equivalent to ~0.9 km depth in the reservoir). Beyond this pressure, denoted as P*, we observed accelerated porosity and permeability reduction with pressure, as the rock underwent non-elastic (destructive) compaction. In comparison, the porosity and permeability of the subsurface core samples was less sensitive to effective pressure and decreased linearly with confinement as the samples compacted elastically (non-destructive) within the conditions tested (to 40 MPa). Although the surficial material underwent destructive compaction, it maintained higher porosity and permeability than the subsurface hyaloclastites throughout.

We constrained the evolution of yield curves of the hyaloclastites subjected to different effective mean stresses beyond P* in a triaxial press. Surficial hyaloclastites underwent a brittle-ductile transition at an effective mean stress of ~10.5 MPa, and peak strength reached 13 MPa. When loaded to effective mean stresses of 33 and 40 MPa, the rocks compacted, respectively producing new yield curves with a brittle-ductile transition at ~12.5 and ~19 MPa. In comparison, the subsurface samples were found to be much stronger, displaying brittle-ductile transitions at higher effective mean stresses (i.e., 37.5 MPa for 70 m sample, >75 MPa for 556 m, 68.5 MPa for 732 m s). Thus, we conclude that compaction upon burial alone is insufficient to explain the physical and mechanical properties of the subsurface hyaloclastites present in the reservoir at Krafla volcano. We discuss how mineralogical alteration, mapped using QEMSCAN, may have further modified the hyaloclastite during evolution in the active geothermal system.

4.1 Introduction

Geothermal and hydrothermal systems are typically found in active volcanic environments (e.g. Axelsson et al., 2014; Bibby et al., 1995; Collar and Browne, 1985; Moran et al., 2000), where fluid convection transfers heat and mass from the magma-derived, relatively high temperature subsurface (e.g. Norton, 1984). As these magma under-rooted systems can be intermittently volcanically active over long periods of time, it is common for the reservoir rock to be of volcanic origin. The initial geomechanical properties, such as permeability and strength, of these reservoir rocks can be as varied as the style of volcanism from which they are formed (Heap et al., 2014d; Lamur et al., 2017; Schaefer et al., 2015), and may be susceptible to subsequent impact from burial, temperature and interaction with saturated fluids (e.g. Julia et al., 2014). Thus, the evolution of geothermal systems fed by

magmatic bodies is intrinsically linked to the petrological and mechanical evolution of the reservoir rocks. The common presence of clay phases in reservoir rocks can be mapped from the surface using electrical resistivity, providing information about the structure of the reservoir (e.g. Kristinsdóttir et al., 2010; Lévy et al., 2018; Mortensen et al., 2015).

In mid-to-high latitude provinces where volcanic activity may commonly be subaqueous or subglacial (e.g., in Iceland, Chile, New Zealand), substantially increased cooling rates and elevated pressure promotes quench-induced fragmentation whilst suppressing exsolution fragmentation (van Otterloo et al., 2015). In basaltic eruptions, the products of such activity includes highly-variable, quench-fragmented glass, termed hyaloclastite (e.g. Cole et al., 2018; Gutierrez et al., 2005; Jakobsson and Gudmundsson, 2008; Lachowycz et al., 2015; Smellie et al., 2011; Tucker and Scott, 2009; Watton et al., 2013; Zierenberg et al., 1995). Through time the glass commonly undergoes extensive alteration, resulting in the generation of a palagonite matrix, dominated by thermally-liable clays such as smectite, and zeolites (e.g. Johnson and Smellie, 2007; Moore, 2001; Stroncik and Schmincke, 2002; Walton and Schiffman, 2003). As such, hyaloclastite comprises a time and temperature dependent, variably-indurated and heterogeneous assortment of palagonite, hydrated glass (Watton et al., 2013), lithics and crystal fragments.

Hyaloclastites are often highly porous (e.g. Alfredsson et al., 2013; Eggertsson et al., 2018b; Loftsson and Steingrímsson, 2010), mechanically weak (e.g. Loftsson and Steingrímsson, 2010; Neuffer et al., 2006; Tentler and Temperley, 2006), and thus highly permeable to fluid circulation (e.g. Eggertsson et al., 2018b; Jarosch et al., 2008). As such, they are often targeted as a preferred reservoir rocks for freshwater aquifers (e.g. Kim et al., 2013) and for hydrothermal fluid extraction in geothermal energy production (e.g. Arnorsson, 1995; Nielson and Stiger, 1996; Zakharova and Spichak, 2012). In active volcanic systems, hyaloclastites are progressively buried by recurrent deposition of eruptive products, such that they are increasingly in contact with, and host to, hydrothermal fluids (e.g. Alfredsson et al., 2013; Jarosch et al., 2008; Mortensen et al., 2014; Mortensen et al., 2015). Thus, they experience elevated pressures, high temperatures, and corrosive fluids (e.g. Alfredsson et al., 2013; Bolognesi and Damore, 1993; Bonafede, 1991; Keiding et al., 2010; Keiding et al., 2008). Such extreme conditions may promote compaction (e.g. Bedford et al., 2018; Eggertsson et al., 2018b; Farquharson et al., 2017; Heap et al., 2015b; Siratovich et al., 2016), precipitation of secondary mineral phases (e.g. Alfredsson et al., 2013; Scott et al., 2017; Thien et al., 2015; Wyering et al., 2015) and variable degrees of alteration (e.g. Heap et al., 2015b; Pola et al., 2012), modifying the mechanical properties and the permeable-porous network through which fluids circulate. Previous mechanical studies of porous rock compaction (Baud et al., 2004; Bedford et al., 2018) have characterised rock strength by evaluating yield curves to identify the stress conditions where permanent inelastic deformation may occur. These investigations have shown that yielding behaviour can vary between different rock types, with many granular materials (e.g. soils and sandstones) typically having elliptical shaped yield curves (e.g. Baud et al., 2004; Baud et al., 2000), whereas volcanic rocks can exhibit linear yield curves (e.g. Gueguen and Fortin, 2013; Heap et al., 2015a). Despite their importance in geothermal fields, the mechanical properties and yielding behaviour of hyaloclastite remain largely unconstrained. An understanding of how pore space evolves during compaction of hyaloclastite is central to our ability to adequately model the evolution of hydrothermal reservoirs for optimising energy production.

Here, we systematically map the physical and mechanical properties of surficial and subsurface hyaloclastites from Krafla volcano, Northeast Iceland, which constitute important reservoir rocks in the active hydrothermal system exploited for geothermal energy. The volcano consists of a large caldera that formed ~100 ka ago, possibly in two eruptions (Sæmundsson, 1991), that has been partly infilled with ignimbrites, lava flows (commonly occurring every 300-1000 years in the Holocene (Sæmundsson, 1991), hyaloclastites, and other fragmental products (Mortensen et al., 2015; Sæmundsson, 1991). Cores and drill cuttings obtained from extensive geothermal exploration of the Krafla hydrothermal system have revealed that the upper >1300 m of the reservoir mostly consists of basaltic lavas and hyaloclastites. Below this depth, the reservoir consists of gabbroic intrusions (Mortensen et al., 2014; Mortensen et al., 2015), which are locally under-rooted by rhyolitic magma at a depth of 2100 m (Elders et al., 2014b). As observed in other areas of Iceland, the hydrothermal reservoir rocks can be divided into five zones based on temperature-induced alteration: 1) a shallow zone of smectite-zeolite, 2) interlayered smectite-chlorite, 3) chlorite, 4) chlorite-epidote and 5) epidote actinolite (Mortensen et al., 2015). Calcite can additionally occur in regions where the rock is at temperatures lower than ~290 °C (Mortensen et al., 2015). Temperature is highly spatially-variable across the field, and does not increase linearly with depth (Lévy et al., 2018), for example previous studies on core samples from borehole KH-6, drilled in 2006, found that the rocks at 556m depth were rather unaltered, but the rock samples collected at 732 m depth had experienced a high intensity of alteration (Lévy et al., 2018).

4.2 Materials and methods

In this study, we investigate the effect of confinement on the physical and mechanical evolution of surficial and subsurface hyaloclastites from Krafla volcano, Northeast Iceland, to assess the degree to which compaction contributes to permeability evolution during burial in the reservoir. The surficial sample was collected at the south-eastern edge of the caldera (65°N 41.067; -16°W 43.089) during a field campaign in August 2015. It is a basaltic hyaloclastite produced during a subglacial eruption, shortly after the formation of the caldera ~100 ka ago (Mortensen et al., 2015; Sæmundsson, 1991). Subsurface samples were selected in August 2016 from cores drilled and collected by Landsvirkjun National Power Company of Iceland: hyaloclastite from a depth of 70 m was selected from borehole KH-4 (65°N 41.411; 16°W 48.140) drilled in 2006 and hyaloclastites from 556 m and 732 m depth were selected from borehole KH-6 (65°N 42.115; 16°W 48.048) drilled in 2007 (Gautason et al., 2007). These core samples are located about 2.5 km away from the main region exploited for geothermal energy (Mortensen et al., 2015). During drilling and after completion of the boreholes, the temperature was measured at some depth intervals. In the KH-4 well a temperature of 40°C was recorded at 65 m. In the KH-6 well, temperature measurements were made at three depths, and showed slight warming from measurements taken over a 5-day interval. During the last measurements, the temperature was measured to be 50 °C at 250 m, increasing rapidly from 75 °C to 200 °C at 345 m, before decreasing beyond 500 m depth; at 550 m, the temperature was approximately 150 °C and at 735 m depth, 125 °C (Gautason et al., 2007). A sample overview is presented in table 4.1.

Table 4.1 Sample suite and test types undertaken.

Depth	Sample ID	Measurement type
0 m	H1 0m	Yield curve
	H2 0m	Yield curve
	H3 0m	Yield curve
	H4 0m	UCS and Young's modulus
	H5 0m	Elastic limit (P*)
	H6 0m	Permeability
70 m	H1 70m	Yield curve
	H2 70m	UCS and Young's modulus
	H3 70m	Permeability
	H4 70m	Elastic limit (P*)
556 m	H1 556m	Yield curve
	H2 556m	UCS and Young's modulus
	H3 556m	Permeability
732 m	H1 732m	Yield curve
	H2 732m	UCS and Young's modulus
	H3 732m	Permeability

4.2.1 Mineralogical and petrological analysis

The petrology of the rock and mineralogical distribution was investigated using an optical microscopy and QEMSCAN® (Quantitative Evaluation of Minerals by SCANning electron microscopy). Analysis was performed using this automated SEM-EDS system using a 15-kV accelerating voltage and ~5 nA beam current (see Wallace et al. 2018 for further detail). A step size of 2 μm was used to map an area of >8 x 12 mm. Two Bruker energy dispersive X-ray spectrometers (EDS) recorded the discrete secondary X-Rays emitted by the sample, which are used to identify and quantify the mineralogy of the thin section by correlation with a composition database. The mineral distribution was summarised numerically by identifying the relative proportions of each mineral in the QEMSCAN images and normalising them to the pore space. All samples were thin sectioned perpendicular to the drilling direction (Pirrie et al., 2004).

4.2.2 Sample Preparation

For experimental purposes, 24.9 ± 0.1-mm diameter by 50.5 ± 1-mm long cylindrical cores were prepared (~2:1 aspect ratio) from the available well cores and surface material. The core samples were all drilled parallel to the drilled well cores. All prepared samples were kept in a drying oven over night at 75°C and then cooled and stored in a desiccator before any measurements were undertaken.

4.2.3 Porosity Determination

The porosity of all sample cores was determined using an AccuPyc 1340 Helium Pycnometer from Micromeritics in the Experimental Volcanology and Geothermal Research Laboratory at the University of Liverpool. The device measures the skeletal sample volume (i.e. rock including isolated pores

inaccessible to helium) in a 100 cm^3 chamber, with an accuracy of ±0.1% of the sample volume. The connected porosity (ϕ) is then determined via:

$$\phi = \frac{V_c - V_m}{V_c} \quad (4.1)$$

Where V_m is the measured skeletal volume and V_c is the volume calculated by the core dimensions.

4.2.4 Porosity and Permeability Evolution with Pressure

To simulate the impact of hyaloclastite burial, we determined the porosity and permeability changes associated with increasing effective pressure (effective pressure = confining pressure - pore pressure) using a hydrostatic 250 MPa pressure cell from Sanchez Technologies in the Experimental Volcanology and Geothermal Research Laboratory at University of Liverpool. This method was employed for samples with permeability greater than $5x10^{-18}$ m^2 (corresponding to the approximate determination limit of the apparatus). Jacketed water-saturated samples were loaded in the pressure vessel to the target confining pressure (at 5 increments up to 40 MPa). [Note that 1 km depth would correspond to a confining pressure of approximately 25 MPa assuming a nominal rock density of 2500 $kg.m^{-3}$.] During each loading phase, the change in porosity experienced by the compacting sample was determined by measuring the volume of water expelled (±0.05% accuracy) with the sample held at a pore pressure of 1MPa (see Eggertsson et al., 2018b; Lamur et al., 2017). Subsequently, following 30 minutes of equilibration at the set confining pressure, permeability was measured via the steady-state flow method (Darcy, 1856; Lamur, 2018), by exerting a pressure differential of 1 MPa (2 MPa upstream; 1 MPa downstream) and monitoring fluid discharge in the pumps (with ±0.002 ml accuracy). To assess for the need of Klinkenberg (1941) or Forchheimer (Whitaker, 1996) corrections, the pressure gradient was increased and decreased (between 0-2 MPa) to ensure the calculated permeability remained constant as flow rate evolved; we found that these corrections were not needed for any of the samples. Following permeability determination, the sample was loaded to the next increment in effective pressure by increasing confinement, whilst monitoring the volume of water expelled from the sample to monitor pore closure once more, and to measure the permeability again.

For samples with a permeability below the detection limit of the apparatus, permeability was quantified using the pulse transient method (Brace et al., 1968) in a triaxial apparatus in the Rock Deformation Laboratory at the University of Liverpool (see Faulkner and Armitage, 2013). The sample was fully saturated in water to a pore fluid pressure of 5 MPa. The fluid pressure was then increased by approximately 0.5 MPa on one side of the sample to set a small pressure differential. This pressure differential across the sample then decays through time, allowing the permeability to be calculated. Once the measurement was completed, the confining pressure was increased to the next increment and the procedure repeated (Brace et al., 1968; Faulkner and Armitage, 2013).

4.2.5 Mechanical Properties

To constrain the elastic limit of the rocks subjected to isotropic loading (P*), samples were loaded in the hydrostatic cell by incrementally increasing the confining and pore pressures to 46 MPa and 45 MPa, respectively, ensuring that the effective pressure never exceeded 1 MPa. Then, the effective pressure was increased by reducing the pore pressure at a rate of 0.1 $MPa.min^{-1}$, whilst monitoring the volume of water expelled from the sample. This provided the continuous porosity change as a function

of effective pressure up to 45 MPa, and P* was defined as the point of negative inflection in porosity-pressure space (after Zhang et al., 1990).

The mechanical properties of the samples were further constrained under unconfined and confined conditions in the Experimental Volcanology and Geothermal Research Laboratory at the University of Liverpool. Uniaxial (unconfined) compressive strength (UCS) measurements were conducted using a 5969 Instron uniaxial press (equipped with a 100 kN load cell with a resolution of 100 N, and actuator with a testing range of 0.001-600 mm.min^{-1}) where the samples were all brought to failure (defined by a stress drop exceeding 10 %) with a strain rate of 10^{-5} s^{-1}. The measurements were corrected for machine compliance by pressing the pistons directly together under the same loading conditions, the displacement was then subtracted from the displacement measured during the rock tests in real time using the Bluehill® software from Instron. The slope of the linear elastic portion of the stress-strain loading curves were used to calculate the Young's modulus.

Confined conditions were tested using a TRIAX100-300 triaxial press, developed by Sanchez Technologies. The apparatus controls the experimental conditions (up to 300 MPa of axial load and 100 MPa confining pressure) using four Stigma 300 pumps (the pumps operate up to 100 MPa with a resolution of 50 kPa, have a volume of 300 cm^3, maximum flow rate of 110 cm^3.min^{-1}, a resolution of 10^{-4} cm^3 and a volume control and determination accuracy of 0.1 %,). Here, only two pumps were used as the triaxial tests were done in absence of pore fluids: the radial confinement was applied using argon in one pump, the axial deformation was controlled using silicon oil in another pump along with a 1.5 kbar Maximator gas booster (pressure ratio of 1:150). The sample assembly consists of the test specimen loaded between alumina cylindrical spacers of 25 mm diameter, jacketed in a 30-cm long Viton sleeve. Compliance was constrained by loading a sample assembly containing a sample of steel (for which the elastic properties had been accurately constrained *a priori*) to 300 MPa. By subtracting the steel predicted deformation during loading, we quantified the compliance as a function of applied axial stress. To test rock samples, a core was placed in the sample assembly and inserted in the press. The confining pressure was increased to a desired testing value, and during loading the axial load was maintained at 2 MPa higher, increasing at the same rate to ensure the confinement did not force the pistons to recede, causing slack in the assembly; during this phase, the samples compacted slightly (as cracks closed; e.g. Wong and Baud, 2012).

To determine the strength of the materials, yield curves were plotted in P-Q space, where P is the effective mean stress ($\mathrm{P} = \frac{\sigma_1+\sigma_2+\sigma_3}{3}$) and Q is the differential stress (($\mathrm{Q} = \sigma_1 - \sigma_3$). Yield curves were mapped following the procedure of Bedford et al., (2018) where a sample is hydrostatically loaded to a given confining pressure (note there was no pore fluid pressure in these tests), before an axial load was applied (strain rate = 10^{-5} s^{-1}) in order to subject the sample to a differential stress. During axial loading, the sample deforms elastically with a quasi-linear stress-strain relationship. The stress build-up was monitored until a deviation from linear loading was observed, marking the onset of yield (i.e. permanent inelastic strain), and the load was immediately removed to ensure the sample did not accumulate inelastic damage. The P and Q values at the deviation from linear loading were recorded as the yield point, and the same sample was then taken to a range different confining pressures and the axial loading procedure was repeated at each pressure increment in order to map out the complete

yield curve in P-Q space. This procedure is useful when the available material is limited, as is the case from recovered core samples, as an entire yield curve can be reconstructed using only one sample. The yield curve intersects the P-axis at the hydrostatic yield point (i.e. no differential stress), typically referred to as P*; beyond this point the rock undergoes compaction and pore collapse (Zhang et al., 1990).

4.3 Results

4.3.1 Mineralogical and Petrological Signatures

The surficial hyaloclastite and the subsurface hyaloclastites cored from different depths in the reservoir exhibit contrasting mineralogical and petrological characteristics (Fig. 4.1). The surface hyaloclastite is light brown with ~10% dark basaltic fragments up to 10 mm in size (Fig. 4.1A). Under plane polarised light (PPL) the heterogenous texture of the clasts and porosity can be seen (Fig. 4.1B). QEMSCAN analysis (Table 4.2; Fig. 4.1C-E) indicates that the surface rock is mostly comprised of glass fragments (58%), smectite (26%), zeolites (8%) and anorthite (7%). The glass is highly variable in size and morphology and is found within both the matrix and as large clasts within the rock (Fig. 4.1C); smectite is visible across the matrix but zeolites and anorthite are limited to small clasts (Fig. 4.1E). At 70 m depth the matrix of the hyaloclastite is darker compared to the surface samples and consists of ~35% basalt fragments (Fig. 4.1F). Under PPL the porosity can be seen as rounded vesicles within individual clasts and more angular patches between clasts (Fig. 4.1G). QEMSCAN (Table 4.2; Fig. 4.1H-J) shows that the rock is comprised of glass (70%), smectite (27%) and calcite (1%), while zeolites and other minerals are only present as accessory minerals (<1% combined). The glass is both found in large clasts and within the matrix (Fig. 4.1H). The smectite is only found in the matrix, along with the few infilled secondary minerals such as zeolites (Fig. 4.1J). The sample from 556 m depth (Fig. 4.1K) contains a brown-green matrix with darker clasts, and in PPL fractures can be seen (Fig. 4.1L). QEMSCAN analysis (Table 4.2; Fig. 4.1M-O) shows the sample contains 49% glass, 24% smectite, 17% zeolites and small amounts of Apatite (2%), Actinolite (2%) and Calcite (1%). The sample has a finer matrix compared to the other samples, clasts are not as visible (Fig. 4.1M) and it is the only sample that contains visible fractures that are filled by zeolites (Fig. 4.1M) and other secondary minerals (Fig. 4.1O). Glass and smectite are common within the matrix along with the secondary minerals (Fig. 4.1M and Fig. 4.1O). The sample from 732 m depth has a grey-greenish colour, with larger basalt clasts within the matrix (Fig. 4.1P) than the 556 m sample. PPL shows rounder clasts than the shallower samples, and QEMSCAN (Table 4.2; Fig. 4.1S), indicates the sample contains mostly glass (58%), smectite (16%) and zeolites (14%), with 3% actinolite (3 %), anorthite (1%) and augite (1%). The glass clasts are hard to distinguish from the ground mass, which is made up of mostly glass and smectite along with zeolites. The zeolite preferentially fills in the pore space (Fig. 4.1R and T). No systematic change in glass content with depth was observed within the samples.

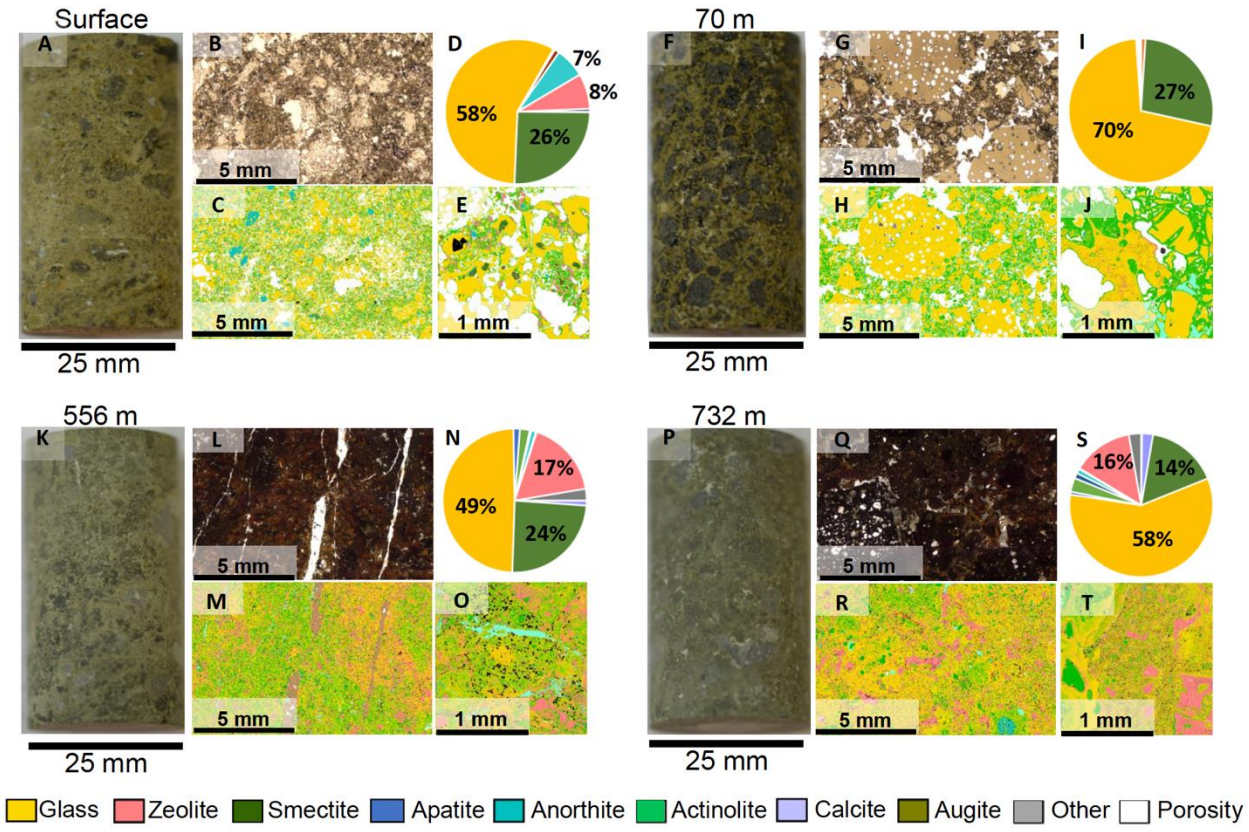

Figure 4.1: Characterisation of the drilled hyaloclastite from different depths within the hydrothermal reservoir at Krafla volcano, NE Iceland : (A-E) surface sample, (F-J) 70m drill core (K-O) 556m and (P-T) 732 m. (A) Sample from surface hyaloclastite containing dark scoria clasts which are matrix supported. (B) Plane-polarised light (PPL) photomicrograph shows angular clasts and heterogeneously distributed porosity (C) A colour-coded mineral distribution map and (D) Pie-chart indicating the fraction of minerals mapped using the QEMSCAN. (E) Zoomed-in version of the colour-coded mineral map shown in panel C. (F) Subsurface 70 m hyaloclastite sample containing prominent dark scoria clasts. (G) PPL photomicrograph showing rounded glassy clasts with vesicles. (H) A colour-coded mineral distribution map and (I) Pie-chart indicating the minerals mapped using QEMSCAN. (J) Zoomed in version of the map in H. (K) Subsurface hyaloclastite from 556 m which is matrix supported and contains some scoria clasts. (L) PPL photomicrograph showing veins/ fractures and finer matrix. (M) A colour-coded mineral distribution obtained by QEMSCAN shows prominent zeolite filled fracture. (N) Pie-chart indicating the quantities of minerals mapped using the QEMSCAN. (O) Zoomed in version of the colour-coded minerals shown in M. (P) Subsurface 732 m hyaloclastite sample containing matrix supported light grey basaltic clasts. (Q) PPL photomicrograph showing a largely dense sample with partly vesicular clasts (R) A colour-coded mineral distribution map obtained by QEMSCAN showing zeolite-filled pore space. (S) Pie-chart indicating the quantities of minerals mapped using QEMSCAN. (T) Zoomed in version of the colour-coded minerals shown in R.

Table 4.2 QEMSCAN quantitative results.

Minerals	0m (Surface)	70 m	556 m	732 m
Glass (%)	57.6	70.3	49.2	58.5
Smectite Fe Mg (%)	25.5	27.3	24.4	16.2
Zeolite (%)	7.9	0.1	17.4	13.6
Anorthite (%)	6.7	0.2	1.1	1.0
Augite (%)	1.1	0.1	0.3	1.2
Quartz (%)	0.1	0.1	0.0	0.2
Actinolite (%)	0.4	0.0	2.2	3.1
Calcite (%)	0.0	1.0	1.1	2.5
Apatite (%)	0.0	0.3	1.5	0.7
Pyrite (%)	0.0	0.0	0.2	0.2
Others (%)	0.6	0.4	2.6	2.8
Total (%)	100	100	100	100

4.3.2 Porosity and Permeability Evolution with Pressure

The hyaloclastites become denser with increasing burial depth within the geothermal system, with porosity reducing from 39.7 % in the surface samples, to 22.1 % in the 70m drill core sample, and reaching an apparent plateau of 12.5 % and 13.3 % in the 556 m and 732m samples respectively (Table 4.3). As an illustrative example, the permeability at an effective pressure of 4 MPa decreases from $2.0x10^{-13}$ m^2 at the surface to $1.4x10^{-15}$ m^2 at 70 m depth as porosity is almost halved, and reduces further to a minimum of $8.7x10^{-20}$ m^2 at 556 m, stabilising to $5.9x10^{-20}$ m^2 at 732 m in the deepest, densest samples (Table 4.3).

Table 4.3 Porosity, permeability, uniaxial compressive strength and Young's modulus results.

Sample		Porosity [%]	Permeability [m^2]*	UCS [MPa]	Young's Modulus [GPa]
Depth	Sample ID				
0 m	H1 0m	39.7			
	H2 0m	39.8			
	H3 0m	38.6			
	H4 0m	40.8		5.4	0.8
	H5 0m	39.7			
	H6 0m	39.8	$2.0x10^{-13}$		
		39.7			
70 m	H1 70m	21.9			
	H2 70m	22.5		10.3	1.4
	H3 70m	19.7	$1.4x10^{-15}$		
	H4 70m	24.0			
		22.1			
556 m	H1 556m	12.1			
	H2 556m	13.8		37.1	8.6
	H3 556m	11.8	$8.7x10^{-20}$		
		12.5			
732 m	H1 732m	13.1			
	H2 732m	12.9		40.0	13.1
	H3 732m	13.9	$5.9x10^{-20}$		
		13.3			

*at Peff = 4 MPa

To simulate burial conditions, we subjected the shallow (surface and 70 m) hyaloclastite samples to isotropic loading (keeping $\sigma_1 = \sigma_2 = \sigma_3$) to observe compaction. Samples were initially loaded to high confining pressure (~40 MPa) and pore pressure, then the pore pressure was gradually reduced to increase the effective pressure whilst continuously monitoring the pore volume. Following an initial consolidation of the sample and the assembly (<2 MPa), the porosity of the surficial sample decreased quasi-linearly until 22-24 MPa, above which, a greater rate of porosity decrease with increasing effective pressure was observed (a steepening of the slope; Fig. 4.2). In contrast, the sample from 70 m depth compacted linearly as effective pressure increased.

In a separate run in which the pore volume and permeability of the sample were evaluated at different, non-continuous pressure increments, we again observed an increase in reduction rate of both porosity and permeability with effective pressure between the 20.2 MPa and 25.9 MPa measurements for the surface sample. Thus, the elastic limit, P*, may be constrained at 22-24 MPa for the surficial hyaloclastite. Following the same procedure, the porosity and permeability of the subsurface 70 m

hyaloclastite both decreased linearly with hydrostatic pressure, demonstrating that P* was not reached up to an effective pressure 40 MPa (Fig. 4.2). The two ways of measuring pore compaction with increasing effective pressure yield similar quantitative changes; compaction is more significant in the more porous surface sample, which reduces by ~8% whilst the lower porosity 70m samples compacted by ~5% (Fig. 4.2).

The sensitivity of permeability reduction to increasing effective pressure also appears to be controlled by the initial porosity and permeability of the samples. The initially most porous, permeable samples from the surface have the largest magnitude decrease in permeability of more than 2 orders of magnitude as effective pressure is increased (Fig 2). The mid-porosity 70m samples have a slightly lesser permeability reduction across the same range of effective pressures. The much lower porosity samples from 556 and 732 m have very low initial permeabilities which are much less sensitive to effective pressure.

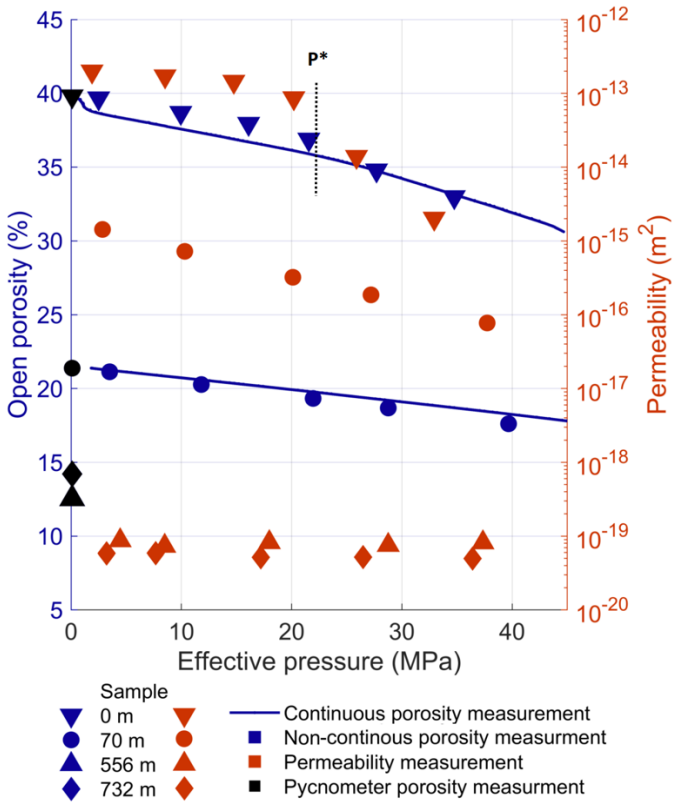

Figure 4.2: Porosity and permeability evolution with increasing effective pressure for the different hyaloclastites. Here, the initial porosity measurement (in black) is made by He-pycnometry for all samples. For the two shallower samples, subsequent measurements are extrapolated by monitoring the volume change in the pumps as the effective pressure is increased via continuous and non-continuous approaches (blue line and blue symbols). Permeability is also measured at increasing pressure increments, highlighting the different susceptibility of the materials to permeability reduction via compaction. For the surface material, we observe a change in the slope of porosity and permeability as a function of effective pressure, marking P.*

4.3.3 Mechanical Fingerprint of Buried Hyaloclastite

The decreasing porosity of the hyaloclastites with increasing depth within the geothermal system corresponds to an increase in uniaxial compressive strength (UCS) from 5.4 MPa in the surface samples, to 10.3 MPa in the 70m drill core sample, 37.1 MPa at 556 m and 40.0 MPa for the deepest samples from 732 m (Table 4.3). Similarly, the Young's modulus increases from 0.8 GPa at the surface to 13.1 GPa at 732 m (Table 4.3).

To understand more about their mechanical fingerprint, systematic, repetitive axial loading of two samples of surficial hyaloclastite was conducted, following the procedure of Bedford et al. (2018), providing reconstructions of the elliptical yield curve. The two yield curves generated for the surficial hyaloclastite were similar and exhibited comparable peaks, marking the transition from the brittle regime (where materials strengthen with pressure and rupture via localised deformation) to the ductile regime (where materials weaken with pressure and compact via pervasive deformation). The peaks occurred at an effective mean stress of 9.2-12.0 MPa, corresponding to a peak strength of ~13 MPa (Fig. 4.3a). Where the sample can no longer withhold any shear stress (differential stress, Q = 0 MPa) the curves (black circles and red triangles; Fig 3a) intersect the effective mean stress (P) axis at a pressure of ~22 MPa, marking P*.

Two samples of surficial hyaloclastite were then compacted by increasing the effective mean stress beyond P*, effectively extending P* to 33 MPa (black boxes; Fig. 4.3a) and 40 MPa (blue triangles; Fig. 4.3a). The resultant yield curves (also mapped via repetitive loading) achieved similar peak strengths of 14 to 15 MPa but the curves are elongate, with shifts in the brittle-ductile transition to a higher effective mean stress of ~12.5 MPa for the sample compacted to 33 MPa and ~ 19 MPa for the sample compacted to 40 MPa (Fig. 4.3a). We further processed the data by normalising each curve against its P* value (where the compacted samples acquired a new apparent P* of 33 and 40 MPa respectively), by dividing the effective mean stress (P) and the differential stress (Q) at each step by the P* value. This was done to allow a direct comparison between different yield curves (after Bedford et al., 2018). The normalised data indicate that Q/P* lowers with the degree of compaction (i.e., with its P* value; Fig. 4.3b).

The strength of the subsurface hyaloclastites collected from boreholes is greater than the surface samples (hollow symbols; Fig. 4.3c) and the yield curves obtained are much greater in magnitude (Fig. 4.3c). The magnitude of the yield curves scales with porosity; the sample from 70 m depth exhibited the brittle-ductile transition at an effective mean stress of ~37.5 MPa, the sample from 556 m did not cross the brittle-ductile transition within the pressure conditions tested (up to 75 MPa) and the deepest sample, from 732 m showed brittle-ductile transition at an effective mean stress of ~68.5 MPa (Fig. 4.3c). The pressure for inelastic compaction (P*) of these hyaloclastites was not met during testing up to >40 MPa for the 70m sample and > 75 MPa for the 556 and 732 m samples.

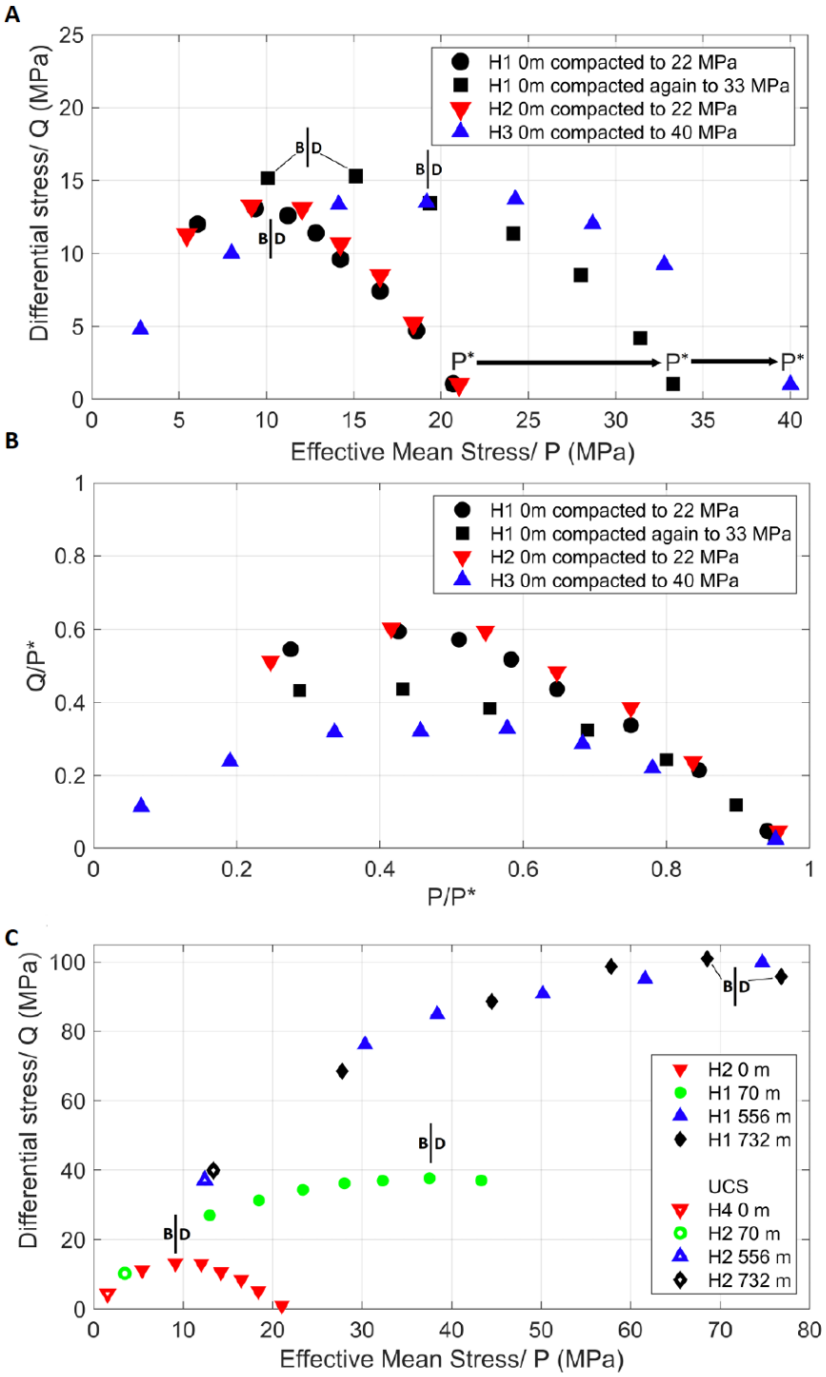

Figure 4.3: Yield curves of hyaloclastites. (A) Yield curves for the surface hyaloclastite, loaded up to P (black circles and red triangles), and compacted by loading past P* to 33 MPa (using the same sample; black squares) and 40 MPa (blue triangles). The samples compacted beyond P* show elongate yield curves. The transition from between brittle to ductile behaviour is shown for each curve (B|D). (B) The data in panel A normalised by dividing each point by its respective P* value. Q/P* decreases as the samples are compacted beyond P*. (C) Yield curves for subsurface hyaloclastite sampled at different depths at Krafla. The yield curve increases in size with decreasing porosity as the samples become stronger. The brittle to ductile transition is shown for each curve, except for the sample from 556 m depth, where it was not met within the pressure conditions tested.*

4.4 Interpretation and Discussion

By mimicking stress conditions from various depths in the geothermal reservoir, we assess and compare the compaction response of surficial and subsurface hyaloclastites during compression. During simulated burial, the surface hyaloclastite transition from elastic to inelastic compaction at an effective pressure of just over 22 MPa (i.e. P*; Fig. 4.2), corresponding to a depth of 1.3 km, assuming that the top part of the reservoir is made of layers of basalt and hyaloclastite with a nominal rock density of ~2,500 $kg.m^{-3}$ and a fluid density of 800 $kg.m^{-3}$ (after Scott et al., 2019). Thus, it is likely that hyaloclastite buried in the geothermal system to depths of at least 1362 m (logged at IDDP-1; Mortensen et al., 2014) at Krafla experienced P*. Moreover, vapour rich hot zones within the reservoir may drop fluid density to below 400 $kg.m^{-3}$ (Scott et al., 2016), causing locally higher effective pressures that could push the hyaloclastite to P*. At higher pressures, the rock compacts, which causes the resultant yield curve of the material to widen, pushing the apparent P* to higher effective pressures without increasing the strength (Fig. 4.3A).

The samples retrieved from depth display much lower porosity and permeability and the porosity and permeability reduction during loading is smaller than the surface samples (Fig. 4.2). The samples also show increasing compressive strength and Young's modulus with burial depth (Table 4.3) and have a greater strength at a given effective pressure (Fig. 4.3C). The subsurface samples have higher magnitude yield curves, with the brittle to ductile transition occurring at significantly higher pressures than the surface samples. Assuming an average rock density of 2,500 $kg.m^{-3}$ and a reservoir fluid density of 800 $kg.m^{-3}$ (Scott et al., 2019) the overburden for the 70 m deep sample would be ~1.2 MPa, the 556 m would be ~9.5 MPa and the 732 m deep sample would be ~12.5 MPa, which places them in the brittle regime at reservoir conditions (Fig. 4.3C). Thus, if high differential stresses were to accumulate, they would cause dilatant rupture. The reservoir is located in a divergent, extensional tectonic setting impacted by recurring volcanic activity (e.g. Einarsson, 1991; Hjartardottir et al., 2012), with a highly varied stress field (Schuler et al., 2016), as such, rupture is not unlikely and would locally enhance fluid circulation (e.g. Eggertsson et al., 2018b; Lamur et al., 2017; Sibson, 1994) within the reservoir.

P* for the reservoir samples would occur at pressures much greater that those experienced in the hyaloclastites in-situ at Krafla, yet, they are likely formed by the inelastic compaction of hyaloclastites similar to those found at the surface, which may have already undergone P*. Such a mechanism however fails to recreate all the characteristics of the hyaloclastites forming the geothermal reservoir (Fig. 4.2; Fig. 4.3), indicating that the porous permeable network within these rocks has been additionally modified.

Several factors may contribute to enhanced closure of porosity and strengthening with burial, including lowering of P* by temperature-induced weakening that enables more complete compaction (Weaver. J et al., In review), and interaction with hydrothermal fluids (Fig. 4.1J, O and T). We observe that the deep hyaloclastites show signs of reactions induced by elevated temperatures and the infill of pores by secondary mineral precipitation. In particular, we note that calcite and zeolite fractions increase with depth, clogging pore space and fractures (Fig. 4.1M and R; Table 4.2) and that the smectite content remains stable with depth until it reduces by ~10% at 732 m. A reduction in the smectite

content may indicate the bottom of the low temperature alteration zone, where smectite is thermodynamically stable. This is often referred to the clay cap within geothermal reservoirs, which is commonly mapped with electrical soundings(e.g. Flovenz et al., 1985; Kristinsdóttir et al., 2010; Lévy et al., 2018; Mortensen et al., 2015), although we note that higher spatial resolution measurements show smectite content is highly variable within the Krafla geothermal field (Lévy et al, 2018).

Comparison of the mineralogical assemblage of the hyaloclastites with the alteration chart of Thien et al. (2015) helps in the assessment of the conditions of alteration. The surficial zeolite-bearing hyaloclastite (with 8% zeolites) indicates a shallow, low-temperature alteration (<50 °C and <5 MPa pressure), whereas the 70 m depth hyaloclastite contains no zeolites, which suggests that it was altered through interaction with volcanic gases and by progressive interaction with meteoric fluids at low pressure (Thien et al., 2015). The deeper samples contain higher amounts of calcite, indicating precipitation from volcanic fluids at higher pressure (25 MPa) and temperature (250 °C). The temperature measurement of ~200 °C within the borehole after drilling (Gautason et al., 2007) suggests the rock may have previously been at a slightly elevated temperature, causing the calcite to fill vesicles in the rock. In combination with burial-induced compaction, modification of the pore space by infilling could result in the low porosity and permeability and increased strength of the subsurface hyaloclastite. Considering that hyaloclastites are variably porous (e.g. Alfredsson et al., 2013; Eggertsson et al., 2018b; Loftsson and Steingrímsson, 2010), it is interesting to note that the model of Thien et al. (2015) suggests that a reduction in porosity slows down the alteration process. This introduces further complexity into the understanding of the hyaloclastite's evolutionary history, including the respective timing of progressive weakening via leaching by fluids (e.g. Thien et al., 2015) or thermal destabilisation (Weaver. J et al., In review) versus strengthening via compaction and secondary mineral precipitation, and how these processes may differ as a function of depth, highlighting the need for dense sampling and high-resolution modelling within these systems.

4.5 Conclusions

This experimental study investigates the mineralogical, physical and mechanical evolution of hyaloclastite upon burial in the active hydrothermal system at Krafla volcano. During the burial of fresh, surficial hyaloclastite in a reservoir, local pressures will increase causing the physical properties (porosity and permeability) of the host material to alter upon exceeding the elastic limit (P*), which prompts collapse of the porous network, resulting in reduced porosity and permeability. This further results in a modification of the yield curve of the rock with a shift in the brittle-ductile transition to a higher effective mean stress. In comparison, subsurface hyaloclastite samples from the reservoir exhibit progressive enhancement of strength and reduction in porosity and permeability with burial depth. The yield curves of the subsurface samples differ significantly from those produced by compaction of fresh surficial hyaloclastite; these samples do not achieve P* within the reservoir conditions and remain within the brittle deformation field at depths where hyaloclastites are present in Krafla. Following compaction of the surficial hyaloclastite beyond P*, the samples fail to recreate the porosity and permeability values measured for subsurface hyaloclastites. Thus, we conclude that burial alone is not sufficient to produce the physical and mechanical properties of the hyaloclastite present in the reservoir. Instead, we invoke the additional importance of mineralogical alteration and

precipitation from hydrothermal fluids occurring at high temperature, which subsequently modified the porous permeable network and led to strengthening of the rock. Mineralogical, physical and mechanical processes are in constant competition during the evolution of rocks within geothermal systems; small spatial and temporal fluctuations in the local pressure-temperature environment will dictate the ability for fluid to flow and the potential for energy extraction.

4.6 Acknowledgements

This study has been supported by Landsvirkjun National Power Company of Iceland and financially supported by Landsvirkjun's Energy Research fund: Y. Lavallée acknowledges grants NÝR-17 – 2015, NÝR-16 – 2016 and NÝR-20 – 2017. This research was further supported by a scholarship from the Institute for Risk and Uncertainty at the University of Liverpool, a Starting Grant from the European Research Council (ERC) to Y. Lavallée on Strain Localisation in Magma (SLiM, no. 306488) and an Early Career Fellowship of the Leverhulme Trust granted to J.E. Kendrick. We acknowledge QEMSCAN technical support of FEI Company, Hillsboro, Oregon, USA.

Chapter 5:

Implications and future work

The nature, formation history and properties of geothermal reservoirs can vary greatly (e.g. Arnorsson, 1995; Bloomberg et al., 2012; Keiding et al., 2010; Rowland and Sibson, 2004; Siratovich et al., 2014; Sæmundsson, 1991). In this project, the permeable and mechanical properties have been investigated, using standard experimental methods that aim to simulate the reservoir conditions at Krafla geothermal system and its response to changes in pressure. The wider context of this work highlights the great variability that can be found in igneous rocks and how rock properties can be affected by fluctuations in pressure within hydrothermal systems and evolution that results from temperature changes or fluid flow. As reservoir models are commonly constructed to simulate the reservoir, to investigate the effects of production, knowledge of the reservoir properties is vital to simulate the reservoir as close as possible (e.g. Bodvarsson, 1988; Cant et al., 2018; Siratovich et al., 2016), or in more recent times, to investigate the fluid flow and temperature distribution close to magmatic conditions (e.g. Axelsson et al., 2014; Scott et al., 2015, 2017).

5.1 Summary of results

In chapter 3, the permeability and storage capacity of both intact and fractured rocks, from the lithologies found within the Krafla reservoir were investigated and constrained. We found that the lithologies exhibit a wide range of porosity and pore structure, having a great effect on their permeability and behaviour under increased pressure. We find that porosity and permeability decrease nonlinearly with increasing effective pressure and that this effect is more pronounced in samples containing a fracture. A fracture within the sample increases the permeability by up to five orders of magnitude and even though increased effective pressure decreased the permeability, it was insufficient to retrieve the intact rock permeability. Imposing a second fracture only increased the permeability slightly but increased the possibility of offset along the fractures and thus persistence of high permeability under confinement. We demonstrated that the fracture surface roughness or fragments lodged within the fracture causes the fracture to stay open and become relatively pressure independent.

Further investigation was also made to investigate the effect of pressure oscillations, thermal stressing and multiple fracturing events on permeability. The results showed that pressurisation/ depressurisation cycles led to the progressive shutting of micro-fractures, which reduced the permeability of the rock. This occurred even though the pore pressure was significantly lower than the confining pressure. This effect may be reversed if the pore pressure locally exceeds the confining pressure, causing the effective pressure to become tensile and allowing fluid flow in the fractures. Thermal stimulation, commonly used to induce a temperature change (i.e. cooling contraction) and therefore stress build-up within a rock, results in an increase in the rock permeability. We correlated this to the formation of micro-fractures, and this was especially effective for the samples that experienced the highest rate of temperature change (caused by water). However, rocks that already contained micro-fractures remained largely unaffected by the thermal stressing.

Overall, the data suggest that thermo-mechanical stimulation should aim to generate fractures in intact materials, or if materials are already damaged within the reservoir then fractures should be generated orthogonal to primary fractures and faults, or at a low angle to the principal stresses, to increase the induced offset at their intersections. Such an approach would favour and maximise fluid flow within the geothermal system.

In chapter 4, the mechanical properties of the different lithologies were investigated to constrain their properties and response to changes in pressure and temperature. The results show that the rock strength is in inversely proportional to the porosity and strongly affected by the abundance of microcracks. As the rock properties vary, some of these rocks can be considered unusually weak, considering their porosity. When buried within the reservoir, the rocks may be subjected to increased pressures exceeding their elastic limit (P*), causing them to compact and resulting in a modification to their pore-structure.

When the induced thermal tensile stress is modelled (chapter 3.4.3), we note that more confined rocks generally have higher Young's modulus, and experience higher induced tensile stresses when subjected to temperature changes. The thermal liability of rocks depends partially on their expansion coefficients (α), in the reservoir rocks expansion of felsite and basalt are very similar, but as the felsite contains quartz, a peak is observed when the quartz crosses the α-β transition within the rock. Integration of the observed mechanical and thermal behaviour and associated permeability into future fluid flow stimulation efforts will aim to increase our understanding and exploitation of geothermal reservoirs, maximising well potential.

Finally, in chapter 5, the evolution of hyaloclastite within an active hydrothermal system has been investigated. As demonstrated in chapters 3 and 4, the hyaloclastite is very weak and permeable, such that under relatively low effective pressures, we pass the elastic limit (P*). As the hyaloclastite gets buried within the reservoir, it is subjected to elevated pressures and temperatures and percolation of potentially corrosive hydrothermal fluids. We find that by applying increased pressure on the rock, it retains permeability far higher than the reservoir hyaloclastites. When the pressure exceeds the elastic limit and the pore structure crumbles however, the permeability decreases rapidly. The yield curve for the surface hyaloclastite reveals that even though we reduce the porosity when we exceed the elastic limit, the strength does not increase but rather forms a plateau of the peak strength. Core samples taken at different depths within the reservoir, show progressive densification and increasing strength as the hyaloclastite were subjected to higher pressures and temperatures. We note that the much higher strength and lower permeability of the reservoir compared to surficial samples may be the result of fracture and pore infilling due to alteration found within the core samples. Comparison of the minerology of the samples also highlights that the alteration history is an influential factor in the evolution of the hyaloclastite within the hydrothermal system.

Overall, the project has constrained the mechanical and permeable properties of the reservoir rocks at Krafla, focusing on the variability found within the different lithologies (e.g. various porosity, mechanical properties and permeability due to their formation history, evolution through time and emplacement). Knowledge of the different rock properties and how they respond to changes in

pressure or temperature allows for more accurate stimulation procedures and ultimately increases the effectiveness of the approaches taken to stimulate the reservoir.

5.2 Implications for hydrothermal systems and Krafla

The work presented here has demonstrated the variability and evolution of rock properties within an active hydrothermal system. When modelling these systems, it is common to assume constant rock properties throughout a single lithology or even on a larger scale. But by assuming the rock properties are constant, the model will not fully capture the potential reservoir response to stimulation or production. Constraining the range of rock properties gives a much better insight into the potential variability expected to be found within each lithology. This also gives good boundary conditions for the model properties, if a single value is used for simplicity. A notable example revealed here is the somewhat unexpected properties of the felsite, with low porosity, high permeability, low UCS and UTS but with significantly higher strengths with increasing confinement, demonstrates the importance of knowledge of the stratigraphy and pressure conditions within the reservoir.

For stimulation and power production from geothermal reservoir, the impact on permeability by imparting fractures has been highlighted. The rock strength is a vital factor here, as to break the rock, its strength must be exceeded. Targeting wells in areas known to have weaker rocks could therefore be beneficial. If the rock is however too weak to withstand the reservoir principal stresses, it could lead to problems during drilling and operation of the reservoir and could eventually a collapse of the well walls. Moreover, it has been noted here that the impact of a fracture on fluid flow is more significantly in initially dense, stronger lithologies.

Krafla also offers one of the most unique and most exciting opportunities for innovative research in volcanology and geothermal power production, as a magma body has been found at shallow depths within the crust (Elders et al., 2014b). This unique opportunity to study shallow magma bodies within the crust and how to utilise the energy potential will both require in-depth knowledge of the rock properties found within the reservoir and close to the magma, and an understanding of how they respond to changes during drilling excursions. Efforts have already been made to try to correlate the drilling data close to the magma with the rock properties and by extrapolation, try to find out which rocks contact the magma body at depth, where no cuttings were retrieved (Saubin et al., 2018).

5.2.1 Well RN-37 within the Reykjanes geothermal field, south-west Iceland

To understand the direct relevance of the results of this thesis to geothermal exploitation in areas outside the Krafla geothermal reservoir, the findings within the thesis have been applied to a drill site in Reykjanes peninsula, south-west Iceland. The knowledge was used to identify a location and select the well trajectory for a new geothermal well within the high temperature field of Reykjanes. The well, RN-37, had the objectives to be a deep well, with feed zones below 2000 m and to reach fluid enthalpy of >1300 $kJ.kg^{-1}$. The results of the thesis were especially applied for three aspects of the well selected trajectory and stimulation procedure; 1) the results highlighted the importance of open fractures for fluid flow. This led to higher emphasis on defining active fractures within the reservoir and its stress field. 2) Stimulation procedures do not need to aim towards rapid heating and cooling during thermal stimulation, as samples experiencing slower thermal cycles experienced very similar effects on the

permeability. This emphasises that the cold waterfront should be pushed further within the well, with longer periods of cold-water injection and allowing the well to heat up for longer (10 days of injection instead of commonly performed 18 hours with and heating up periods of 8 days instead of 10 hours). Therefore, the drill used to drill the well can be removed after drilling, as lower capacity water pumps can be used during the stimulation procedure. 3) Alteration of hyaloclastite at Krafla emphasised the effect alteration can have, so active faults with previously noted damage zones that had been identified within this area were targeted, as their permeability was elevated.

Right after drilling, the well heated up much quicker than previously seen within the Reykjanes field and it is currently being flow tested, but results already show that it is a very successful well, which will become a producing well before the end of the year, which makes the turnaround for the well very fast, compared to other wells.

5.3 Suggestions for future work

Even though the work within this project has demonstrated the importance of defining rock properties within the hydrothermal reservoir at Krafla volcano, and many questions are addressed, new ones also arise from these results.

One of the main questions within the geothermal sector regards thermal stimulation and how to optimise the stimulation procedure (e.g. Axelsson et al., 2006). From our simulation within the laboratory, we see clearly that cycling the temperature from 450°C to room temperature causes increased micro-fracturing within the dense rock for the first 5 cycles, but for the already microfractured rocks, the temperature change does not cause any further increase in permeability. From a small dataset that was collected on the same basalt, but with lower temperature thresholds (Eggertsson et al., 2018a), this change in permeability cannot be seen. Within a reservoir, where the lithological boundaries and orientation and magnitudes of the principal stresses will affect the stimulation process, it is important to investigate what the main controlling factors are, to ensure the success of the stimulation and optimising the well.

A second interesting question that arises, is how permeability is affected by temperature of the hydrothermal system. This has been looked into in the laboratory (e.g. Kushnir et al., 2017) and even directly recorded within reservoirs (e.g. Gunnarsson, 2011), but further constraints for fractured reservoirs are important. The experience from Hellisheiði hydrothermal system in Iceland (Gunnarsson, 2011) shows that the relationship is reversible, such that if the fluid temperature is cycled, the permeability of the well also cycles, causing changes in the injectivity index of the well. This might play a role in the alteration state of the reservoir and the triggering of mineral precipitation. In Krafla, this becomes especially important due the shallow magma chamber within the system at 2.1 km depth (Elders et al., 2014b). At this depth, the principal stresses are not very great, compared to deeper within the reservoir, and the magma chamber seems to be in good equilibrium with its surrounding pressures (Elders et al., 2011). Pressure changes that occur due to drilling and exploration around the magma may cause changes in circulation and temperature that might prove to be challenging to deal with.

With the great opportunity in Krafla, to study and exploit magma at shallow depth within the crust, more focus needs to be shifted towards the in-situ stresses within the reservoir and how the physical properties of the rocks respond to the changes that occur. To date, no geo-mechanical model has been constructed that considers all the various datasets available for the Krafla reservoir. Earthquake data (e.g. Schuler et al., 2016), along with geological indicators found within the reservoir, provide a partial understanding but a complete model would be of great benefit to the proposition to drill into or close to the magma. Dealing with very hot rocks and magma bodies during drilling is poorly understood. For example, the expansion coefficient for the felsite, which is thought to overlay the rhyolitic magma body, showed small changes in expansion until it reached the α-β transition in quartz, when it increased by an order of magnitude over the temperature threshold of 573°C. The full effect this has within the reservoir, once a drill penetrates the rock is unclear. The felsite found at >2000 m depth in Krafla might already be heavily micro-fractured from the formation of Víti crater (from a phreatomagmatic explosion in 1724), so this transition threshold could help open the rock up for increased permeability. Circulation loss was experienced around this depth when the well IDDP-1 was drilled (Palsson et al., 2014), which therefore suggests it has great potential for the extraction of steam.

Further attention should also be given to the importance of cores from active hydrothermal reservoirs. During drilling, it is very uncommon to collect cores at depth, however some experience has been gained through the IDDP project (Fowler and Zierenberg, 2016; Fowler et al., 2015; Friðleifsson et al., 2017; Marks et al., 2015). It has been shown that the evolution of hyaloclastite, from the surface into the hydrothermal system, can have a great effect on its properties. To fully understand these systems, hands-on samples from within them is the best way to gain knowledge, when coupled with other commonly utilised methods.

References

Al-Harthi, A. A., Al-Amri, R. M., and Shehata, W. M., 1999, The porosity and engineering properties of vesicular basalt in Saudi Arabia: Eng Geol, v. 54.

Alam, A. K. M. B., Niioka, M., Fujii, Y., Fukuda, D., and Kodama, J.-i., 2014, Effects of confining pressure on the permeability of three rock types under compression: International Journal of Rock Mechanics and Mining Sciences, v. 65, p. 49-61.

Alfredsson, H. A., Oelkers, E. H., Hardarsson, B. S., Franzson, H., Gunnlaugsson, E., and Gislason, S. R., 2013, The geology and water chemistry of the Hellisheidi, SW-Iceland carbon storage site: International Journal of Greenhouse Gas Control, v. 12, p. 399-418.

Allis, R., Bromley, C., and Currie, S., 2009, Update on subsidence at the Wairakei-Tauhara geothermal system, New Zealand: Geothermics, v. 38, no. 1, p. 169-180.

Allis, R. G., and Zhan, X. Y., 2000, Predicting subsidence at Wairakei and Ohaaki geothermal fields, New Zealand: Geothermics, v. 29, no. 4-5, p. 479-497.

Anderson, E. M., 1951, The Dynamics of Faulting and Dyke Formation With Applications to Britain, Edinburgh, UK, Oliver and Boyd.

Annen, C., Blundy, J. D., Leuthold, J., and Sparks, R. S. J., 2015, Construction and evolution of igneous bodies: Towards an integrated perspective of crustal magmatism: Lithos, v. 230, p. 206-221.

Aqui, A. R., and Zarrouk, S., Permeability enhancement of conventional geothermal wells, *in* Proceedings New Zealand Geothermal Workshop, Auckland, New Zealand, 2011.

Armannsson, H., 2016, The fluid geochemistry of Icelandic high temperature geothermal areas: Applied Geochemistry, v. 66, p. 14-64.

Arnorsson, S., 1995, Geothermal systems in Iceland: Structure and conceptual models .1. High-temperature areas: Geothermics, v. 24, no. 5-6, p. 561-602.

Arnorsson, S., Axelsson, G., and Saemundsson, K., 2008, Geothermal systems in Iceland: Jokull, v. 58, p. 269-302.

Ashwell, P. A., Kendrick, J. E., Lavallée, Y., Kennedy, B. M., Hess, K. U., von Aulock, F. W., Wadsworth, F. B., Vasseur, J., and Dingwell, D. B., 2015, Permeability of compacting porous lavas: Journal of Geophysical Research: Solid Earth, v. 120, no. 3, p. 2014JB011519.

Austin-Erickson, A., Buttner, R., Dellino, P., Ort, M. H., and Zimanowski, B., 2008, Phreatomagmatic explosions of rhyolitic magma: Experimental and field evidence: Journal of Geophysical Research-Solid Earth, v. 113, no. B11.

Axelsson, G., Egilson, T., and Gylfadottir, S. S., 2014, Modelling of temperature conditions near the bottom of well IDDP-1 in Krafla, Northeast Iceland: Geothermics, v. 49, p. 49-57.

Axelsson, G., Thórhallsson, S., and Björnsson, G., 2006, Stimulation of geothermal wells in basaltic rock in Iceland, ENGINE – ENhanced Geothermal Innovative Network for Europe, Workshop 3, "Stimulation of reservoir and microseismicity": Kartause Ittingen, Zürich.

Ayling, M. R., Meredith, P. G., and Murrell, S. A. F., 1995, Microcracking during triaxial deformation of porous rocks monitored by changes in rock physical properties, I. Elastic-wave propagation measurements on dry rocks: Tectonophysics, v. 245 p. 205-225.

Bachmann, O., Miller, C. F., and de Silva, S. L., 2007, The volcanic-plutonic connection as a stage for understanding crustal magmatism: Journal of Volcanology and Geothermal Research, v. 167, no. 1-4, p. 1-23.

Barton, C. A., and Zoback, M. D., 1992, Self-similar distribution and properties of macroscopic fractures at depth in crystalline rock in the Cajon Pass Scientific Drill Hole: J Geophys Res, v. 97.

Barton, C. A., Zoback, M. D., and Moos, D., 1995, Fluid-flow along potentially active faults in crystalline rock: Geology, v. 23, no. 8, p. 683-686.

Baud, P., Klein, E., and Wong, T. F., 2004, Compaction localization in porous sandstones: spatial evolution of damage and acoustic emission activity: Journal of Structural Geology, v. 26, no. 4, p. 603-624.

Baud, P., Schubnel, A., and Wong, T. F., 2000, Dilatancy, compaction, and failure mode in Solnhofen limestone: Journal of Geophysical Research-Solid Earth, v. 105, no. B8, p. 19289-19303.

Baud, P., Wong, T.-F., and Zhu, W., 2014, Effects of porosity and crack density on the compressive strength of rocks, Int J Rock Mech Min Sci.

Bauer, S. J., Friedman, M., and Handin, J., 1981, Effects of water-saturated on strength and ductility of three igneous rocks at effective pressures to 50 MPa and temperatures to partial melting., *in* Einstein, H. H., Scandriato, D.P. , ed., Rock Mechanics from Research to Application.: Rotterdam,, Balkema, p. pp. 79-84.

Bedford, J. D., Faulkner, D. R., Leclere, H., and Wheeler, J., 2018, High-Resolution Mapping of Yield Curve Shape and Evolution for Porous Rock: The Effect of Inelastic Compaction on Porous Bassanite: Journal of Geophysical Research-Solid Earth, v. 123, no. 2, p. 1217-1234.

Benson, P. M., Meredith, P. G., Platzman, E. S., and White, R. E., 2005, Pore fabric shape anisotropy in porous sandstones and its relation to elastic wave velocity and permeability anisotropy under hydrostatic pressure: International Journal of Rock Mechanics and Mining Sciences, v. 42, no. 7-8, p. 890-899.

Bibby, H. M., Caldwell, T. G., Davey, F., and Webb, T., 1995, Geophysical evidence on the structure of the Taupo Volcanic Zone and its hydrothermal circulation: J Volcanol Geotherm Res, v. 68.

Bjarnason, I. P., 2008, An Iceland hotspot saga: Jokull, v. 58, p. 3-16.

Bjornsson, A., Saemundsson, K., Einarsson, P., Tryggvason, E., and Gronvold, K., 1977, Current rifting episode in North Iceland: Nature, v. 266, no. 5600, p. 318-323.

Björnsson, A., Sæmundsson, K., Sigmundsson, F., Halldórsson, P., Sigbjörnsson, R., and Snæbjörnsson, J. Þ., 2007, Geothermal Projects in NE Iceland at Krafla, Bjarnarflag, Gjástykki and Theistarreykir - Assessment of geo-hazards affecting energy production and transmission systems emphasizing structural design criteria and mitigation of risk: Landsvirkjun.

Bloomberg, S., Rissmann, C., Mazot, A., Oze, C., Horton, T., Kennedy, B., Werner, C., Christenson, B., and Pawson, J., 2012, Soil gas flux exploration at the Rotokawa Geothermal Field and White Island, New Zealand, Proceedings, Thirty Sixth Workshop on Geothermal Reservoir Engineering: Stanford, California, Stanford University.

Blundy, J., Cashman, K., and Humphreys, M., 2006, Magma heating by decompression-driven crystallization beneath andesite volcanoes: Nature, v. 443, no. 7107, p. 76-80.

Bodvarsson, G. S., 1988, Model predictions of Svartsengi reservoir, Iceland: Water Resources Research, v. 24, no. 10, p. 1740-1746.

Bodvarsson, G. S., Pruess, K., Stefansson, V., Bjornsson, S., and Ojiambo, S. B., 1987, East Olkaria geothermal-fueld, Kenya. 1. History match with production and pressure decline data: Journal of Geophysical Research-Solid Earth and Planets, v. 92, no. B1, p. 521-539.

Bodvarsson, G. S., Pruess, K., Stefansson, V., and Eliasson, E. T., 1984, The Krafla Geothermal Field, Iceland: 2. The Natural State of the System: Water Resource research, v. 20, no. 11, p. 14.

Bolognesi, L., and Damore, F., 1993, Isotopic variation of the hydrothermal system on Volcano-Island, Italy: Geochimica Et Cosmochimica Acta, v. 57, no. 9, p. 2069-2082.

Bonafede, M., 1991, Hot fluid migration - An efficient source of ground deformation - application to the 1982 - 1985 crisis at Campi Flegrei - Italy: Journal of Volcanology and Geothermal Research, v. 48, no. 1-2, p. 187-198.

Bourbie, T., and Zinszner, B., 1985, Hydraulic and acoustic properties as a function of porosity in Fontainebleau Sandstone: Journal of Geophysical Research: Solid Earth, v. 90, no. B13, p. 11524-11532.

Brace, W. F., 1980, Permeability of crystalline and argillaceous rocks: International Journal of Rock Mechanics and Mining Sciences, v. 17, no. 5, p. 241-251.

Brace, W. F., Paulding, B., and Scholz, C., 1966, Dilatancy in the fracture of crystalline rocks: J Geophys Res, v. 71.

Brace, W. F., Walsh, J. B., and Frangos, W. T., 1968, Permeability of granite under high pressure: Journal of Geophysical Research, v. 73, no. 6, p. 2225-2236.

Brinton, D., McLin, K., and Moore, J., The chemical stability of Bauxite and quartz sand proppants under geothermal conditions, *in* Proceedings 36th Stanford Geothermal workshop on Geothermal Reservoir Engineering, Stanford, California, 2011.

Bromley, C., Brockbank, K., Glynn-Morris, T., Rosenberg, M., Pender, M., O'Sullivan, M., and Currie, S., 2013, Geothermal subsidence study at Wairakei-Tauhara, New Zealand: Proceedings of the Institution of Civil Engineers-Geotechnical Engineering, v. 166, no. 2, p. 211-223.

Browning, J., Meredith, P., and Gudmundsson, A., 2016, Cooling-dominated cracking in thermally stressed volcanic rocks: Geophysical Research Letters, v. 43, no. 16, p. 8417-8425.

Bubeck, A., Walker, R. J., Healy, D., Dobbs, M., and Holwell, D. A., 2017, Pore geometry as a control on rock strength: Earth and Planetary Science Letters, v. 457, p. 38-48.

Byerlee, J. D., 1978, Friction of rocks: Pure Appl Geophys, v. 116.

Camacho, G. T., and Ortiz, M., 1996, Computational modelling of impact damage in brittle materials: International Journal of Solids and Structures, v. 33, no. 20-22, p. 2899-2938.

Cant, J. L., Siratovich, P. A., Cole, J. W., Villeneuve, M. C., and Kennedy, B. M., 2018, Matrix permeability of reservoir rocks, Ngatamariki geothermal field, Taupo Volcanic Zone, New Zealand: Geothermal Energy, no. 6:2.

Carlino, S., Somma, R., Troise, C., and De Natale, G., 2012, The geothermal exploration of Campanian volcanoes: Historical review and future development: Renewable & Sustainable Energy Reviews, v. 16, no. 1, p. 1004-1030.

Carman, P., 1937, Fluid flow though a granular bed: Transactions, Institution of Chemical Engineers, no. 15, p. 150-167.

Castro, J. M., and Dingwell, D. B., 2009, Rapid ascent of rhyolitic magma at Chaiten volcano, Chile: Nature, v. 461, no. 7265, p. 780-U729.

Coats, R., Kendrick, J. E., Wallace, P. A., Miwa, T., Hornby, A. J., Ashworth, J. D., Matsushima, T., and Lavallee, Y., 2018, Failure criteria for porous dome rocks and lavas: a study of Mt. Unzen, Japan: Solid Earth, v. 9, no. 6, p. 1299-1328.

Cole, R. P., White, J. D. L., Conway, C. E., Leonard, G. S., Townsend, D. B., and Pure, L. R., 2018, The glaciovolcanic evolution of an andesitic edifice, South Crater, Tongariro volcano, New Zealand: Journal of Volcanology and Geothermal Research, v. 352, p. 55-77.

Collar, R. J., and Browne, P. R. L., 1985, Hydrothermal eruptions at The Rotokawa Geothermal Field, Taupo Volcanic Zone, New Zealand, Proceedings of the seventh New Zealand geothermal workshop, University of Auckland: Auckland, New Zealand, Geothermal Institute.

Colombier, M., Wadsworth, F. B., Gurioli, L., Scheu, B., Kueppers, U., Di Muro, A., and Dingwell, D. B., 2017, The evolution of pore connectivity in volcanic rocks: Earth and Planetary Science Letters, v. 462, p. 99-109.

Cooper, H. W., and Simmons, G., 1977, The effect of cracks on the thermal expansion of rocks: Earth and Planetary Science Letters, v. 36, no. 3.

Cooper, K. M., 2019, Time scales and temperatures of crystal storage in magma reservoirs: implications for magma reservoir dynamics: Philosophical Transactions of the Royal Society a-Mathematical Physical and Engineering Sciences, v. 377, no. 2139.

Costa, A., 2006, Permeability-porosity relationship: a re-examination of the Kozeny-Carman equation based on a fractal pore-space geometry assumption, Geophys Res Lett.

Curewitz, D., and Karson, J. A., 1997, Structural settings of hydrothermal outflow: Fracture permeability maintained by fault propagation and interaction: Journal of Volcanology and Geothermal Research, v. 79, no. 3-4, p. 149-168.

Darcy, H., 1856, Les fontaines publiques de la ville de Dijon, Paris, Dalmont.

Darling, W. G., and Armannsson, H., 1989, Stable isotopic aspects of fluid-flow in the Krafla, Namufjall and Theistareykir geothermal system of north Iceland: Chemical Geology, v. 76, no. 3-4, p. 197-213.

David, C., Menendez, B., and Darot, M., 1999, Influence of stress-induced and thermal cracking on physical properties and microstructure of La Peyratte granite: International Journal of Rock Mechanics and Mining Sciences, v. 36, no. 4, p. 433-448.

Degraff, J. M., and Aydin, A., 1993, Effect of thermal regime on growth increment and spacing of contraction joints in basaltic lava: Journal of Geophysical Research-Solid Earth, v. 98, no. B4, p. 6411-6430.

Degruyter, W., Bachmann, O., and Burgisser, A., 2010, Controls on magma permeability in the volcanic conduit during the climactic phase of the Kos Plateau Tuff eruption (Aegean Arc): Bulletin of Volcanology, v. 72, no. 1, p. 63-74.

Demets, C., Gordon, R. G., Argus, D. F., and Stein, S., 1994, Effect of recent revisions to the geomagnetic reversal time-scale on estimates of current plate movements: Geophysical Research Letters, v. 21, no. 20, p. 2191-2194.

Dolino, G., Bachheimer, J. P., and Zeyen, C. M. E., 1983, Observation of an intermediate phase near the alpha-beta transition of quartz by heat-capacity and neutron-scattering measurements: Solid State Communications, v. 45, no. 3, p. 295-299.

Drief, A., and Schiffman, P., 2004, Very low-temperature alteration of sideromelane in hyaloclastites and hyalotuffs from Kilauea and Mauna Kea volcanoes: Implications for the mechanism of palagonite formation: Clays and Clay Minerals, v. 52, no. 5, p. 622-634.

Druitt, T. H., and Kokelaar, B. P., 2002, The Eruption of Soufrière Hills Volcano, Montserrat, from 1995 to 1999. : The Geological Society Memoir 21. London.

Edmonds, M., Cashman, K. V., Holness, M., and Jackson, M. D., 2019, Architecture and dynamics of magma reservoirs: Philosophical Transactions of the Royal Society a-Mathematical Physical and Engineering Sciences, v. 377, no. 2139, p. 29.

Edmonds, M., and Herd, R. A., 2007, A volcanic degassing event at the explosive-effusive transition: Geophys. Res. Lett., v. 34, no. 21, p. L21310.

Eggertsson, G. H., Lavallée, Y., and Kendrick, J. E., 2018a, Impact of thermo-mechanical stimulation on the reservoir rocks of the geothermal system at Krafla, Iceland, Stanford Geothermal Workshop 43rd annual: Stanford.

Eggertsson, G. H., Lavallée, Y., Kendrick, J. E., Lamur, A., and Markússon, S., 2016, Enhancing permeability by multiple fractures in the Krafla geothermal reservoir, Iceland, European Geothermal Congress: Strasbourg, European Geothermal Congress.

Eggertsson, G. H., Lavallée, Y., Kendrick, J. E., and Markússon, S. H., 2018b, Improving fluid flow in geothermal reservoirs by thermal and mechanical stimulation: The case of Krafla volcano, Iceland: Journal of Volcanology and Geothermal Research.

Eichelberger, J., Ingolfsson, H. P., Carrigan, C., Lavallee, Y., Tester, J. W., and Markusson, S. H., 2018, Krafla magma testbed: Understanding and using the magma-hydrothermal connection, Geothermal Resources Council Vol. 42: Reno, NV, Geothermal Reserouce Council, p. 2396-2405.

Eichelberger, J. C., Carrigan, C. R., Westrich, H. R., and Price, R. H., 1986, Non-explosive silicic volcanism: Nature, v. 323, no. 6089, p. 598-602.

Einarsson, P., 1978, S-wave shadows in the Krafla caldera in NE Iceland: evidence for a magma chamber in the crust: Bulletin of Volcanology, v. 41, no. 3, p. 8.

-, 1991, The Krafla rifting episode 1975–1989 (Umbrotin við Kröflu 1975-89 in Icelandic), Reykjavík, Hið íslenska náttúrufræðifélag, Náttúra Mývatns, 43 p.:

Einarsson, P., Sigmundsson, F., Sturkell, E., Árnadóttir, Þ., Pedersen, R., Pagli, C., and Geirsson, H., Geodynamic signals detected by geodetic methods in Iceland, *in* Proceedings Wissenschaftliche Arbeiten der Fachrichtung Geodäsie und Geoinformatik der Universität Hannover, Hannover, 2006, p. 39–57.

Elders, W. A., Fridleifsson, G. O., and Albertsson, A., 2014a, Drilling into magma and the implications of the Iceland Deep Drilling Project (IDDP) for high-temperature geothermal systems worldwide: Geothermics, v. 49, p. 111-118.

Elders, W. A., Fridleifsson, G. O., and Palsson, B., 2014b, Iceland Deep Drilling Project: The first well, IDDP-1, drilled into magma Preface: Geothermics, v. 49, p. 1-1.

Elders, W. A., Frioleifsson, G. O., Zierenberg, R. A., Pope, E. C., Mortensen, A. K., Guomundsson, A., Lowenstern, J. B., Marks, N. E., Owens, L., Bird, D. K., Reed, M., Olsen, N. J., and Schiffman, P., 2011, Origin of a rhyolite that intruded a geothermal well while drilling at the Krafla volcano, Iceland: Geology, v. 39, no. 3, p. 231-234.

Fakhimi, A., and Gharahbagh, E. A., 2011, Discrete element analysis of the effect of pore size and pore distribution on the mechanical behavior of rock: International Journal of Rock Mechanics and Mining Sciences, v. 48, no. 1, p. 77-85.

Farquharson, J., Heap, M. J., Varley, N. R., Baud, P., and Reuschlé, T., 2015, Permeability and porosity relationships of edifice-forming andesites: A combined field and laboratory study: Journal of Volcanology and Geothermal Research, v. 297, p. 52-68.

Farquharson, J. I., Wadsworth, F. B., Heap, M. J., and Baud, P., 2017, Time-dependent permeability evolution in compacting volcanic fracture systems and implications for gas overpressure: Journal of Volcanology and Geothermal Research, v. 339, p. 81-97.

Faulkner, D. R., and Armitage, P. J., 2013, The effect of tectonic environment on permeability development around faults and in the brittle crust: Earth and Planetary Science Letters, v. 375, p. 71-77.

Fialko, Y. A., and Rubin, A. M., 1997, Numerical simulation of high-pressure rock tensile fracture experiments: Evidence of an increase in fracture energy with pressure?: Journal of Geophysical Research-Solid Earth, v. 102, no. B3, p. 5231-5242.

Flores, M., Davies, D., Couples, G., and Palsson, B., Stimulation of Geothermal Wells, Can We Afford It?, *in* Proceedings World Geothermal Congress, Antalya, Turkey, 2005.

Flovenz, O. G., Georgsson, L. S., and Arnason, K., 1985, Resestivity structure of the upper crust in Iceland: Journal of Geophysical Research-Solid Earth and Planets, v. 90, no. NB12, p. 136-150.

Fournier, R. O., 1999, Hydrothermal processes related to movement of fluid from plastic into brittle rock in the magmatic-epithermal environment: Economic Geology and the Bulletin of the Society of Economic Geologists, v. 94, no. 8, p. 1193-1211.

Fowler, A. P. G., and Zierenberg, R. A., 2016, Geochemical bias in drill cutting samples versus drill core samples returned from the Reykjanes Geothermal System, Iceland: Geothermics, v. 62, p. 48-60.

Fowler, A. P. G., Zierenberg, R. A., Schiffman, P., Marks, N., and Frioleifsson, G. O., 2015, Evolution of fluid-rock interaction in the Reykjanes geothermal system, Iceland: Evidence from Iceland Deep Drilling Project core RN-17B: Journal of Volcanology and Geothermal Research, v. 302, p. 47-63.

Fridleifsson, G. O., and Elders, W. A., 2005, The Iceland Deep Drilling Project: a search for deep unconventional geothermal resources: Geothermics, v. 34, no. 3, p. 269-285.

Fridleifsson, G. O., Elders, W. A., and Albertsson, A., 2014, The concept of the Iceland deep drilling project: Geothermics, v. 49, p. 2-8.

Fridleifsson, G. O., Elders, W. A., Zierenberg, R. A., Stefansson, A., Fowler, A. P. G., Weisenberger, T. B., Hardarson, B. S., and Mesfin, K. G., 2017, The Iceland Deep Drilling Project 4.5km deep well, IDDP-2, in the seawater-recharged Reykjanes geothermal field in SW Iceland has successfully reached its supercritical target: Scientific Drilling, v. 23, p. 1-12.

Friðleifsson, G. Ó., Elders, W. A., Zierenberg, R., Weisenberger, T. B., Harðarson, B. S., Stefánsson, A., Gíslason, Þ., Sigurðsson, Ó., Þórólfsson, G., Mesfin, K. G., Sverrisdóttir, S. B., Hafnadóttir, M. Ó., Kruszewski, M., Calicki, A., Einarsson, G. M., Níelsson, S., Gunnarsdóttir, S. H., and Poux, B., 2017, The drilling of the Iceland Deep Drilling Project geothermal well at Reykjanes has been successfully completed.: DeepEGS.

Fukuhara, M., and Sampei, A., 2001, Stress-induced pyroelectric properties of devitrified fused quartz in elevated temperature: Journal of Materials Science-Materials in Electronics, v. 12, no. 2, p. 131-135.

Gaherty, J. B., 2001, Seismic evidence for hotspot-induced buoyant flow beneath the Reykjanes Ridge: Science, v. 293, no. 5535, p. 1645-1647.
Gallois, R., 2007, The formation of the hot springs at Bath Spa, UK: Geological Magazine, v. 144, no. 4, p. 741-747.
Gaunt, H. E., Sammonds, P. R., Meredith, P. G., Smith, R., and Pallister, J. S., 2014, Pathways for degassing during the lava dome eruption of Mount St. Helens 2004–2008: Geology, v. 42, no. 11, p. 947-950.
Gautason, B., Egilson, Þ., Blishke, A., and Daníelsen, P. E., 2007, KRAFLA: Borun tveggja kjarnaholna, KH-5 og KH-6 veturinn 2006-2007 (e. KRAFLA: Drilling of two core holes, KH-5 and KH-6 winter 2006-2007).
Ghassemi, A., 2012, A Review of Some Rock Mechanics Issues in Geothermal Reservoir Development: Geotechnical and Geological Engineering, v. 30, no. 3, p. 647-664.
Gislason, S. R., and Arnorsson, S., 1993, Dissolution of primary basaltic minerals in natural waters: saturation state and kinetics: Chemical Geology, v. 105, no. 1-3, p. 117-135.
Glover, P. W. J., Baud, P., Darot, M., Meredith, P. G., Boon, S. A., LeRavalec, M., Zoussi, S., and Reuschle, T., 1995, alpha/ beta phase transition in quartz monitored using acoustic emissions: Geophysical Journal International, v. 120, p. 775-782.
Grant, M. A., Clearwater, J., Quinão, J., Bixley, P. F., and Le Brun, M., Thermal stimulation of geothermal wells: a review of field data, *in* Proceedings Proceedings2013.
Griffith, A. A., 1920, The phenomena of rupture and flow in rocks: Philosophical transactions of the Royal Society of London, v. 221, no. Series A, p. 163-197.
Griffiths, L., Heap, M. J., Xu, T., Chen, C. F., and Baud, P., 2017, The influence of pore geometry and orientation on the strength and stiffness of porous rock: Journal of Structural Geology, v. 96, p. 149-160.
Gruber, J. A., 2018, Accurate Data Reduction for the Uniaxial Compression Test: Experimental Techniques, v. 42, no. 2, p. 209-221.
Gudmundsson, A., 1995, Infrastructure and mecahnics of volcanic systems in Iceland: Journal of Volcanology and Geothermal Research, v. 64, no. 1-2, p. 1-22.
Gudmundsson, J. S., and Thorhallsson, S., 1986, THE SVARTSENGI RESERVOIR IN ICELAND: Geothermics, v. 15, no. 1, p. 3-15.
Gudmundsson, M. T., Larsen, G., Hoskuldsson, A., and Gylfason, A. G., 2008, Volcanic hazards in Iceland: Jokull, v. 58, p. 251-268.
Gueguen, Y., and Fortin, J., 2013, Elastic envelopes of porous sandstones: Geophysical Research Letters, v. 40, no. 14, p. 3550-3555.
Guillou-Frottier, L., Carre, C., Bourgine, B., Bouchot, V., and Genter, A., 2013, Structure of hydrothermal convection in the Upper Rhine Graben as inferred from corrected temperature data and basin-scale numerical models: Journal of Volcanology and Geothermal Research, v. 256, p. 29-49.
Gunnarsson, G., Mastering reinjection in the Hellisheidi field, SW-Iceland: a story of successes and failuers, *in* Proceedings Thirty-Sixth Workshop on Geothermal Reservoir Engineering, Stanford, California, 2011.
Gutierrez, F., Gioncada, A., Ferran, O. G., Lahsen, A., and Mazzuoli, R., 2005, The Hudson Volcano and surrounding monogenetic centres (Chilean Patagonia): An example of volcanism associated with ridge-trench collision environment: Journal of Volcanology and Geothermal Research, v. 145, no. 3-4, p. 207-233.
Guðmundsson, Á., 2001, An expansion of the Krafla Power Plant from 30 to 60 MWe - Geothermal considerations: Geothermal Resources council transactions, v. 25, p. 6.
Hansell, A., and Oppenheimer, C., 2004, Health hazards from volcanic gases: A systematic literature review: Archives of Environmental Health, v. 59, no. 12, p. 628-639.
Hashida, T., and Takahashi, H., 1993, Significance of Ae Crack Monitoring in Fracture-Toughness Evaluation and Nonlinear Rock Fracture-Mechanics: International Journal of Rock Mechanics and Mining Sciences & Geomechanics Abstracts, v. 30, no. 1, p. 47-60.

Hauksson, T., Markusson, S., Einarsson, K., Karlsdottir, S. N., Einarssond, A., Moller, A., and Sigmarsson, P., 2014, Pilot testing of handling the fluids from the IDDP-1 exploratory geothermal well, Krafla, NE Iceland: Geothermics, v. 49, p. 76-82.

Heap, M., Xu, T., and Chen, C.-f., 2014a, The influence of porosity and vesicle size on the brittle strength of volcanic rocks and magma: Bulletin of Volcanology, v. 76, no. 9, p. 1-15.

Heap, M. J., Baud, P., Meredith, P. G., Vinciguerra, S., Bell, A. F., and Main, I. G., 2011, Brittle creep in basalt and its application to time-dependent volcano deformation: Earth and Planetary Science Letters, v. 307, no. 1–2, p. 71-82.

Heap, M. J., Baud, P., Meredith, P. G., Vinciguerra, S., and Reuschlé, T., 2014b, The permeability and elastic moduli of tuff from Campi Flegrei, Italy: implications for ground deformation modelling: Solid Earth, v. 5, no. 1, p. 25-44.

Heap, M. J., Farquharson, J. I., Baud, P., Lavallee, Y., and Reuschle, T., 2015a, Fracture and compaction of andesite in a volcanic edifice: Bulletin of Volcanology, v. 77, no. 6.

Heap, M. J., and Kennedy, B. M., 2016, Exploring the scale-dependent permeability of fractured andesite: Earth and Planetary Science Letters, v. 447, p. 139-150.

Heap, M. J., Kennedy, B. M., Pernin, N., Jacquemard, L., Baud, P., Farquharson, J. I., Scheu, B., Lavallee, Y., Gilg, H. A., Letham-Brake, M., Mayer, K., Jolly, A. D., Reuschle, T., and Dingwell, D. B., 2015b, Mechanical behaviour and failure modes in the Whakaari (White Island volcano) hydrothermal system, New Zealand: Journal of Volcanology and Geothermal Research, v. 295, p. 26-42.

Heap, M. J., Kolzenburg, S., Russell, J. K., Campbell, M. E., Welles, J., Farquharson, J. I., and Ryan, A., 2014c, Conditions and timescales for welding block-and-ash flow deposits: Journal of Volcanology and Geothermal Research, v. 289, p. 202-209.

Heap, M. J., Lavallee, Y., Laumann, A., Hess, K. U., Meredith, P. G., and Dingwell, D. B., 2012, How tough is tuff in the event of fire?: Geology, v. 40, no. 4, p. 311-314.

Heap, M. J., Lavallee, Y., Petrakova, L., Baud, P., Reushcle, T., Varley, N. R., and Dingwell, D. B., 2014d, Microstructural controls on the physical and mechanical properties of edifice-forming andesites at Volcán de Colima Mexico: J Geophys Res, v. 119.

Heap, M. J., Lavallée, Y., Petrakova, L., Baud, P., Reuschlé, T., Varley, N. R., and Dingwell, D. B., 2014e, Microstructural controls on the physical and mechanical properties of edifice-forming andesites at Volcán de Colima, Mexico: Journal of Geophysical Research: Solid Earth, v. 119, no. 4, p. 2925-2963.

Heap, M. J., Mollo, S., Vinciguerra, S., Lavallée, Y., Hess, K. U., Dingwell, D. B., Baud, P., and Iezzi, G., 2013, Thermal weakening of the carbonate basement under Mt. Etna volcano (Italy): Implications for volcano instability: Journal of Volcanology and Geothermal Research, v. 250, p. 42-60.

Heap, M. J., Russell, J. K., and Kennedy, L. A., 2016, Mechanical behaviour of dacite from Mount St. Helens (USA): A link between porosity and lava dome extrusion mechanism (dome or spine)?: Journal of Volcanology and Geothermal Research, v. 328, p. 159-177.

Heap, M. J., Vinciguerra, S., and Meredith, P. G., 2009, The evolution of elastic moduli with increasing crack damage during cyclic stressing of a basalt from Mt. Etna volcano: Tectonophysics, v. 471, p. 153-160.

Heard, H. C., 1960, Transition from brittle fracture to ductile flow in Solnhofen limestone as a function of temperature, confining pressure and interstitial fluid pressure, *in* Griggs, D. T., and Handin, J., eds., Rock Deformation, Volume 79: New York, Geological Society of America, p. 193-226.

Heimisson, E. R., Einarsson, P., Sigmundsson, F., and Brandsdottir, B., 2015, Kilometer-scale Kaiser effect identified in Krafla volcano, Iceland: Geophysical Research Letters, v. 42, no. 19, p. 7958-7965.

Hjartardottir, A. R., and Einarsson, P., 2012, The Kverkfjoll fissure swarm and the eastern boundary of the Northern Volcanic Rift Zone, Iceland: Bulletin of Volcanology, v. 74, no. 1, p. 143-162.

Hjartardottir, A. R., Einarsson, P., Bramham, E., and Wright, T. J., 2012, The Krafla fissure swarm, Iceland, and its formation by rifting events: Bulletin of Volcanology, v. 74, no. 9, p. 2139-2153.

Hjartarson, S., Saevarsdottir, G., Ingason, K., Palsson, B., Harvey, W. S., and Palsson, H., 2014, Utilization of the chloride bearing, superheated steam from IDDP-1: Geothermics, v. 49, p. 83-89.

Hoek, E., and Brown, E. T., 1980, Empirical strength criterion for rock masses: Journal of the Geotechnical Engineering Division-Asce, v. 106, no. 9, p. 1013-1035.

Hoek, E., Carranza-Torres, C. T., and Corkum, B., Hoek-Brown failure criterion - 2002 edition, *in* Proceedings Proceedings of the Fifth North American Rock Mechanics Symposium (NARMS_TAC), Toronto, 2002, p. 267-273.

Hofmann, H., Blocher, G., Milsch, H., Babadagli, T., and Zimmermann, G., 2016, Transmissivity of aligned and displaced tensile fractures in granitic rocks during cyclic loading: International Journal of Rock Mechanics and Mining Sciences, v. 87, p. 69-84.

Hornby, A., Lavallée, Y., Kendrick, J. E., Angelis, S. D., Lamur, A., Lamb, O. D., Rietbrock, A., and Chigna, G., 2019, Brittle ‐ ductile deformation and tensile rupture of dome lava during inflation at Santiaguito, Guatemala: Journal of Geophysical Research: Solid Earth.

Hornby, A. J., Kendrick, J. E., Lamb, O. D., Hirose, T., De Angelis, S., von Aulock, F. W., Umakoshi, K., Miwa, T., Henton De Angelis, S., Wadsworth, F. B., Hess, K.-U., Dingwell, D. B., and Lavallée, Y., 2015, Spine growth and seismogenic faulting at Mt. Unzen, Japan: Journal of Geophysical Research: Solid Earth, p. 2014JB011660.

Ingason, K., Kristjansson, V., and Einarsson, K., 2014, Design and development of the discharge system of IDDP-1: Geothermics, v. 49, p. 58-65.

Jakobsson, S. P., and Gudmundsson, M. T., 2008, Subglacial and intraglacial volcanic formations in Iceland: Jokull, v. 58, p. 179-196.

Jansen, J. D., 2011, Adjoint-based optimization of multi-phase flow through porous media - A review: Computers & Fluids, v. 46, no. 1, p. 40-51.

Jarosch, A., Gudmundsson, M. T., Hognadottir, T., and Axelsson, G., 2008, Progressive cooling of the Hyaloclastite ridge at Gjalp, Iceland, 1996-2005: Journal of Volcanology and Geothermal Research, v. 170, no. 3-4, p. 218-229.

Johnson, J. S., and Smellie, J. L., 2007, Zeolite compositions as proxies for eruptive paleoenvironment: Geochemistry Geophysics Geosystems, v. 8, p. 19.

Jonasson, K., 1994, Rhyolite volcanism in the Krafla Central Volcano, northeast Iceland: Bulletin of Volcanology, v. 56, no. 6-7, p. 516-528.

Jouniaux, L., Bernard, M. L., Zamora, M., and Pozzi, J. P., 2000, Streaming potential in volcanic rocks from Mount Pelee: Journal of Geophysical Research-Solid Earth, v. 105, no. B4, p. 8391-8401.

Ju, Y., Yang, Y., Peng, R., and Mao, L., 2013, Effects of pore structures on static mechanical properties of sandstone: J Geotech Geoenvironmental Eng, v. 139.

Julia, F., Vladimir, L., Sergey, R., and David, Z., 2014, Effects of hydrothermal alterations on physical and mechanical properties of rocks in the Kuril–Kamchatka island arc: Engineering Geology, v. 183, p. 80-95.

Kantha, L. H., 1981, Basalt fingers - Origin of columnar joints: Geological Magazine, v. 118, no. 3, p. 251-&.

Karlsdottir, S. N., Ragnarsdottir, K. R., Moller, A., Thorbjornsson, I. O., and Einarsson, A., 2014, On-site erosion-corrosion testing in superheated geothermal steam: Geothermics, v. 51, p. 170-181.

Keiding, M., Arnadottir, T., Jonsson, S., Decriem, J., and Hooper, A., 2010, Plate boundary deformation and man-made subsidence around geothermal fields on the Reykjanes Peninsula, Iceland: Journal of Volcanology and Geothermal Research, v. 194, no. 4, p. 139-149.

Keiding, M., Arnadottir, T., Sturkell, E., Geirsson, H., and Lund, B., 2008, Strain accumulation along an oblique plate boundary: the Reykjanes Peninsula, southwest Iceland: Geophysical Journal International, v. 172, no. 2, p. 861-872.

Kendrick, J., Smith, R., Sammonds, P., Meredith, P., Dainty, M., and Pallister, J., 2013a, The influence of thermal and cyclic stressing on the strength of rocks from Mount St. Helens, Washington: Bulletin of Volcanology, v. 75, no. 7, p. 1-12.

Kendrick, J. E., Lavallee, Y., Varley, N. R., Wadsworth, F. B., Lamb, O. D., and Vasseur, J., 2016, Blowing Off Steam: Tuffisite Formation As a Regulator for Lava Dome Eruptions: Frontiers in Earth Science, v. 4.

Kendrick, J. E., Lavallée, Y., Ferk, A., Perugini, D., Leonhardt, R., and Dingwell, D. B., 2012, Extreme frictional processes in the volcanic conduit of Mount St. Helens (USA) during the 2004–2008 eruption: Journal of Structural Geology, v. 38, no. 0, p. 61-76.

Kendrick, J. E., Lavallée, Y., Hess, K. U., Heap, M. J., Gaunt, H. E., Meredith, P. G., and Dingwell, D. B., 2013b, Tracking the permeable porous network during strain-dependent magmatic flow: Journal of Volcanology and Geothermal Research, v. 260, p. 117-126.

Keshavarz, M., Pellet, F. L., and Loret, B., 2010, Damage and changes in mechanical properties of a gabbro thermally loaded up to 1,000°C: Pure Appl Geophys, v. 167.

Kim, K. Y., Han, W. S., and Park, E., 2013, The impact of highly permeable layer on hydraulic system in a coastal aquifer: Hydrological Processes, v. 27, no. 22, p. 3128-3138.

Klinkenberg, L. J., 1941, The permeability of porous media to liquids and gases. Drilling and production practice, New York, American Petroleum Institute.

Klug, C., and Cashman, K. V., 1996, Permeability development in vesiculating magmas: Implications for fragmentation: Bulletin of Volcanology, v. 58, no. 2-3, p. 87-100.

Kolzenburg, S., Heap, M. J., Lavallée, Y., Russell, J. K., Meredith, P. G., and Dingwell, D. B., 2012, Strength and permeability recovery of tuffisite-bearing andesite: Solid Earth, v. 3, no. 2, p. 191-198.

Koudina, N., Garcia, R. G., Thovert, J. F., and Adler, P. M., 1998, Permeability of three-dimensional fracture networks: Physical Review E, v. 57, no. 4, p. 4466-4479.

Kozeny, J., 1927, Ueber kapillare Leitung der Wasser in Boden: Sitzungsber. Akad. Wiss, p. 271-306.

Kristinsdóttir, L. H., Flóvenz, Ó. G., Árnason, K., Bruhn, D., Milsch, H., Spangenberg, E., and Kulenkampff, J., 2010, Electrical conductivity and P-wave velocity in rock samples from high-temperature Icelandic geothermal fields: Geothermics, v. 39.

Krupp, R. E., and Seward, T. M., 1987, The Rotokawa geothermal system, New Zealand; an active epithermal gold-depositing environment: Econ Geol, v. 82.

Kushnir, A. R. L., Heap, M. J., and Baud, P., 2018, Assessing the role of fractures on the permeability of the Permo-Triassic sandstones at the Soultz-sous-Forêts (France) geothermal site: Geothermics, v. 74, p. 181-189.

Kushnir, A. R. L., Martel, C., Bourdier, J.-L., Heap, M. J., Reuschlé, T., Erdmann, S., Komorowski, J.-C., and Cholik, N., 2016, Probing permeability and microstructure: Unravelling the role of a low-permeability dome on the explosivity of Merapi (Indonesia): Journal of Volcanology and Geothermal Research, v. 316, p. 56-71.

Kushnir, A. R. L., Martel, C., Champallier, R., and Wadsworth, F. B., 2017, Permeability Evolution in Variably Glassy Basaltic Andesites Measured Under Magmatic Conditions: Geophysical Research Letters, v. 44, no. 20, p. 10262-10271.

Lachowycz, S. M., Pyle, D. M., Gilbert, J. S., Mather, T. A., Mee, K., Naranjo, J. A., and Hobbs, L. K., 2015, Glaciovolcanism at Volcan Sollipulli, southern Chile: Lithofacies analysis and interpretation: Journal of Volcanology and Geothermal Research, v. 303, p. 59-78.

Lamur, A., Kendrick, J. E., Eggertsson, G. H., Wall, R. J., Ashworth, J. D., and Lavallee, Y., 2017, The permeability of fractured rocks in pressurised volcanic and geothermal systems: Scientific Reports, v. 7.

Lamur, A., Kendrick, J. E., Wadsworth, F. B., and Lavallee, Y., 2019, Fracture healing and strength recovery in magmatic liquids: Geology, v. 47, no. 3, p. 195-198.

Lamur, A., Lavallee, Y., Iddon, F. E., Hornby, A. J., Kendrick, J. E., von Aulock, F. W., and Wadsworth, F. B., 2018, Disclosing the temperature of columnar jointing in lavas: Nature Communications, v. 9, p. 7.

Lamur, A. L. H., 2018, Development, impact and longevity of fractures in magmatic, volcanic and geothermal systems [PhD: University of Liverpool, 132 p.

Langella, G., Paoletti, V., DiPippo, R., Amoresano, A., Steinunnardottir, K., and Milano, M., 2017, Krafla geothermal system, northeastern Iceland: Performance assessment of alternative plant configurations: Geothermics, v. 69, p. 74-92.

Lavallée, Y., Benson, P., Hess, K.-U., Flaws, A., Schillinger, B., Meredith, P. G., and Dingwell, D. B., 2013a, Reconstructing magma failure and the permeable degassing network: Geology, v. 41, p. 515-518.

Lavallée, Y., Benson, P. M., Heap, M. J., Hess, K. U., Flaws, A., Schillinger, B., Meredith, P. G., and Dingwell, D. B., 2013b, Reconstructing magma failure and the degassing network of dome-building eruptions: Geology, v. 41.

Lavallée, Y., Meredith, P. G., Dingwell, D. B., Hess, K. U., Wassermann, J., Cordonnier, B., Gerik, A., and Kruhl, J. H., 2008, Seismogenic lavas and explosive eruption forecasting: Nature, v. 453, no. 7194, p. 507-510.

Lay, T., Hernlund, J., and Buffett, B. A., 2008, Core-mantle boundary heat flow: Nature Geoscience, v. 1, no. 1, p. 25-32.

Legarth, B., Huenges, E., and Zimmermann, G., 2005, Hydraulic fracturing in a sedimentary geothermal reservoir: Results and implications: International Journal of Rock Mechanics and Mining Sciences, v. 42, no. 7-8, p. 1028-1041.

Li, D. Y., and Wong, L. N. Y., 2013, The Brazilian Disc Test for Rock Mechanics Applications: Review and New Insights: Rock Mechanics and Rock Engineering, v. 46, no. 2, p. 269-287.

Lim, S. S., Martin, C. D., and Åkesson, U., 2012, In-situ stress and microcracking in granite cores with depth: Eng Geol, v. 147–148.

Lin, W. R., 2002, Permanent strain of thermal expansion and thermally induced microcracking in Inada granite: Journal of Geophysical Research-Solid Earth, v. 107, no. B10, p. 16.

Loftsson, M., and Steingrímsson, B. Ó., 2010, Tæknilegir eiginleikar mismunandi berggerða: Mannvit.

Lévy, L., Gibert, B., Sigmundsson, F., Flóvenz, Ó., Hersir, G., Briole, P., and Pezard, P., 2018, The role of smectites in the electrical conductivity of active hydrothermal systems: electrical properties of core samples from Krafla volcano, Iceland: *Geophysical Journal International*, v. 215, no. 3, p. 1558–1582.

Majer, E. L., and Peterson, J. E., 2007, The impact of injection on seismicity at The Geysers, California Geothermal Field: International Journal of Rock Mechanics and Mining Sciences, v. 44, no. 8, p. 1079-1090.

Marks, N., Zierenberg, R. A., and Schiffman, P., 2015, Strontium and oxygen isotopic profiles through 3 km of hydrothermally altered oceanic crust in the Reykjanes Geothermal System, Iceland: Chemical Geology, v. 412, p. 34-47.

McClure, M. W., and Horne, R. N., 2014, An investigation of stimulation mechanisms in Enhanced Geothermal Systems: International Journal of Rock Mechanics and Mining Sciences, v. 72, p. 242-260.

Miller, S. A., 2015, Modeling enhanced geothermal systems and the essential nature of large-scale changes in permeability at the onset of slip: Geofluids, v. 15, no. 1-2, p. 338-349.

Milsch, H., Hofmann, H., and Blocher, G., 2016, An experimental and numerical evaluation of continuous fracture permeability measurements during effective pressure cycles: International Journal of Rock Mechanics and Mining Sciences, v. 89, p. 109-115.

Mock, J. E., Tester, J. W., and Wright, P. M., 1997, Geothermal energy from the earth: Its potential impact as an environmentally sustainable resource: Annual Review of Energy and the Environment, v. 22, p. 305-356.

Moore, J. G., 2001, Density of basalt core from Hilo drill hole, Hawaii: Journal of Volcanology and Geothermal Research, v. 112, no. 1-4, p. 221-230.

Moran, S. C., Zimbelman, D. R., and Malone, S. D., 2000, A model for the magmatic-hydrothermal system at Mount Rainier, Washington, from seismic and geochemical observations: Bulletin of Volcanology, v. 61, no. 7, p. 425-436.

Mortensen, A. K., Egilson, P., Gautason, B., Arnadottir, S., and Gudmundsson, A., 2014, Stratigraphy, alteration mineralogy, permeability and temperature conditions of well IDDP-1, Krafla, NE-Iceland: Geothermics, v. 49, p. 31-41.

Mortensen, A. K., Guðmundsson, Á., Steingrímsson, B., Sigmundsson, F., Axelsson, G., Ármannsson, H., Björnsson, H., Ágústsson, K., Sæmundsson, K., Ólafsson, M., Karlsdóttir, R., Halldórsdóttir, S., and Hauksson, T., 2015, The Krafla Geothermal System Research summary and conceptual model revision: Landsvirkjun.

Mueller, S., Melnik, O., Spieler, O., Scheu, B., and Dingwell, D. B., 2005, Permeability and degassing of dome lavas undergoing rapid decompression: An experimental determination: Bulletin of Volcanology, v. 67, no. 6, p. 526-538.

Murphy, H. D., Tester, J. W., Grigsby, C. O., and Potter, R. M., 1981, Energy extraction from fractured geothermal reservoirs in low-permeability crystalline rock: Journal of Geophysical Research, v. 86, no. NB8, p. 7145-7158.

Nara, Y., Meredith, P. G., Yoneda, T., and Kaneko, K., 2011, Influence of macro-fractures and micro-fractures on permeability and elastic wave velocities in basalt at elevated pressure: Tectonophysics, v. 503.

Nara, Y., Morimoto, K., Hiroyoshi, N., Yoneda, T., Kaneko, K., and Benson, P. M., 2012, Influence of relative humidity on fracture toughness of rock: implications for subcritical crack growth: Int J Solids Struct, v. 49.

Neuffer, D. P., Schultz, R. A., and Watters, R. J., 2006, Mechanisms of slope failure on Pyramid Mountain, a subglacial volcano in Wells Gray Provincial Park, British Columbia: Canadian Journal of Earth Sciences, v. 43, no. 2, p. 147-155.

Nielson, D. L., and Stiger, S. G., 1996, Drilling and evaluation of Ascension #1, a geothermal exploration well on Ascension Island, South Atlantic Ocean: Geothermics, v. 25, no. 4-5, p. 543-560.

Nordgren, R. P., 1972, Propagation of a vertical hydraulic fracture: Society of Petroleum Engineers Journal, v. 12, no. 4, p. 306-&.

Norton, D. L., 1984, Theory of hydrothermal systems: Annual Review of Earth and Planetary Sciences, v. 12, p. 155-177.

Norton, D. L., and Dutrow, B. L., 2001, Complex behavior of magma-hydrothermal processes: Role of supercritical fluid: Geochimica Et Cosmochimica Acta, v. 65, no. 21, p. 4009-4017.

Okumura, S., and Sasaki, O., 2014, Permeability reduction of fractured rhyolite in volcanic conduits and its control on eruption cyclicity: Geology, v. 42, no. 10, p. 843-846.

Palchik, V., and Hatzor, H. Y., 2004, The Influence of Porosity on Tensile and Compressive Strength of Porous Chalks: Rock Mechanics and Rock Engineering, v. 37, no. 4, p. 331-341.

Palsson, B., Holmgeirsson, S., Gudmundsson, A., Boasson, H. A., Ingason, K., Sverrisson, H., and Thorhallsson, S., 2014, Drilling of the well IDDP-1: Geothermics, v. 49, p. 23-30.

Paterson, M. S., and Wong, T. F., 2005, Experimental Rock Deformation - The Brittle Field, Berlin Heidelberg, Springer, 347 p.:

Pearson, C., 1981, The relationship between micro-seismicity and high pore pressure during hydraulic stimulation experiments in low permeability granitic-rocks: Journal of Geophysical Research, v. 86, no. NB9, p. 7855-7864.

Perez-Flores, P., Wang, G., Mitchell, T. M., Meredith, P. G., Nara, Y., Sarkar, V., and Cembrano, J., 2017, The effect of offset on fracture permeability of rocks from the Southern Andes Volcanic Zone, Chile: Journal of Structural Geology, v. 104, p. 142-158.

Petrakova, L., Heap, M. J., Lavallée, Y., Baud, P. and Dingwell, D. B., 2012. The effect of thermal stresses on the strength and physical properties of edifice-forming andesites: the case study of Volcan de Colima, , 2012, The effect of thermal stresses on the strength and physical properties of edifice-forming andesites: the case study of Volcan de Colima.: Journal of Volcanology and Geothermal Research, submitted.

Pirrie, D., Butcher, A. R., Power, M. R., Gottlieb, P., and Miller, G. L., 2004, Rapid quantitative mineral and phase analysis using automated scanning electron microscopy (QemSCAN); potential

applications in forensic geoscience, London, Geological Society, Special Publications, Forensic Geoscience: Principles, Techniques and Applications.
Pola, A., Crosta, G., Fusi, N., Barberini, V., and Norini, G., 2012, Influence of alteration on physical properties of volcanic rocks: Tectonophysics, v. 566–567.
Pola, A., Crosta, G. B., Fusi, N., and Castellanza, R., 2014, General characterization of the mechanical behaviour of different volcanic rocks with respect to alteration: Eng Geol, v. 169.
Pollack, H. N., Hurter, S. J., and Johnson, J. R., 1993, Heat-flow from the Earths interior - analysis of the global data set: Reviews of Geophysics, v. 31, no. 3, p. 267-280.
Rocchi, V., Sammonds, P. R., and Kilburn, C. R. J., 2002, Flow and fracture maps for basaltic rock deformation at high temperatures: Journal of Volcanology and Geothermal Research, v. 120, p. 25-42.
Rowland, J. V., and Sibson, R. H., 2004, Structural controls on hydrothermal flow in a segmented rift system, Taupo Volcanic Zone, New Zealand: Geofluids, v. 4.
Rozhko, A. Y., Podladchikov, Y. Y., and Renard, F., 2007, Failure patterns caused by localized rise in pore-fluid overpressure and effective strength of rocks: Geophysical Research Letters, v. 34, no. 22.
Saar, M. O., and Manga, M., 1999, Permeability-porosity relationship in vesicular basalts: Geophys Res Lett, v. 26.
Sammis, C. G., and Ashby, M. F., 1986, The failure of brittle porous solids under compressive stress state: Acta Metallurgica, v. 34, no. 3, p. 511-526.
Samuelson, J., Marone, C., Voight, B., and Elsworth, D., 2008, Laboratory investigation of the frictional behavior of granular volcanic material: Journal of Volcanology and Geothermal Research, v. 173, no. 3-4, p. 265-279.
Sanyal, S. K., 2005, Classification of Geothermal Systems – A Possible Scheme, The Thirtieth Workshop on Geothermal Reservoir Engineering,: Stanford University, Stanford, California.
Saubin, E., Villeneuve, M., Mortensen, A., and Kennedy, B., Drilling in the blind zone: how it can inform geological interpretation, *in* Proceedings Georg Geothermal Workshop, Reykjavík, 2018, Georg Geothermal cluster.
Scandone, R., Cashman, K., and Malone, S. D., 2007, Magma supply, magma ascent and the style of volcanic eruptions: Earth and Planetary Science Letters, v. 253, no. 3-4, p. 513-529.
Schaefer, L. N., Kendrick, J. E., Lavallée, Y., Oommen, T., and Chigna, G., 2015, Geomechanical rock properties of a basaltic volcano: Frontiers in Earth Science, v. 3.
Scholz, C. H., 1968, Microfracturing and the inelastic deformation of rock in compression: Journal of Geophysical Research, v. 73, p. 1417-1432.
Schuler, J., Pugh, D. J., Hauksson, E., White, R. S., Stock, J. M., and Brandsdottir, B., 2016, Focal mechanisms and size distribution of earthquakes beneath the Krafla central volcano, NE Iceland: Journal of Geophysical Research-Solid Earth, v. 121, no. 7, p. 5152-5168.
Schöpfer, M. P. J., Abe, S., Childs, C., and Walsh, J. J., 2009, The impact of porosity and crack density on the elasticity, strength and friction of cohesive granular materials: insights from DEM modelling: Int J Rock Mech Min Sci, v. 46.
Scott, B. J., Gordon, D. A., and Cody, A. D., 2005, Recovery of Rotorua geothermal field, New Zealand: Progress, issues and consequences: Geothermics, v. 34, no. 2, p. 159-183.
Scott, S., Driesner, T., and Weis, P., 2015, Geologic controls on supercritical geothermal resources above magmatic intrusions: Nature Communications, v. 6, p. 6.
-, 2016, The thermal structure and temporal evolution of high-enthalpy geothermal systems: Geothermics, v. 62, p. 33-47.
-, 2017, Boiling and condensation of saline geothermal fluids above magmatic intrusions: Geophysical Research Letters, v. 44, no. 4, p. 1696-1705.
Scott, S. W., Covell, C., Júlíusson, E., Valfells, Á., Newson, J., Hrafnkelsson, B., Pálsson, H., and Gudjónsdóttir, M., 2019, A probabilistic geologic model of the Krafla geothermal system constrained by gravimetric data: Geothermal Energy, v. 7, no. 1, p. 29.

Sella, G. F., Dixon, T. H., and Mao, A. L., 2002, REVEL: A model for Recent plate velocities from space geodesy: Journal of Geophysical Research-Solid Earth, v. 107, no. B4, p. 31.

Sibson, R. H., 1994, Crustal stress, faulting and fluid flow: Geological Society, London, Special Publications, v. 78, no. 1, p. 69.

Sigmundsson, F., Hreinsdottir, S., Hooper, A., Arnadottir, T., Pedersen, R., Roberts, M. J., Oskarsson, N., Auriac, A., Decriem, J., Einarsson, P., Geirsson, H., Hensch, M., Ofeigsson, B. G., Sturkell, E., Sveinbjornsson, H., and Feigl, K. L., 2010, Intrusion triggering of the 2010 Eyjafjallajokull explosive eruption: Nature, v. 468, no. 7322, p. 426-U253.

Simmons, G., and Cooper, H. W., 1978, Thermal cycling cracks in three igneous rocks: International Journal of Rock Mechanics and Mining Sciences, v. 15, p. 145-148.

Siratovich, P. A., Heap, M. J., Villeneuve, M. C., Cole, J. W., Kennedy, B. M., Davidson, J., and Reuschle, T., 2016, Mechanical behaviour of the Rotokawa Andesites (New Zealand): Insight into permeability evolution and stress-induced behaviour in an actively utilised geothermal reservoir: Geothermics, v. 64, p. 163-179.

Siratovich, P. A., Heap, M. J., Villenueve, M. C., Cole, J. W., and Reuschlé, T., 2014, Physical property relationships of the Rotokawa Andesite, a significant geothermal reservoir rock in the Taupo Volcanic Zone, New Zealand: Geothermal Energy, v. 2, no. 1, p. 1-31.

Siratovich, P. A., Villeneuve, M. C., Cole, J. W., Kennedy, B. M., and Begue, F., 2015a, Saturated heating and quenching of three crustal rocks and implications for thermal stimulation of permeability in geothermal reservoirs: International Journal of Rock Mechanics and Mining Sciences, v. 80, p. 265-280.

Siratovich, P. A., von Aulock, F. W., Y., L., J.W., C., B.M., K., and M.C., V., 2015b, Thermoelastic properties of the Rotokawa Andesite: a geothermal reservoir constraint: Journal of Volcanology and Geothermal Research v. 301.

Smellie, J. L., Rocchi, S., and Armienti, P., 2011, Late Miocene volcanic sequences in northern Victoria Land, Antarctica: products of glaciovolcanic eruptions under different thermal regimes: Bulletin of Volcanology, v. 73, no. 1, p. 1-25.

Stefánsson, V., Guðmundsson, Á., Steingrímsson, B., Halldórsson, G. K., Ármannsson, H., Franzson, H., and Hauksson, T., 1982, Krafla - Hola KJ-14 - Borun, rannsóknir og vinnslueiginleikar.

Stimac, J. A., Powell, T. S., and Golla, G. U., 2004, Porosity and permeability of the Tiwi geothermal field, Philippines, based on continuous and spot core measurements: Geothermics, v. 33.

Strehlow, K., Gottsmann, J. H., and Rust, A. C., 2015, Poroelastic responses of confined aquifers to subsurface strain and their use for volcano monitoring: Solid Earth, v. 6, no. 4, p. 1207-1229.

Stroncik, N. A., and Schmincke, H. U., 2002, Palagonite - a review: International Journal of Earth Sciences, v. 91, no. 4, p. 680-697.

Sæmundsson, K., 1991, Geology of the Krafla Volcanic system (Jarðfræði Kröflukerfisins in Icelandic), *in* Garðarsson, A., and Einarsson, Á., eds., Náttúra Mývatns, Volume 1: Reykjavík, Hið íslenska náttúrufræðifélag, p. 24-95.

Takarli, M., Prince, W., and Siddique, R., 2008, Damage in granite under heating/cooling cycles and water freeze thaw condition: Int J Rock Mech Min Sci, v. 45.

Tanikawa, W., and Shimamoto, T., 2009, Comparison of Klinkenberg-corrected gas permeability and water permeability in sedimentary rocks: International Journal of Rock Mechanics and Mining Sciences, v. 46, no. 2, p. 229-238.

Tentler, T., and Temperley, S., 2006, Rock control of faulting: A case study from the Icelandic rift zone: Journal of Geology, v. 114, no. 4, p. 449-470.

Thien, B. M. J., Kosakowski, G., and Kulik, D. A., 2015, Differential alteration of basaltic lava flows and hyaloclastites in Icelandic hydrothermal systems: Geothermal Energy, v. 3, p. 32.

Thomas, M. E., Petford, N., and Bromhead, E. N., 2004, Volcanic rock-mass properties from Snowdonia and Tenerife: implications for volcano edifice strength: Journal of the Geological Society, v. 161, no. 6, p. 939-946.

Thordarson, T., and Larsen, G., 2007, Volcanism in Iceland in historical time: Volcano types, eruption styles and eruptive history: Journal of Geodynamics, v. 43, no. 1, p. 118-152.

Timoshenko, S. P., and Goodier, J. N., 1970, Theory of Elasticity. 3rd ed., McGraw-Hill,New York, NY.
Tiwari, G. N., and Ghosal, M. K., 2005, Renewable Energy Resources: Basic Principles and Applications, Alpha Science International.
Tomac, I., and Gutierrez, M., 2017, Coupled hydro-thermo-mechanical modeling of hydraulic fracturing in quasi-brittle rocks using BPM-DEM: Journal of Rock Mechanics and Geotechnical Engineering, v. 9, no. 1, p. 92-104.
Tucker, D. S., and Scott, K. M., 2009, Structures and facies associated with the flow of subaerial basaltic lava into a deep freshwater lake: The Sulphur Creek lava flow, North Cascades, Washington: Journal of Volcanology and Geothermal Research, v. 185, no. 4, p. 311-322.
Tuffen, H., Dingwell, D. B., and Pinkerton, H., 2003, Repeated fracture and healing of silicic magma generate flow banding and earthquakes?: Geology, v. 31, no. 12, p. 1089-1092.
Tuffen, H., Gilbert, J., and McGarvie, D., 2001, Products of an effusive subglacial rhyolite eruption: Blahnukur, Torfajokull, Iceland: Bulletin of Volcanology, v. 63, no. 2-3, p. 179-190.
van Otterloo, J., Cas, R. A. F., and Scutter, C. R., 2015, The fracture behaviour of volcanic glass and relevance to quench fragmentation during formation of hyaloclastite and phreatomagmatism: Earth-Science Reviews, v. 151, p. 79-116.
Varley, N., Arámbula-Mendoza, R., Reyes-Dávila, G., Sanderson, R., and Stevenson, J., 2010, Generation of Vulcanian activity and long-period seismicity at Volcán de Colima, Mexico: Journal of Volcanology and Geothermal Research, v. 198, no. 1–2, p. 45-56.
Vinciguerra, S., Trovato, C., Meredith, P. G., and Benson, P. M., 2005, Relating seismic velocities, thermal cracking and permeability in Mt. Etna and Iceland basalts: International Journal of Rock Mechanics and Mining Sciences, v. 42, no. 7-8, p. 900-910.
Violay, M., Gibert, B., Mainprice, D., Evans, B., Dautria, J.-M., Azais, P., and Pezard, P., 2012, An experimental study of the brittle-ductile transition of basalt at oceanic crust pressure and temperature conditions: Journal of geophysical reserach, v. 117.
Violay, M., Heap, M. J., Acosta, M., and Madonna, C., 2017, Porosity evolution at the brittle-ductile transition in the continental crust: Implications for deep hydro-geothermal circulation: Scientific Reports, v. 7, p. 10.
Vishal, V., Pradhan, S. P., and Singh, T. N., 2011, Tensile Strength of Rock Under Elevated Temperatures: Geotechnical and Geological Engineering, v. 29, no. 6, p. 1127-1133.
Walsh, J. B., 1981, Effect of pore pressure and confining pressure on fracture permeability: International Journal of Rock Mechanics and Mining Sciences & Geomechanics Abstracts, v. 18, no. 5, p. 429-435.
Walton, A. W., and Schiffman, P., 2003, Alteration of hyaloclastites in the HSDP 2 Phase 1 Drill Core - 1. Description and paragenesis: Geochemistry Geophysics Geosystems, v. 4, p. 31.
Warpinski, N. R., and Teufel, L. W., 1987, Influence of geologic discontinuities on hydraulic fracture propagation: Journal of Petroleum Technology, v. 39, no. 2, p. 209-220.
Watton, T. J., Jerram, D. A., Thordarson, T., and Davies, R. J., 2013, Three-dimensional lithofacies variations in hyaloclastite deposits: Journal of Volcanology and Geothermal Research, v. 250, p. 19-33.
Weaver. J, G.H., E., Utley, J. E. P., Wallace, P. A., Lamur, A., J.E., K., H., T., Markússon, S. H., and Y., L., In review, Thermal liability of hyaloclastite in the Krafla geothermal reservoir, Iceland: the impact of phyllosilicates on permeability and rock strength.: Geofluids.
Weng, X., Kresse, O., Cohen, C., Wu, R., and Gu, H., 2011, Modeling of Hydraulic-Fracture-Network Propagation in a Naturally Fractured Formation: Spe Production & Operations, v. 26, no. 4, p. 368-380.
Whitaker, S., 1996, The Forchheimer equation: A theoretical development: Transport in Porous Media, v. 25, no. 1, p. 27-61.
Wolfe, C. J., Bjarnason, I. T., VanDecar, J. C., and Solomon, S. C., 1997, Seismic structure of the Iceland mantle plume: Nature, v. 385, no. 6613, p. 245-247.
Wong, T.-f., and Baud, P., 2012, The brittle-ductile transition in porous rock: A review: Journal of Structural Geology, v. 44, p. 25-53.

Wright, T. J., Sigmundsson, F., Pagli, C., Belachew, M., Hamling, I. J., Brandsdottir, B., Keir, D., Pedersen, R., Ayele, A., Ebinger, C., Einarsson, P., Lewi, E., and Calais, E., 2012, Geophysical constraints on the dynamics of spreading centres from rifting episodes on land: Nature Geoscience, v. 5, no. 4, p. 242-250.

Wu, X. Y., Baud, P., and Wong, T. F., 2000, Micromechanics of compressive failure and spatial evolution of anisotropic damage in Darley Dale sandstone: Int J Rock Mech Min Sci, v. 37.

Wyering, L. D., Villeneuve, M. C., Wallis, I. C., Siratovich, P. A., Kennedy, B. M., and Gravley, D. M., 2015, The development and application of the alteration strength index equation: Engineering Geology, v. 199, p. 48-61.

Yagi, M., Ohguch, T., Akiba, F., Yoshida, T., and Tiba, T., 2009, The Fukuyama volcanic rocks: Submarine composite volcano in the Late Miocene to Early Pliocene Akita-Yamagata back-arc basin, northeast Honshu, Japan: Sedimentary Geology, v. 220, no. 3-4, p. 243-255.

Ylagan, R. F., Altaner, S. P., and Pozzuoli, A., 1996, Hydrothermal alteration of a rhyolitic hyaloclastite from Ponza island, Italy: Journal of Volcanology and Geothermal Research, v. 74, no. 3-4, p. 215-231.

Yoshinobu, A. S., Wolak, J. M., Paterson, S. R., Pignotta, G. S., and Anderson, H. S., 2009, Determining relative magma and host rock xenolith rheology during magmatic fabric formation in plutons: Examples from the middle and upper crust: Geosphere, v. 5, no. 3, p. 270-285.

Zakharova, O. K., and Spichak, V. V., 2012, Geothermal fields of Hengill Volcano, Iceland: Journal of Volcanology and Seismology, v. 6, no. 1, p. 1-14.

Zang, A. N., Oye, V., Jousset, P., Deichmann, N., Gritto, R., McGarr, A., Majer, E., and Bruhn, D., 2014, Analysis of induced seismicity in geothermal reservoirs - An overview: Geothermics, v. 52, p. 6-21.

Zhang, J. X., Wong, T. F., and Davis, D. M., 1990, Micromechanics of pressure-induced grain crushing in porous rocks: Journal of Geophysical Research-Solid Earth and Planets, v. 95, no. B1, p. 341-352.

Zierenberg, R. A., Schiffman, P., Barfod, G. H., Lesher, C. E., Marks, N. E., Lowenstern, J. B., Mortensen, A. K., Pope, E. C., Bird, D. K., Reed, M. H., Friðleifsson, G. Ó., and Elders, W. A., 2013, Composition and origin of rhyolite melt intersected by drilling in the Krafla geothermal field, Iceland: Contributions to Mineralogy and Petrology, v. 165, no. 2, p. 327-347.

Zierenberg, R. A., Schiffman, P., Jonasson, I. R., Tosdal, R., Pickthorn, W., and McClain, J., 1995, Alteration of basalt hyaloclastite at the off-axis Sea Cliff hydrothermal field, Gorda Ridge: Chemical Geology, v. 126, no. 2, p. 77-99.

Zimmermann, G., Blocher, G., Reinicke, A., and Brandt, W., 2011, Rock specific hydraulic fracturing and matrix acidizing to enhance a geothermal system - Concepts and field results: Tectonophysics, v. 503, no. 1-2, p. 146-154.

Zimmermann, G., Tischner, T., Legarth, B., and Huenges, E., 2009, Pressure-dependent Production Efficiency of an Enhanced Geothermal System (EGS): Stimulation Results and Implications for Hydraulic Fracture Treatments: Pure and Applied Geophysics, v. 166, no. 5-7, p. 1089-1106.

Zoback, M. D., 2010, Reservoir Geomechanics, Camebridge University Press, NY, USA, Camebridge University Press.

Ármannsson, H., 1989, Gas changes in the Krafla geothermal system, Iceland: Water-rock interaction, v. 76, no. 3-4, p. 19.

Appendix I:
Impact of thermo-mechanical stimulation on the reservoir rocks of the geothermal system at Krafla, Iceland

Guðjón H. Eggertsson[1*], Yan Lavallée[1], Jackie E. Kendrick[1] and Sigurður Markússon[2]

[1]Department of Earth, Ocean and Ecological Sciences, University of Liverpool, 4 Brownlow Street, Liverpool, U.K.

[2]Landsvirkjun, Háaleitisbraut 68, 110 Reykjavík, Iceland

*g.eggertsson@liverpool.ac.uk

Keywords: Laboratory testing, High temperature, Thermal stimulation, Krafla

Abstract

The controlled enhancement of fluid flow within a geothermal reservoir is a challenge as knowledge of stress distribution and rock response eludes us. One of the most common ways to improve fluid flow in a well, is through thermal stimulation. Here we investigate the influence of thermal stressing of basalt (present in the geothermal field of Krafla volcano, Iceland) on the development of thermal stresses and fracture creation leading to changes in rock permeability. We first measure the linear thermal expansivity of the basalt, noting that it increases slightly, ~linearly with temperature up to 750 ˚C. We tested the effect of heating/cooling cycles on basalt and noted that the permeability of the basalt tested was not affected by thermal stimulation (within the resolution of the permeability measurements), for the range of heating/cooling conditions, even after five cycles. Simple modelling of the experimental results shows however that small temperature changes can be sufficient to create thermal stresses that exceed the rocks' tensile strength at ambient pressures (not considering additional contributions from the local stress field in the system). We discuss the implication of these results, both for the development of laboratory methods and field site exploration.

Introduction

The flow capacity from a geothermal well and the commercial potential of a geothermal reservoir is dependent on the permeability of the reservoir (e.g. Murphy et al., 1981). To enhance the natural, near-well permeability of a reservoir, geoengineering methods such as fracking (e.g. Legarth et al., 2005; McClure and Horne, 2014; Miller, 2015; Tomac and Gutierrez, 2017; Zimmermann et al., 2011) or thermal stimulation (e.g. Grant et al., 2013; Siratovich et al., 2015b) have been developed to increase the presence of fractures that provide additional fluid pathways in reservoirs (e.g. Aqui and Zarrouk, 2011; Eggertsson et al., 2016; Heap and Kennedy, 2016; Lamur et al., 2017). Several factors

may contribute to the generation of thermal stresses in rocks, such as anisotropic thermal expansions of minerals, thermo-chemical reactions and heterogeneous temperature gradients (e.g. Siratovich et al., 2015a). Anisotropy in thermal expansion is thought to be the main contributor to thermal cracking in igneous rocks (e.g. Browning et al., 2016; Siratovich et al., 2015a). Although thermal stimulation of wells has been a common practice for decades, and it has the potential to be a cheap way to enhance the fluid flow and be very beneficial, its impact on the magnitude of *in-situ* stress and extent of fracture opening remains difficult to ascertain (Flores et al., 2005).

In Iceland, thermal stimulation of wells is common (e.g. Axelsson et al., 2006). It is often performed upon well completion, before any flow tests have been made. Circulation loss has been monitored and used as a proxy for a well's permeability (Figure 1; Stefánsson et al., 1982). It has also been shown that thermal properties of the reservoir (as well as lithology) can influence injection capacity (Injection Index) of wells, depending on the temperature of the fluid that is being injected (Gunnarsson, 2011). Due to the high temperatures (>200 °C) of exploited geothermal reservoirs (e.g. Axelsson et al., 2014), the potential for high thermal gradients between the reservoir temperature and the temperature of the injection fluids is high and therefore, cracks are more likely to occur (Siratovich et al., 2015a). The induced thermo-elastic stress change (Eq. 1), occurring as a result of temperature change within the rock, is given as (Siratovich et al., 2015b; Timoshenko and Goodier, 1970):

$$\sigma_t = \frac{\alpha \mathrm{E} \Delta \mathrm{T}}{(1-\nu)} \quad (1)$$

σt = induced tensile thermal stress (MPa)
α = linear expansion coefficient (m/ (m K))
E = Young's modulus (MPa)
ΔT = temperature difference (°C)
ν = Poisson's ratio

Here, we assess the extent of thermal stimulation in wells drilled in a basaltic environment, using the results of laboratory experiments, conducted in the Volcanology and Geothermal Research Laboratory at the University of Liverpool. This focuses on the case of Krafla volcano, in North-East Iceland, where geothermal production has been ongoing since 1978 from a high temperature reservoir (reservoir temperature >200 °C). Geological investigation from drill-cuttings has revealed that the upper most part of the reservoir (<1000-1300 m) is primarily made up of basaltic lavas and hyaloclastites. At greater depths (>1000-1300 m) intrusions become more common (Mortensen et al., 2015).

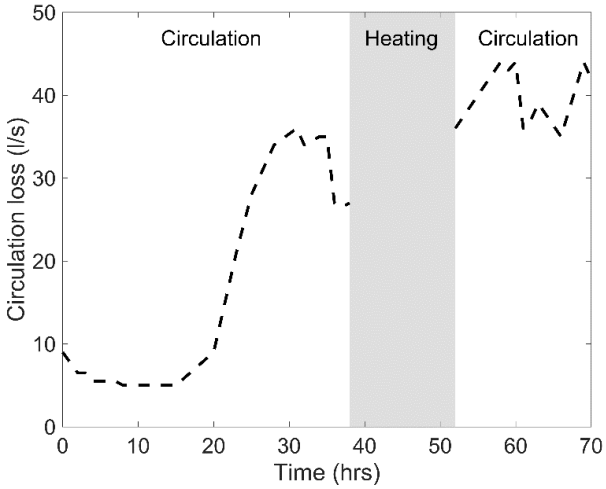

Figure 1. Circulation loss during thermal stimulation of well KJ-14 in Krafla, NE-Iceland (there is no loss during the heating phase). The stimulation of the well made it one of the most productive well in Krafla at that time (Stefánsson et al., 1982).

Methods and materials

To evaluate the magnitude of induced thermal stresses and evaluate changes in matrix permeability, we combine drilling reservoir data from Krafla with laboratory testing of basalt from Krafla. The material used for testing is a basalt erupted during the Mývatns fires in 1724-29 (Sæmundsson, 1991). Cylindrical core samples with a diameter and length of 25 mm were prepared for testing.

Experimental methods

The permeability of basalt samples (with 10% ±1 vol. % porosity) was measured using a benchtop permeameter. The permeability was measured by imposing a small pressure gradient where the flow of water was measured through the sample using a steady-state flow method. All measurements were conducted at a low confining pressure of 1 MPa to ensure fractures remained open (Lamur et al., 2017). To test the effects of thermal stimulation on the basalt, 9 cores were split into groups of 3 after permeability was measured. Each group was then heated at a steady rate of 5°C/min to set temperatures of 125 °C, 225 °C or 325 °C and held for 60 minutes. After that time, one core of each group was cooled in a bucket of water at ~20 °C, another was allowed to cool on the benchtop at ~20 °C and the third one was allowed to cool under a slow, controlled, cooling rate (~1 °C/min) in the furnace. Once the samples had cooled down, the permeability was re-measured. Then, the process was repeated for a further four heating/ cooling cycles and the permeability was measured again.

The thermal expansion of the basalt from Krafla was measured using a Netzsch TMA 402 F1 Hyperion Thermomechanical Analyzer (TMA). Following a baseline run, to accurately determine the thermal expansion of the sample assembly, the sample was heated up at a rate of 5 °C/min to 850 °C and cooled at the same rate. For the temperature range tested here, complementary simultaneous thermal analysis (combining the measurements of thermogravimetric analysis (TG) and differential scanning calorimetry (DSC) were carried out using a Netzsch STA 449 F1 Jupiter analyser, to ensure that no reactions would occur and overprint the effects of thermal stressing on the porous network upon heating (Siratovich et al., 2015b).

Properties of Icelandic basalt

Estimates of stress induced by cooling rely on a knowledge of the rock mechanical properties (i.e. tensile strength, Young's modulus and Poisson's ratio), which have been presented for a large dataset of Icelandic basalt in a report to the Road Administration of Iceland (Table 1; Loftsson and Steingrímsson, 2010). For our sample set, the porosity of the basalt chosen falls within the anticipated range (Table 1), having porosity of 10% ±1% and tensile strength of 5-15 MPa (Loftsson and Steingrímsson, 2010). For the model, we use the values relevant to our samples for which the porosity was measured

Table 1. Mechanical properties of Icelandic basalt presented in Loftsson and Steingrímsson (2010) and thermal properties of the Krafla basalt (as measured here).

Measured rock property	Range of values from Loftsson and Steingrímsson (2010)	Chosen properties for model
Porosity	1 – 33 %*	10% ±1%
Uniaxial strength (UCS)	4 – 330 MPa*	-
Tensile strength (TS)	0.25 – 20 MPa*	5-15 MPa**
Young's modulus	2.22 – 43.48 GPa*	40 GPa**
Poisson's ratio	0.18 – 0.20*	0.2**
Average thermal expansion (α)	N/A	6.09 x10-6 (1/K) ***

*From (Loftsson and Steingrímsson, 2010).

** Representative value chosen.

***Results presented in figure 2.

Results

Thermal expansivity determination

The linear thermal expansion and contraction (α) was calculated from change in length of the sample as it was heated 5 °C/min for the thermomechanical analyses (Figure 2). We note that the expansion was ~linear as a function of temperature to 500 °C before stabilising.

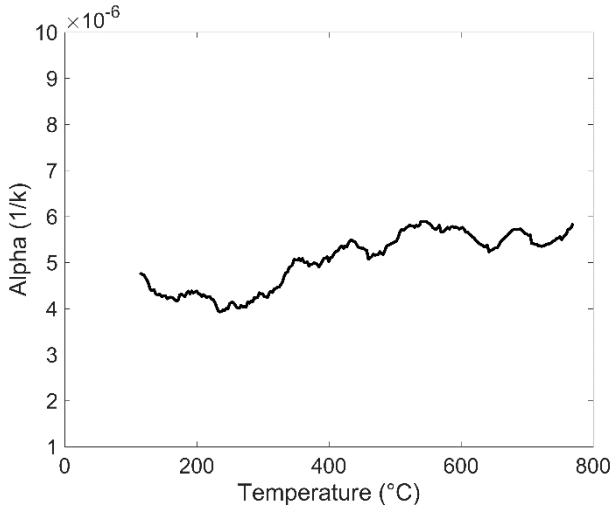

Figure 2. Thermomechanical analysis, showing the linear thermal expansion of basalt at 5 °C/min.

Thermally induced tensile stress modelling

By using the thermal properties of the basalt from Krafla (Figure 2), and its mechanical properties reported in Table 1, we can constrain the thermo-elastic stress resulting from cooling of reservoir rock via Equation 1 (Figure 3). For comparison, we show the range of tensile strength of the Icelandic basalt from Loftsson and Steingrímsson (2010). We observe that changes in the Young's modulus can have significant effects on the tensile stress induced by cooling; the analysis suggest that 15-20°C of cooling is needed to induce thermal cracks in rocks with high Young's modulus, whereas as much as 25-30 °C cooling is needed in rocks with lower Young's modulus. This cooling range would further depend on the local stress conditions (i.e. pore pressure and local stress anisotropy) in the reservoir (not assessed here).

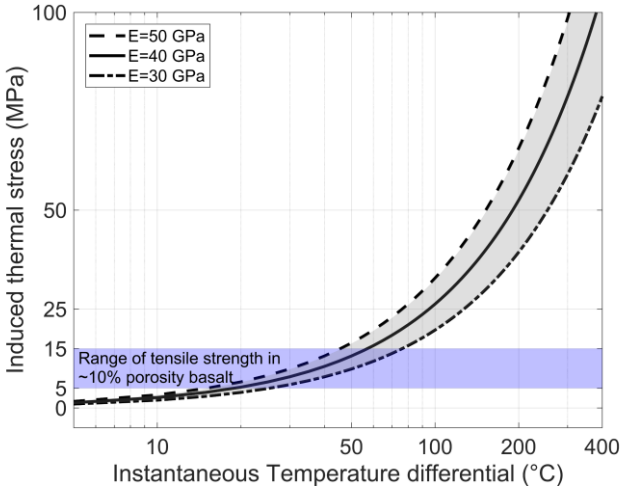

Figure 3. Model results of thermally induced tensile stress changes resulting from cooling of the basalt from the Mývatns Fires. The range of tensile strength of basalt containing 10% porosity is also shown in blue.

Impact of thermal stressing on basalt permeability

To investigate further the potential effect of thermally stressing rocks around wells with imposed temperature change, basalt cores were thermally stressed with different temperatures and cooling rates. During well construction and operation, temperature fluctuations occur in addition to thermal stimulation methods. The data shows that the changes in permeability following thermal stressing was trivial (Table 2); and thus, any changes may have remained within the resolution limit of permeability determination for the conditions tested.

Table 2. Impact of thermal stress cycles on the permeability of basalt. Thermal stressing was undergone by heating to 125, 225 or 325 °C and cooling to room temperature in water (rapid), in air or in a furnace (under slow, controlled, cooling rate).

Set temperature (°C)	Sample	Cooling environment	Permeability (m2)		
			Initial	1 cycle	5 cycles
125	Basalt_6w	Water	1.2x10-15	1.1 x10-15	1.3 x10-15
	Basalt_3b	Air	4.0x10-15	4.0 x10-15	4.0 x10-15
	Basalt_7f	Furnace	5.4 x10-15	5.1 x10-15	5.2 x10-15
225	Basalt_13w	Water	1.7 x10-15	1.5 x10-15	1.5 x10-15
	Basalt_14b	Air	2.6 x10-15	2.3 x10-15	2.5 x10-15
	Basalt_12f	Furnace	5.2 x10-15	4.4 x10-15	4.8 x10-15
325	Basalt_9w	Water	4.7 x10-16	4.5 x10-16	4.9 x10-16
	Basalt_2b	Air	3.2 x10-15	3.9 x10-15	5.1 x10-15
	Basalt_4f	Furnace	5.7 x10-15	5.0 x10-15	5.4 x10-15

Discussion and conclusions

A better understanding of the magnitude and extent of tensile stresses generated by thermal stimulation will improve our understanding of reservoir geoengineering to increase fluid flow and energy production. Thermal stimulation may induce a new fracture when the tensile stress imparted by contraction from the imposed temperature change exceeds the tensile strength of the rock. The presence of pressurised fluids in vesicles and cracks, and the anisotropy of the local stress field may alleviate the magnitude of thermal stress needed to fracture the rock. If we do not consider this local stress, we find in our model of thermal stress (Figure 3) that small changes in temperature can induce thermal stresses greater than the lower limit of tensile strengths. Yet, we found that permeability of the basalt was not changed when subjected to thermal stressing; we surmise that the nature of thermal stimulation tests commonly conducted in the laboratory may not fully mimic the nature of thermal stimulation from fluid injection in a borehole. Even though these tests are very helpful in the description of the material response to temperature changes, these tests are conducted on a cylindrical sample, free to expand and contract during heating/cooling cycles, without being constricted (as it would be in a natural environment). We posit that further experimental considerations may be required to widen the applicability of such tests. It remains that the permeability of geothermal reservoirs is certainly strongly influenced by fractures, but the influence of

thermal stressing – as a trigger to generate new fractures or open pre-existing ones – still deserves close attention in order to develop accurate methods to efficiently enhance fluid flow within reservoirs in a controlled manner.

Acknowledgements

This study has been partially financed by research funds from Landsvirkjun National Power Company of Iceland as well as a scholarship from the Institute for Risk and Uncertainty at the University of Liverpool and the European Research Council Starting Grant on Strain Localisation in Magma (SLiM, no. 306488). Attendance to the Stanford Geothermal Workshop 2018 is partly funded by a travel grant from GEORG Geothermal cluster.

Appendix II:

Supplementary information: Improving fluid flow in geothermal reservoirs by thermal and mechanical stimulation: The case of Krafla volcano, Iceland

Supplementary information published with the paper [Chapter 2]

Rock Type	Sample Name	Length (mm)	Diameter (mm)	Connected porosity (%)	Permeability at 3.75 MPa (m^2)	Permeability at 3.75 MPa with 1 fracture (m^2)	Permeability at 3.75 MPa with 2 fracture (m^2)
Felsite	KRA_FEL__01	14.65	26.06	12.95	$5.19x10^{-14}$	$3.48x10^{-14}$	N/A
Felsite	KRA_FEL__08	12.73	26.02	14.21	$3.85x10^{-14}$	$6.12x10^{-14}$	N/A
Felsite	KRA_FEL__09	16.10	26.03	13.88	$4.02x10^{-14}$	$1.45x10^{-14}$	N/A
Felsite	KRA_FEL__13	15.21	26.02	11.10	$3.77x10^{-15}$	$3.69x10^{-14}$	N/A
Felsite	KRA_FEL__02	12.25	25.98	12.54	$1.13x10^{-14}$	N/A	N/A
Felsite	KRA_FEL__03	11.89	26.00	11.15	$9.53x10^{-15}$	N/A	N/A
Felsite	KRA_FEL__04	12.73	26.01	12.04	$1.00x10^{-14}$	N/A	N/A
Felsite	KRA_FEL__05	12.92	26.02	11.46	$2.19x10^{-14}$	N/A	N/A
Felsite	KRA_FEL__06	12.01	25.99	12.28	$1.24x10^{-14}$	N/A	N/A
Felsite	KRA_FEL__07	13.10	26.08	15.24	$8.39x10^{-14}$	N/A	N/A
Felsite	KRA_FEL__10	10.62	26.05	16.26	$1.05x10^{-13}$	N/A	N/A
Felsite	KRA_FEL__12	14.56	25.96	10.73	$1.82x10^{-15}$	N/A	N/A
Felsite	KRA_FEL__18	15.20	26.05	12.08	$2.05x10^{-15}$	N/A	N/A
Felsite	KRA_FEL__11	14.07	25.95	18.33	$1.00x10^{-13}$	N/A	N/A
Felsite	KRA_FEL__19	12.33	25.84	10.79	$5.83x10^{-15}$	N/A	N/A
Felsite	KRA_FEL_TRI_21	49.77	24.85	9.31	$1.80x10^{-15}$	N/A	N/A
Felsite	KRA_FEL_TRI_22	50.06	24.87	9.42	$4.41x10^{-15}$	N/A	N/A
Felsite	KRA_FEL_PP_01	28.28	25.93	9.55	$1.18x10^{-14}$	N/A	N/A
Felsite	KRA_FEL_TRI_23	52.19	24.83	9.36	$1.19x10^{-14}$	N/A	N/A
Felsite	KRA_FEL_PP_02	50.29	24.88	9.80	$7.27x10^{-15}$	N/A	N/A
Felsite	KRA_FEL_TRI_24	48.20	25.88	9.45	$4.40x10^{-15}$	N/A	N/A
Felsite	KRA_FEL_TRI_25	48.84	25.95	10.88	$2.51x10^{-14}$	N/A	N/A
Felsite	KRA_FEL_TRI_26	51.85	24.88	9.94	$1.34x10^{-14}$	N/A	N/A
Felsite	KRA_FEL_TRI_27	52.72	24.89	9.83	$5.55x10^{-15}$	N/A	N/A
Felsite	KRA_FEL_TRI_28	51.15	24.95	10.03	$1.08x10^{-14}$	N/A	N/A
Felsite	KRA_FEL_TRI_29	48.36	24.88	10.28	$1.31x10^{-14}$	N/A	N/A
Felsite	KRA_FEL_TRI_30	52.11	24.87	9.74	$9.57x10^{-15}$	N/A	N/A
Felsite	KRA_FEL_TRI_31	51.92	24.87	10.47	$1.00x10^{-14}$	N/A	N/A
Felsite	KRA_FEL_TRI_32	49.01	24.89	10.87	$1.28x10^{-14}$	N/A	N/A
Basalt - Dense	KRA_BAS__04	15.83	26.10	15.88	$4.01x10^{-14}$	$1.30x10^{-13}$	$1.54x10^{-13}$
Basalt - Dense	KRA_BAS__05	11.26	26.07	16.89	$1.00x10^{-13}$	$1.00x10^{-13}$	N/A
Basalt - Dense	KRA_BAS__06	12.10	26.07	11.22	$2.03x10^{-16}$	$9.90x10^{-14}$	N/A

Basalt - Dense	KRA_BAS__07	11.91	26.06	14.16	$6.58x10^{-16}$	$7.85x10^{-14}$	N/A
Basalt - Dense	KRA_BAS__08	15.78	26.06	13.45	$2.04x10^{-15}$	$1.20x10^{-13}$	$1.30x10^{-13}$
Basalt - Dense	KRA_BAS__10	15.24	26.10	14.79	$2.75x10^{-14}$	$1.15x10^{-13}$	$1.00x10^{-13}$
Basalt - Dense	KRA_BAS__14	14.80	26.05	12.93	$1.30x10^{-15}$	$6.40x10^{-13}$	$1.35x10^{-13}$
Basalt - Dense	KRA_BAS__16	14.35	26.06	11.94	$5.96x10^{-16}$	$8.61x10^{-13}$	N/A
Basalt - Dense	KRA_BAS__19	13.45	26.06	10.88	$3.49x10^{-16}$	$7.03x10^{-14}$	$7.86x10^{-13}$
Basalt - Dense	KRA_BAS__20	13.44	26.07	21.33	$2.94x10^{-14}$	$1.02x10^{-13}$	N/A
Basalt - Dense	KRA_BAS__12	14.05	26.05	15.13	$2.67x10^{-14}$	N/A	N/A
Basalt - Dense	KRA_BAS__13	15.29	26.11	26.84	$8.89x10^{-14}$	N/A	N/A
Basalt - Dense	KRA_BAS__17	16.60	26.09	22.02	$1.03x10^{-13}$	N/A	N/A
Basalt - Dense	KRA_BAS_UCS_08	50.69	26.10	17.44	$1.74x10^{-15}$	N/A	N/A
Basalt - Dense	KRA_BAS_TRI_40	52.81	24.95	22.90	$1.10x10^{-13}$	N/A	N/A
Basalt - Dense	KRA_BAS_TRI_41	51.74	24.93	11.90	$1.05x10^{-15}$	N/A	N/A
Basalt - Dense	KRA_BAS_TRI_43	52.13	24.93	11.46	$6.41x10^{-16}$	N/A	N/A
Basalt - Dense	KRA_BAS_TRI_44	51.80	24.90	12.46	$1.58x10^{-15}$	N/A	N/A
Basalt - Dense	KRA_BAS_TRI_45	51.20	24.92	12.38	$1.01x10^{-15}$	N/A	N/A
Basalt - Dense	KRA_BAS_TRI_51	49.10	24.93	12.11	$6.04x10^{-16}$	N/A	N/A
Basalt - Dense	KRA_BAS_TRI_52	50.40	24.92	12.45	$1.01x10^{-15}$	N/A	N/A
Basalt - Dense	KRA_BAS_TRI_55	50.82	24.92	11.13	$4.79x10^{-16}$	N/A	N/A
Basalt - Dense	KRA_BAS_TRI_56	51.25	24.95	18.19	$1.61x10^{-13}$	N/A	N/A
Basalt - Dense	KRA_BAS_TRI_57	52.67	24.90	14.05	$4.26x10^{-14}$	N/A	N/A
Basalt - Dense	KRA_BAS_TRI_58	52.38	24.71	23.50	$1.59x10^{-13}$	N/A	N/A
Basalt - Dense	KRA_BAS_TRI_61	51.80	24.95	13.42	$1.75x10^{-14}$	N/A	N/A
Basalt - Dense	KRA_BAS_TRI_62	50.78	24.92	12.79	$7.34x10^{-16}$	N/A	N/A
Basalt - Dense	KRA_BAS_TRI_63	52.03	24.93	10.92	$2.15x10^{-16}$	N/A	N/A
Basalt - Dense	KRA_BAS_TRI_66	51.18	24.87	15.58	$1.96x10^{-13}$	N/A	N/A
Basalt - porous	KRA_BAS_01_01	12.80	26.00	60.39	$1.17x10^{-13}$	N/A	N/A
Basalt - porous	KRA_BAS_01_02	10.63	26.00	49.06	$1.91x10^{-13}$	$1.04x10^{-13}$	N/A
Basalt - porous	KRA_BAS_01_03	10.95	26.01	41.91	$1.45x10^{-13}$	$1.51x10^{-13}$	N/A
Basalt - porous	KRA_BAS_01_04	9.65	26.00	54.64	$7.91x10^{-14}$	$8.07x10^{-14}$	N/A
Basalt - porous	KRA_BAS_01_05	12.01	26.01	46.88	$1.93x10^{-13}$	$1.04x10^{-13}$	N/A
Basalt - porous	KRA_BAS__09	14.56	26.06	34.28	$9.96x10^{-14}$	$8.51x10^{-14}$	N/A
Basalt - porous	KRA_BAS__01	11.02	16.14	58.13	$8.95x10^{-14}$	N/A	N/A
Basalt - porous	KRA_BAS__02	8.83	13.39	60.14	$2.53x10^{-13}$	N/A	N/A
Basalt - porous	KRA_BAS__27	14.28	25.88	36.73	$1.03x10^{-13}$	N/A	N/A
Basalt - porous	KRA_BAS_TRI_02	50.22	24.82	49.34	$2.38x10^{-13}$	N/A	N/A
Basalt - porous	KRA_BAS_TRI_46	50.69	24.87	48.23	$2.29x10^{-13}$	N/A	N/A
Basalt - porous	KRA_BAS_TRI_48	52.23	24.88	48.16	$1.30x10^{-13}$	N/A	N/A
Basalt - Dyke	KRA_BAS_TRI_65	50.80	24.84	35.87	$1.93x10^{-16}$	N/A	N/A
Basalt - Dyke	KRA_BAS_UCS_23	51.65	25.92	31.89	$9.72x10^{-15}$	N/A	N/A
Basalt - Dyke	KRA_BAS_UCS_25	48.76	24.73	31.73	$9.61x10^{-15}$	N/A	N/A
Basalt - Dyke	KRA_BAS_UCS_27	53.22	25.91	31.06	$7.52x10^{-15}$	N/A	N/A
Basalt - Dyke	KRA_BAS_TRI_26	51.55	24.85	31.58	$1.96x10^{-13}$	N/A	N/A
Basalt - Dyke	KRA_BAS_TRI_30	50.14	24.84	32.61	$8.12x10^{-15}$	N/A	N/A
Basalt - Dyke	KRA_BAS_TRI_32	50.13	24.85	31.66	$6.61x10^{-15}$	N/A	N/A
Basalt - Dyke	KRA_BAS_TRI_33	50.85	24.90	32.02	$1.15x10^{-14}$	N/A	N/A

Basalt - Dyke	KRA_BAS_TRI_36	50.85	24.90	33.70	$8.96x10^{-16}$	N/A	N/A
Basalt - Dyke	KRA_BAS_TRI_67	49.70	24.94	32.25	$4.24x10^{-16}$	N/A	N/A
Gabbro	KRA_GAB__03	16.70	26.05	12.95	$1.22x10^{-15}$	$1.18x10^{-13}$	N/A
Gabbro	KRA_GAB__05	13.87	26.07	13.30	$7.85x10^{-16}$	$6.88x10^{-14}$	N/A
Gabbro	KRA_GAB__09	15.06	26.12	11.60	$2.70x10^{-15}$	$5.52x10^{-14}$	N/A
Gabbro	KRA_GAB__10	14.90	26.06	14.96	Below apparatus limit	$6.18x10^{-14}$	N/A
Gabbro	KRA_GAB__11	18.36	26.07	12.53	$8.32x10^{-16}$	$1.39x10^{-13}$	N/A
Gabbro	KRA_GAB__13	16.34	26.08	12.26	$2.17x10^{-15}$	$5.23x10^{-14}$	N/A
Gabbro	KRA_GAB__01	13.54	26.08	14.68	$7.60x10^{-16}$	N/A	N/A
Gabbro	KRA_GAB__04	11.37	26.07	11.46	$7.21x10^{-16}$	N/A	N/A
Gabbro	KRA_GAB__07	14.51	26.06	12.11	$7.32x10^{-16}$	N/A	N/A
Gabbro	KRA_GAB__12	17.61	26.05	10.57	$3.36x10^{-16}$	N/A	N/A
Gabbro	KRA_GAB__08	15.21	26.06	12.80	$7.68x10^{-16}$	N/A	N/A
Gabbro	KRA_GAB_UCS_01	58.41	24.88	11.93	$1.68x10^{-15}$	N/A	N/A
Gabbro	KRA_GAB_TRI_11	51.00	24.89	11.58	$2.67x10^{-15}$	N/A	N/A
Gabbro	KRA_GAB_TRI_12	49.91	24.86	11.61	$1.04x10^{-14}$	N/A	N/A
Gabbro	KRA_GAB_TRI_15	49.07	24.87	13.31	$3.46x10^{-15}$	N/A	N/A
Gabbro	KRA_GAB_TRI_17	51.44	24.91	12.59	$7.00x10^{-15}$	N/A	N/A
Gabbro	KRA_GAB_TRI_20	51.85	24.86	11.40	$1.50x10^{-15}$	N/A	N/A
Gabbro	KRA_GAB_TRI_21	50.92	24.88	11.46	$2.77x10^{-15}$	N/A	N/A
Hyaloclastite	KRA_HYA__01	13.50	25.95	38.81	$1.37x10^{-13}$	N/A	N/A
Hyaloclastite	KRA_HYA__02	12.45	25.80	39.30	$6.33x10^{-14}$	N/A	N/A
Hyaloclastite	KRA_HYA__03	12.32	25.93	41.65	$1.30x10^{-13}$	N/A	N/A
Hyaloclastite	KRA_HYA__05	11.80	25.97	40.03	$1.41x10^{-13}$	N/A	N/A
Hyaloclastite	KRA_HYA__06	11.83	25.85	43.62	$1.55x10^{-13}$	N/A	N/A
Hyaloclastite	KRA_HYA__07	12.67	25.98	40.07	$1.77x10^{-13}$	N/A	N/A
Hyaloclastite	KRA_HYA__08	14.47	25.92	42.23	$1.73x10^{-13}$	N/A	N/A
Hyaloclastite	KRA_HYA__09	15.83	25.90	44.94	$9.63x10^{-14}$	N/A	N/A
Hyaloclastite	KRA_HYA__10	14.32	25.80	41.95	$9.63x10^{-14}$	N/A	N/A
Hyaloclastite	KRA_HYA_TRI_07	51.81	24.66	35.22	$7.83x10^{-14}$	N/A	N/A
Hyaloclastite	KRA_HYA_TRI_08	50.98	24.77	34.87	$9.23x10^{-14}$	N/A	N/A
Hyaloclastite	KRA_HYA_PP_02	51.08	24.65	38.70	$7.73x10^{-14}$	N/A	N/A
Hyaloclastite	KRA_HYA_TRI_09	54.10	24.70	34.98	$5.95x10^{-14}$	N/A	N/A
Ignimbrite	KRA_IGN_03_03	13.95	25.96	15.92	Below apparatus limit	$7.34x10^{-14}$	N/A
Ignimbrite	KRA_IGN_03_04	11.80	26.03	14.63		$3.12x10^{-14}$	N/A
Ignimbrite	KRA_IGN_03_05	11.59	26.05	14.88		$1.30x10^{-15}$	N/A
Ignimbrite	KRA_IGN_03_02	10.87	26.05	13.91		$2.07x10^{-14}$	N/A
Ignimbrite	KRA_IGN__01	11.40	26.03	16.78		$9.38x10^{-14}$	N/A
Obsidian	KRA_OBS__01	13.08	26.01	5.28	Below apparatus limit	$3.33x10^{-14}$	N/A
Obsidian	KRA_OBS_02_01	13.73	26.01	1.53		$4.83x10^{-14}$	N/A
Obsidian	KRA_OBS_02_02	14.25	26.02	1.40		N/A	N/A
Obsidian	KRA_OBS_01_01	14.80	25.97	1.04		N/A	N/A
Obsidian	KRA_OBS_01_02	18.07	26.08	1.26		N/A	N/A
Obsidian	KRA_OBS_03_01	15.40	26.00	2.20		N/A	N/A
Obsidian	KRA_OBS__02	13.98	26.07	1.44		N/A	N/A

Appendix III:
Supplementary figures: Compaction of hyaloclastite from the active geothermal system at Krafla volcano, Iceland

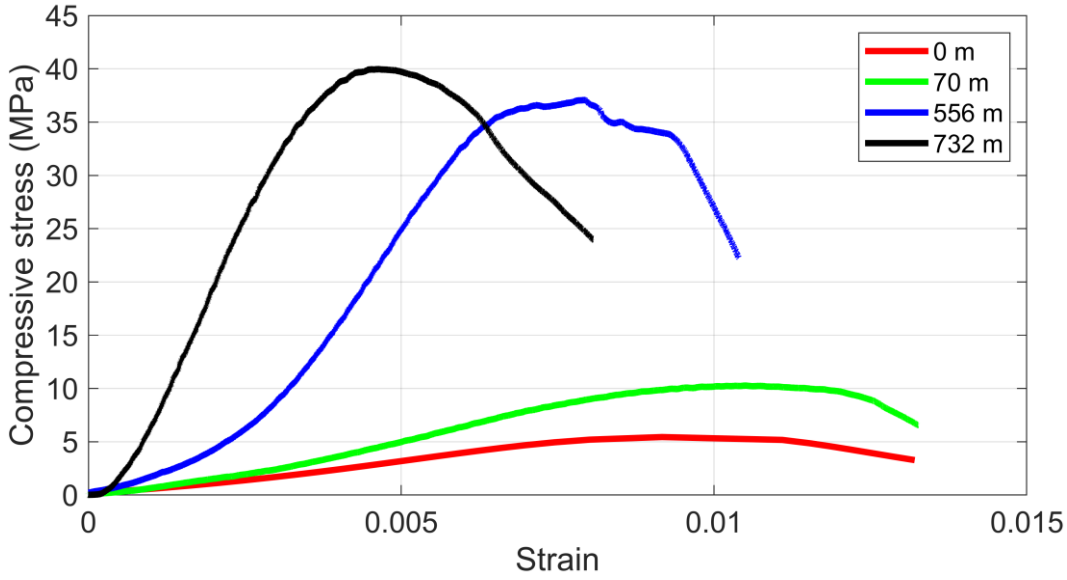

Figure 1. The UCS data showing the stress-strain loading paths for each of the samples tested within the uniaxial press, where the sample is loaded until a stress drop of >10 % is observed. Strength increases with increasing sampling depth within the reservoir, and the slope of the stress strain curves is steeper with increasing sampling depth, corresponding to a lower porosity.

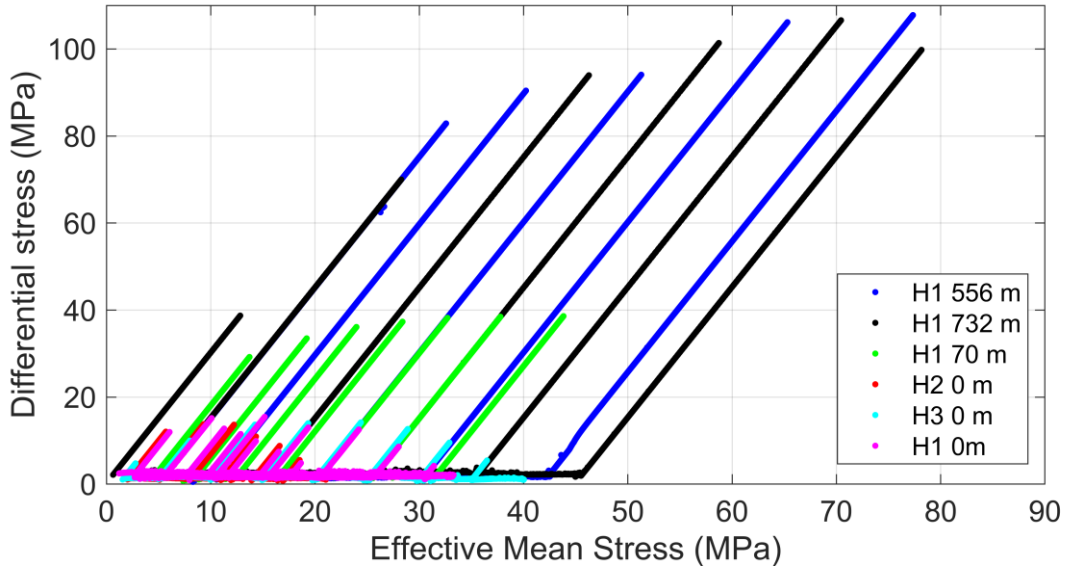

Figure 2. The raw loading data for each sample, showing the loading paths for each of the samples tested within the triaxial apparatus. The raw loading data for each sample, showing the loading paths for each of the samples tested within the triaxial apparatus. The samples are loaded to the target confining pressure and then axially stressed until they exhibit their elastic limit (P) before removing the axial load, reducing the effective mean stress again. However, if the sample is loaded past P* (the surface samples) then the effective mean stress is reduced slightly before the axial load is increased on the sample.*